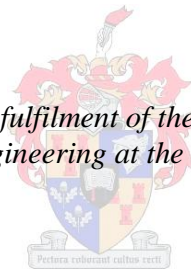


An evaluation of inertial motion capture technology for use in the analysis and optimization of road cycling kinematics

by
Stephen John Cockcroft

*Thesis presented in partial fulfilment of the requirements for the degree
Master of Science in Engineering at the University of Stellenbosch*



Supervisor: Prof. C. Scheffer
Faculty of Engineering
Department of Mechanical and Mechatronic Engineering

March 2011

DECLARATION

By submitting this thesis electronically, I declare that the entirety of the work contained therein is my own, original work, that I am the owner of the copyright thereof (unless to the extent explicitly otherwise stated) and that I have not previously in its entirety or in part submitted it for obtaining any qualification.

March 2011

Copyright © 2011 Stellenbosch University

All rights reserved

ABSTRACT

Optical motion capture (Mocap) systems measure 3D human kinematics accurately and at high sample rates. One of the limitations of these systems is that they can only be used indoors. However, advances in inertial sensing have led to the development of inertial Mocap technology (IMCT). IMCT measures kinematics using inertial measurement units (IMUs) attached to a subject's body without the need for external sensors. It is thus completely portable which opens up new horizons for clinical Mocap. This study evaluates the use of IMCT for improving road cycling kinematics. Ten male sub-elite cyclists were recorded with an IMCT system for one minute while cycling at 2, 3.5 and 5.5 W.kg⁻¹ on a stretch of road and on a stationary trainer. A benchmark test was also done where cycling kinematics was measured simultaneously with the IMCT and a gold-standard Vicon optical system. The first goal was to assess the feasibility of conducting field measurements of cycling kinematics. Magnetic analysis results showed that the IMUs near the pedals and handlebars experienced significant magnetic interference (up to 50% deviation in intensity) from ferrous materials in the road bicycles, causing significant errors in kinematic measurement. Therefore, it was found that the IMCT cannot measure accurate full-body kinematics with the subject on a road bicycle. However, the results of the benchmark test with the Vicon showed that the IMCT can still measure accurate hip (root mean square error (RMSE) < 1°), knee (RMSE < 3.5°) and ankle (RMSE < 3°) flexion using its Kinematic Coupling algorithm. The second goal was to determine whether there is a significant difference between road cycling kinematics captured on the road and in a laboratory. The outdoor flexion results were significantly different to the indoor results, especially for minimum flexion (P < 0.05 for all joints). Changes in rider kinematics between high and low power were also found to have significantly more variability on the road (R² = 0.36, 0.61, 0.08) than on the trainer (R² = 0.93, 0.89, 0.56) for the hip, knee and ankle joints respectively. These results bring into question the ecological validity of laboratory cycling. Lastly, applications of IMCT for optimizing cycling performance were to be identified. Several aspects of kinematic analysis and performance optimization using the IMCT were evaluated. It was determined that IMCT is most suited for use as a dynamic bicycle fitting tool for analysis of biomechanical efficiency, bilateral asymmetry and prevention of overuse injuries. Recommendations for future work include the elimination of the magnetic interference and integration of the IMCT data with kinetic measurements to develop an outdoor dynamic fitting protocol.

OPSOMMING

Optiese bewegingswaarnemingstelsels (BWS) meet drie-dimensionele menslike kinematika met hoë akkuraatheid en teen hoë monstertempo's. Een van die nadele van BWS is dat hulle slegs binnenshuis gebruik kan word. Onlangse ontwikkelings in sensor tegnologie het egter gelei na die beskikbaarheid van traagheids-BWS-tegnologie (TBT). TBT gebruik traagheidsmetingseenhede (TMEs) wat aan 'n persoon se liggaam aangeheg kan word om die kinematika te verkry sonder enige eksterne sensore. TBT is dus volkome draagbaar, wat nuwe geleenheide skep vir kliniese bewingsanalises. Hierdie projek evalueer die gebruik van TBT vir die verbetering van fietsry kinematika. Tien kompeterende fietsryers (manlik) was getoets met 'n TBT terwyl hulle teen 2, 3.5 and 5.5 W.kg⁻¹ gery het op 'n pad, en op 'n stilstaande oefenfietsraam. 'n Maatstaftoets was ook uitgevoer waar fietsry-kinematika gelyktydig met die TBT en die Vicon optiese BWS opgeneem was. Die eerste doel van die navorsing was om die moontlikheid te ondersoek of fietsryer kinematika op die pad gemeet kan word. Die resultate toon dat die ferro-magnetiese materiale wat in meeste padfietsse voorkom, 'n beduidende magnetiese steuring (tot 50% afwyking in intensiteit) op die TMEs naby die pedale en handvatsels veroorsaak, wat lei tot aansienlike foute in die kinematiese metings. Gevolglik was dit gevind dat die TBT nie volle-liggaam kinematika op 'n fiets kan meet nie. Nogtans, het die resultate van die Vicon maatstaftoets bewys dat die TBT nog steeds akkurate heup (wortel van die gemiddelde kwadraad fout (WGKF) < 1°), knie (WGKF < 4°) en enkel (WGKF < 3°) fleksie kan meet met die "Kinematiese Koppeling" algoritme. Die tweede doel was om te bepaal of daar 'n beduidende verskil tussen die laboratorium en pad fietsry-kinematika is. Die buitelug fleksie data het beduidend verskil van die binnenshuise resultate, veral vir minimum fleksie ($P < 0.05$ vir alle gewigte). Veranderinge in fietsryer kinematika tussen hoë en lae krag het ook beduidend meer variasie op die pad ($R^2 = 0.36, 0.61, 0.08$) as op die oefenfietsraam ($R^2 = 0.93, 0.89, 0.56$) vir die heup, knie en enkel gewigte, onderskeidelik, gehad. Hierdie resultate bevraagteken die ekologiese geldigheid van kinematiese toetse op fietsryers in 'n laboratorium. 'n Laaste doel was om die toepassings van TBT vir die optimalisering van fietsry kinematika te ondersoek. 'n Verskeidenheid aspekte van die analise en verbetering van fietsry kinematika met die TBT word bespreek. Die gevolgtrekking is dat TBT geskik is vir gebruik as 'n dinamiese instrument vir die analise van biomeganiese doetreffendheid, bilaterale asimmetrie en die voorkoming van beserings. Aanbevelings vir toekomstige werk, sluit in die uitskakeling van die magnetiese inmenging, asook die integrasie van die TBT data met kinetiese metings.

DEDICATION

To the Lord Jesus Christ; for all things are from Him, through Him and to Him

ACKNOWLEDGEMENTS

The author would like to acknowledge the help of researcher and road cyclist Andrew Smith, from the Department of Physiology at Stellenbosch University, for his valuable technical guidance and practical assistance during the study. Similarly, thanks must go to Sjan-Mari van Niekerk, from the Physiotherapy and Movement Science Clinic at Tygerberg Campus, who assisted with the Vicon benchmark testing.

Furthermore, a word of special thanks to Professor Cornie Scheffer, for being a great mentor as well as supervisor, and for creating a wonderful environment for professional growth and development during the last two years. Dr. Dillon also deserves mention for his insightful technical input, which was tremendously helpful in expanding the horizons of the biomechanical analysis. The author also acknowledges the financial support of the Biomedical Engineering Research Group.

On a more personal note, the author would also like to extend thanks to loyal friend and colleague Albert Smit, for all the countless hours of help during the study; for driving the pursuit vehicle, acting as pseudo-patient in the unflattering MVN suit and providing companionship in the office during the late-night shifts. Two are better than one.

Finally, to my darling Rose; who was a pillar of support and encouragement from start to finish, and read through every word I wrote with a red pen. I could not have made it through to the end without you. Thank you.

CONTENTS

LIST OF TABLES.....	ix
LIST OF FIGURES	x
LIST OF ABBREVIATIONS.....	xii
LIST OF SYMBOLS	xiii
1. INTRODUCTION	1
1.1. Background	1
1.2. Primary Objective and Motivation.....	4
1.3. Problem Statement and Research Questions.....	7
1.4. Scope of Work.....	8
1.4.1. Research activities	8
1.4.2. Document outline.....	9
2. LITERATURE STUDY	10
2.1. The MVN BIOMECH System	10
2.1.1. Sensor fusion scheme overview.....	10
2.1.2. Inertial navigation system.....	11
2.1.3. Segment kinematics	16
2.1.4. Joint updates and contact points	21
2.2. Research Review.....	23
2.2.1. Validations of Xsens Mocap technology.....	23
2.2.2. Sports performance research using Mocap.....	24
2.2.3. The ecological validity of laboratory cycling.....	25
2.2.4. Cycling kinematics and bicycle fit.....	26
3. DATA COLLECTION	29
3.1. Background Information	29
3.1.1. Scope of testing.....	29

3.1.2.	Test subjects.....	29
3.1.1.	Instrumentation	30
3.2.	Experimental Setup	30
3.2.1.	MVN suit	30
3.2.2.	Laboratory test	31
3.2.3.	Field test.....	33
3.3.	Test Procedure.....	33
3.3.1.	Indoor protocol	33
3.3.2.	Outdoor protocol.....	35
3.4.	Data Pre-processing	36
4.	DATA ANALYSIS.....	38
4.1.	Validation of MVN Measurements	38
4.1.1.	Magnetic interference	38
4.1.2.	Background to kinematic analysis	49
4.1.3.	Benchmark test with Vicon system	51
4.1.4.	Comparison of results with other studies.....	54
4.2.	Comparison Between Indoor and Outdoor Data.....	56
4.2.1.	Laboratory and field measurements during medium power test.....	56
4.2.2.	Correlations between low and high power sessions	57
4.3.	Applications of the MVN Data	59
4.3.1.	Dynamic measurement and analysis.....	60
4.3.2.	Bilateral asymmetry	63
4.3.3.	Prevention of knee injuries	66
4.4.	Conclusions	67
5.	DISCUSSION	69
5.1.	Research Conclusions	69
5.2.	Lessons Learned.....	72
5.2.1.	MVN operating principles	72

5.2.2.	Practicalities of data collection using the MVN	73
5.2.3.	Indoor and outdoor measurement of road cycling kinematics.....	74
5.2.4.	Recommendations for future testing.....	76
5.3.	Recommendations for Future Cycling Research.....	77
5.4.	Significance of Research.....	79
APPENDIX A	THEORETICAL WORK	81
A.1	Mocap Overview	81
A.1.1	General working principles.....	81
A.1.2	Types of Mocap	82
A.2	MVN Inertial Measurement Units	84
A.3	Road Cycling.....	87
A.3.1	Cycling kinematics and performance	87
A.3.2	General principles of bicycle fit.....	89
APPENDIX B	EXPERIMENTAL WORK	92
B.1	The MVN Hardware	92
B.2	Powerbeam Trainer	93
B.3	Miscellaneous.....	95
APPENDIX C	ANALYSIS WORK.....	97
C.1	Data Management	97
C.1.1	Importing MVNX data files into Matlab	97
C.1.2	Data structuring.....	97
C.2	Numerical Analysis.....	100
C.2.1	Magnetic flux and inclination calculation	100
C.2.2	Cadence and crank angle calculation.....	106
C.2.3	Joint flexion calculations	109
REFERENCES	111

LIST OF TABLES

Table 1: Summary of Powerbeam workout for data collection	34
Table 2: Entire indoor test protocol	35
Table 3: Flexion measurements taken of outdoor cycling with MVN	53
Table 4: Summary of flexion outdoor cycling measurements	55
Table 5: Comparison between indoor and outdoor flexion measurements	57
Table 6: Comparison of flexion measurements at high and low power	59
Table 7: MVN XBus Master specifications.....	92
Table 8: MVN MTx sensor specifications.....	93
Table 9: Powerbeam specifications	95

LIST OF FIGURES

Figure 1: The MVN (a) suitcase (b) Lycra suit and (c) wireless transmitters	4
Figure 2: MVN sensor fusion scheme	11
Figure 3: MVN MTx module containing MEMS sensors	12
Figure 4: Kalman filter error model for eliminating gyroscope drift error.....	13
Figure 5: MVN model consisting of (a) 23 segments tracked by (b) 17 MTxs.....	16
Figure 6: The (a) rigged skeleton and (b) XYZ coordinate system conventions.....	17
Figure 7: Anthropometry values used for MVN biomechanical model	18
Figure 8: a) Neutral b) T-position- c) squat and d) hand-touch calibrations	19
Figure 9: Calculation sequence for estimation of segment kinematics	20
Figure 10: Joint centre uncertainty (a) before and (b) after joint updates	21
Figure 11: Basic bicycle fit parameters	27
Figure 12: Laboratory setup for indoor tests	32
Figure 13: Road test with pursuit car transporting laptop and wireless receivers	35
Figure 14: MVN interface containing test recording.....	37
Figure 15: Inclination angle and intensity near head segment sensor	39
Figure 16: Magnetic readings for (a) sternum and (b) pelvis sensors	40
Figure 17: Magnetic readings for (a) left and (b) right shoulder sensors	42
Figure 18: Magnetic readings for (a) left and (b) right upper arm sensors.....	42
Figure 19: Magnetic readings for (a) left and (b) right forearm sensors	43
Figure 20: Magnetic readings for (a) left and (b) right hand sensors	43
Figure 21: Magnetic readings for (a) left and (b) right upper leg sensors	44
Figure 22: Magnetic readings for (a) left and (b) right lower leg sensors	44
Figure 23: Magnetic readings for (a) left and (b) right foot sensors.....	45
Figure 24: Increasing magnetic interference toward hands	46
Figure 25: Increasing magnetic interference towards feet.....	47
Figure 26: Example of (a) negligible and (b) severe interference	48
Figure 27: Definition of (a) crank, (b) joint angles, (c) TDC and (d) BDC	49
Figure 28: Five-bar linkage model for (a) kinematic and (b) kinetic analysis	50
Figure 29: Comparison of Vicon and MVN (a) right and (b) left leg flexion	52
Figure 30: Flexion angles for (a) hip and (b) knee at different seat heights	54
Figure 31: Indoor and outdoor (a) Θ_{MAX} (b) Θ_{MIN} right Θ_K	56
Figure 32: Θ_H , Θ_K and Θ_A in (a) indoor and (b) outdoor power sessions	58
Figure 33: Examples of Θ_H , Θ_K and Θ_A for left and right legs.....	61
Figure 34: Asymmetry in (a) pelvic tilt and (b) Θ_H , (c) Θ_K and (d) Θ_A	64

Figure 35: The (a) forces leading to PFJ pain and the (b) ITB friction zone.....	66
Figure 36: Basic universal Mocap principles	81
Figure 37: The (a) outside-in (b) inside-out and (c) inside-in Mocap methods.....	82
Figure 38: Accelerometer (a) principles and (b) signal output vector diagram.....	84
Figure 39: Schematic of vibrating mass gyroscope working principals	86
Figure 40: An AMR (a) sensor and (b) the AMR principle.....	87
Figure 41: Basic bicycle fit parameters	89
Figure 42: The Powerbeam Pro stationary bicycle trainer	94
Figure 43: Powerbeam wireless handlebar display unit	95
Figure 44: Manufactured aluminium frame for trainer.....	96
Figure 45: Flow of measurement data from MVN Studio into Matlab	97
Figure 46: Matlab Data structure	98
Figure 47: The MVNX data table for joint ankles.....	99
Figure 48: Contents of Matlab data structures.....	99
Figure 49: Example of magnetometer readings over time.....	101
Figure 50: Method used to obtain the magnetic inclination angle.....	102
Figure 51: Cosine method used to obtain angle $\Theta_{MA,t}$	103
Figure 52: Hand sensor acceleration (a) indoors and (b) outdoors	104
Figure 53: Acceleration vectors for indoor (a) hand and (b) foot sensors.....	105
Figure 54: Example of severely disturbed magnetometer readings.....	106
Figure 55: Crank angle as calculated using the position of the pedal.....	107
Figure 56: (a) Raw position data and (b) path of toe segment.....	108
Figure 57: Corrected pedal path using Y-data	109
Figure 58: Method used to calculate the kinematic parameters.....	110

LIST OF ABBREVIATIONS

AMR	-	Anisotropic magnetoresistance
BERG	-	Biomedical engineering research group
BDC	-	Bottom dead centre of pedal stroke
DOF	-	Degrees of freedom
IMC	-	Inertial motion capture
IMCT	-	Inertial motion capture technology
IMU	-	Inertial measurement unit
INS	-	Inertial navigation system
ISB	-	International society of biomechanics
ITB	-	Iliotibial Band
ITBFS	-	Iliotibial band friction syndrome
KiC	-	Kinetic coupling
Mocap	-	Motion capture
MEMS	-	Micro-electromechanical systems
MT _x	-	Motion tracker X
MVNX	-	MVN file in XML format
PFJ	-	Patellofemoral joint
RMS	-	Root mean square
RMSE	-	Root mean square error
TDC	-	Top dead centre of pedal stroke
XML	-	Extensible markup language

LIST OF SYMBOLS

Θ_A	-	Ankle flexion
Θ_C	-	Crank angle
Θ_H	-	Hip flexion
Θ_{IN}	-	Indoor flexion
Θ_K	-	Knee flexion
Θ_{LEFT}	-	Left leg flexion
$\Theta_{MA,t}$	-	Angle between MTx intensity and acceleration measurement
Θ_{MAX}	-	Average maximum flexion
Θ_{MIN}	-	Average minimum flexion
Θ_{OUT}	-	Outdoor flexion
Θ_{RANGE}	-	Average range of flexion
Θ_{RIGHT}	-	Right leg flexion
a_c	-	Coriolis acceleration
A_t	-	MVN MTx accelerometer output signal
F_C	-	Coriolis force
FS_t	-	Scalar magnitude of the magnetic field intensity vector
I_t	-	Magnetic field inclination angle
L_C	-	Length of bicycle crank arm
M_t	-	MVN MTx magnetometer output signal

1. INTRODUCTION

This study contributes towards research being conducted with inertial motion capture (Mocap) by the Biomedical Engineering Research Group (BERG) to investigate applications of the technology in a variety of fields. BERG is a research group housed within the Department of Mechanical and Mechatronic Engineering at Stellenbosch University. This chapter presents some background information on the study as well as the research motivation, goals and scope.

1.1. Background

The need for a greater understanding of the causes and effects of human movement has driven the study of human locomotion for hundreds of years (Baker, R, 2007). Increased knowledge in this field has significant benefits. For example, if clear links between pathologies and the resulting pathological gait can be established, there is the possibility of an earlier, more confident diagnosis (Ephanov, A and Hurmuzlu, Y, 2002). Similarly, further understanding of normal motion may lead to enhanced ergonomics for employees in the workplace (Mavrikios, D *et al.*, 2006) and better rehabilitation techniques for injured patients (Steinwender, G *et al.*, 2000). It can also help to produce more realistic humanoid animations and improved performance or training regimes for sports athletes. In fact, the benefits of an improved understanding of human motion are almost endless. However, human motion must be measured and interpreted in ever increasing detail and scope to accomplish this.

Mündermann *et al.* (2006) provide a concise early history of the development of scientific understanding of human locomotion, covering almost two centuries. One of the first quantitative studies was carried out as early as 1836 (Weber, W and Weber, E, 1836). Approximately fifty years later, the first photographic techniques were already being developed to identify patterns in human motion (Muybridge, E, 1887). Around the same time, significant progress was also being made in the understanding of joint forces and energy expenditure during human locomotion (Braune, W and Fischer, O, 1988). However, the most significant advances in the field of biomechanics were made much later; during the 1950's. Due to the need for treating World War II amputees, groundbreaking research on human movement was conducted at the University of California to develop artificial limbs (Eberhart, H and

Inman, V, 1947). This provided the foundational understanding of human motion that led to the development of numerous techniques for quantification and analysis of gait.

Soon after this, in the 1960's and 1970's, the advent of computer processing enabled the production of automated technologies for the measurement and analysis of motion. These simple systems afforded researchers the computational power needed to implement their complex analysis techniques faster and with higher accuracy. More recently, with the rapid evolution of technology and instrumentation, a new generation of advanced 3D Mocap systems has emerged with ever improving resolutions and response times. These technologies offer new opportunities for a diversity of fields. They are increasingly popular in the entertainment industry, where the realism of movie and computer game character motion is improved with human Mocap data. Clinical measurements of motion have also been conducted using Mocap systems for research in the movement sciences. Gait analysis, sports biomechanics and interventions in the physical tasks of factory workers to reduce back pain are but a few examples of the modern clinical applications of Mocap data.

Most Mocap systems track individual bony landmarks on a subject's body and then use some form of digital biomechanical model to reconstruct full-body motion. Current Mocap technologies are primarily differentiated by each system's method of tracking these anatomical points in space. For example, the current gold-standard optical Mocap systems use reflective markers placed on the skin and high-tech cameras positioned around the subject to capture marker movement. However, there are two major constraints for these camera-marker systems. Firstly, skin-based marker systems introduce artefact errors due to the movement of skin over the bony landmarks during locomotion. Secondly, they are generally not very portable and the subject is usually restricted by spatial boundaries. Optical systems are restricted to laboratory use due to the fixed position of the cameras, and since the cameras need to surround the subject there is generally a small recording space (usually a section of a room). These two problems have been addressed in different ways, leading to the development of different technologies (Appendix A.1 gives more background detail on Mocap as well as comparisons of current types of systems on the market).

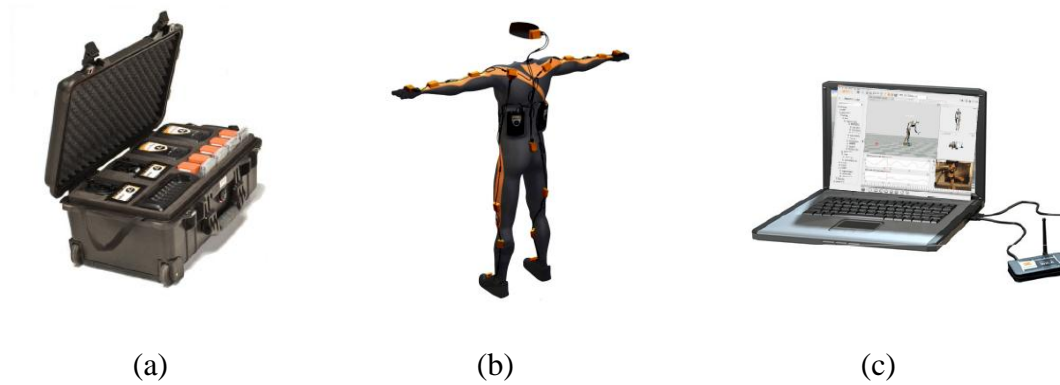
On the one hand, the problem of skin artefacts has produced greater interest in markerless optical Mocap technologies. Markerless systems, which use computer software to automatically locate bony landmarks without anything being attached to the subject, are now recognized by many researchers as the future of numerous

laboratory-based Mocap applications (Mündermann, L *et al.*, 2006). On the other hand, the narrow capture window has always reduced the scope of activities and types of movement analyzed with optical systems. There was thus a need for a more flexible and portable technology which could capture human motion in a variety of environments, uninhibited by camera limitations.

It is a well known fact that inertial sensors, such as accelerometers and gyroscopes, can be used to track motion. However, recent advances in micromachining and the development of microelectromechanical systems (MEMS) have finally made it feasible to measure human kinematics unobtrusively by placing small accelerometers and gyroscopes on different parts of the body (Luinge, H.J, 2002). This has led to the development of, among others, inertial Mocap technology (IMCT). IMCT, like optical systems, makes use of markers that are placed on the subject's body. However, these markers also perform the function of the cameras in optical systems by measuring their own kinematics, thus alleviating the need for external sensors. Each marker is a compact inertial measurement unit which can be tracked wirelessly in 3D space by means of an inertial navigation system and then used to locate the bony landmarks through complex biomechanical modelling. Therefore, IMCT is completely portable and has a theoretically unlimited capture window. It is light and unobtrusive, making it ideal for outdoor kinematic measurement. Furthermore, it is the first portable non-optical system which offers clinical Mocap accuracy.

The Biomedical Engineering Research Group at Stellenbosch University acquired an IMCT system, called the MVN BIOMECH (previously called Moven), in 2006 (Xsens Technologies B.V., Enschede, Netherlands). The first research conducted by BERG with the MVN was an investigation of telemedicine applications for IMCT. This resulted in a gait analysis study where an automated diagnostic tool was successfully implemented for identifying stroke patients using the MVN data and neural networking (Cloete, T, 2008). Using an optical Mocap system as a benchmark, the study also successfully validated the MVN for use in clinical research of gait.

As shown in Figure 1a, the MVN system, can be easily transported in a compact suitcase. It consists of a tight-fitting Lycra bodysuit, which houses 17 inertial MTx sensor units and two wireless transmitters called XBus Masters, as shown in Figure 1b. The inertial sensor data is transmitted wirelessly to two USB receivers connected to a computer (Figure 1c).



(Source: MVN user's manual)

Figure 1: The MVN (a) suitcase (b) Lycra suit and (c) wireless transmitters

Another research field relating to Mocap that is of interest to BERG is sport technologies, which is an emerging field worldwide. The MVN could potentially be used to measure physical technique of athletes for analysis and performance optimization. The portability of the MVN opens up unexplored territory with regard to field-based Mocap in a number of sporting disciplines.

1.2. Primary Objective and Motivation

The primary objective of this study is to evaluate IMCT for use in the analysis and optimization of road cycling kinematics. The first question which might be asked is: why choose road cycling as a case study for sports analysis using IMCT? There are several reasons. Due to the standardized geometry of road bicycles, road cycling technique is to a large extent uniform. It is also fairly regular due to the rhythmical and repetitive nature of pedalling. This makes cycling kinematics easier to optimize. Furthermore, significant gains can be made in performance from small adaptations in body position and pedalling technique in road cycling, which is not the case in all sporting codes. Therefore, the high resolution kinematic measurements offered by the MVN system are most relevant to activities such as cycling where competitive cyclists seek to gain an edge over competitors. Lastly, due to the highly technical approach adopted in road cycling, the level of kinematic research is already fairly developed. This allows for comparisons between experimental results and other studies. Furthermore, the within-day and between-day repeatability and accuracy of the MVN system were previously verified for the lower body kinematics by Cloete (2008), which indicated that the system might be capable to accurately measure

cycling biomechanics. Considering the fact that no other Mocap system exists that can measure outdoor cycling kinematics, and that there is currently no record of data collected for cycling kinematics “on the road”, this study has a strong novel element.

The research work is also motivated by major developments in its three major themes: Mocap, sports science and road cycling. Firstly, the Mocap entertainment industry has experienced a boom since the emergence of portable Mocap systems such as IMCT. According to Ted Price, CEO of highly successful games developer Insomniac Games,

"The flexibility and short turnaround times of the MVN system is unparalleled. With the MVN system, Xsens is changing the rules of the motion capture game: we're saving time and money" (3D Allusions Studio).

On the other hand, traditional optical systems, although constantly improving, have always been extremely expensive, difficult to use and limited to laboratory use. However, the adoption of the significantly cheaper, simpler and portable IMCT is increasing around the world in different fields. For example, the recent blockbuster movies Avatar and Iron Man both used the MVN IMCT system to create the next generation of special effects in entertainment (ICG Magazine; Design News Magazine).

On the other hand, as far as research-grade measurement goes, the MVN system has not yet found wide acceptance within the field of clinical Mocap and is still considered an adolescent technology. However, recent validation studies indicate that the measurement accuracy of the MVN is equivalent to the currently accepted gold-standard Vicon optical systems in a laboratory setting (Cutti, A *et al.*, 2010; Ferrari, A *et al.*, 2010). Nonetheless, wider assessments of the MVN system’s clinical performance are lacking, especially of its field-measurement capability. Considering that the MVN is portable, and that it is currently impossible to accurately measure outdoor kinematics with optical systems, this is a glaring omission. There is thus a need for studies which evaluate the feasibility of valid outdoor measurements using the MVN. Therefore, this study seeks to contribute to the body of knowledge concerning IMCT’s application and performance in clinical research.

One of the most obvious fields which could benefit from clinical outdoor Mocap is sport. However, according to Professor Tim Noakes (2010), world-renowned sports scientist from the Sports Science Institute of South Africa, the sports science

community has been slow in the past to adopt engineering technologies. However, in the last decade there has been a renewed interest worldwide in the applications of technology in sports, which has led to the emergence of the field of sports technology engineering. Global bodies such as the International Sports and Engineering Association and several journals and conferences now represent this distinct field, covering research in everything from measurement devices for analysis of performance to improved materials and design for sporting equipment. Therefore, the use of IMCT for measuring and analyzing sports technique is a typical example of sports technology engineering. This study thus seeks to demonstrate the capability of IMCT to provide sports science researchers and practitioners with novel outdoor kinematic measurements for superior analysis of sports technique.

Thirdly, there have been interesting developments in the road cycling community both worldwide and locally in the last few years. On the international scene, the practise of dynamic bicycle fitting has received increasing exposure and is now widely accepted as superior to traditional static fits. With advances in measurement technology, fitters are able to get more and more detailed and accurate data while the cyclist pedals on a trainer. Now, even Mocap is being used for dynamic fits; many professional cycling teams are using systems such as the Retul to perform analysis of 3D cycling kinematics for improved body positioning on their bicycles (Retul Studios). Similarly, the MVN is an advanced technology which offers more accurate and comprehensive kinematic data than manual static methods or approximations using cinematography, at a much lower price than optical systems. However, the MVN can perform Mocap measurements where other systems (such as Retul) cannot; on the road. MVN field measurements would bring kinematic testing one step closer to the natural setting of road cycling and eliminate the indoor factors which may affect testing realism. Therefore, the MVN system could transform the cutting edge of dynamic bicycle fitting by providing the technology to perform dynamic bicycle fitting on the road with outdoor kinematic measurements.

Locally, road cycling in South Africa is growing both professionally and on the amateur level. South Africa hosts the largest open road race in the world, the Argus, and the Iron Man and Triathlon events are also enjoying increasing numbers. Just recently, Cycling SA (the governing body of cycling in South Africa) unveiled their ambitious plan for cycling called the “2020 vision”, which aims at radically uplifting the sport in the country (Cycling SA, 2010). The impetus behind the “2020 vision” was to boost development and support of both elite and recreational cyclists in South

Africa by, among others, including more national and international events on the South African Tour and improving infrastructure for training and facilities. According to Hendrik Lemmer, director of Cycling South Africa's Road Cycling Commission, South Africa has "*the most active recreational cycling culture in the world*" which is "*growing daily as more people discover the health and fitness benefits of the sport*" (IOL Sport, 2010). Therefore, this research occurs within the context of promising changes in the local cycling community and supports the "2020 vision" goals for South African cycling.

1.3. Problem Statement and Research Questions

The most obvious benefit of the MVN system is outdoor kinematic measurements. Therefore, determining the feasibility of measuring cycling kinematics outdoors with the MVN is of first importance in achieving the research objective. However, it is not certain whether the MVN system can accurately measure the kinematics cyclists out on the road (or even in the laboratory). There are two main reasons for this. Firstly, there is no published case of it ever being done successfully. Secondly, and more critically, the MVN inertial sensors contain magnetometers which make the system sensitive to magnetic disturbances. Therefore, there is a risk of magnetic interference to the MVN system due to ferrous metals in road bicycles. Secondly, since outdoor cycling kinematics has never been measured, the difference between rider kinematics in a traditional research laboratory environment and out on the road has not yet been scientifically investigated. Therefore, it is necessary to determine whether there is a significant difference between indoor and outdoor cycling kinematics. In doing so, it can be established whether or not the MVN outdoor data is novel and of additional value compared to indoor Mocap data recorded with traditional systems. Thirdly, there is also considerable debate as to the optimal body position and pedalling technique for competitive road cyclists due to the anthropometrical and physiological diversity of road cycling athletes. It is therefore important to identify key aspects of road cycling performance optimization that can be addressed with the MVN data.

Therefore, validating the MVN outdoor measurements, assessing the ecological validity of indoor measurements and determining applications of the MVN data for optimization of cycling kinematics are the most relevant research aspects to be addressed in order to fulfil the research objective. As a result, three research questions were formulated for the study:

- Can the MVN be used to obtain field measurements of cycling kinematics?
- Is there a significant difference between cycling kinematics measured on a trainer in a laboratory and on the road?
- How can the MVN be used for improving road cycling kinematics?

1.4. Scope of Work

The following section gives an outline of the study activities as well as the content of this report.

1.4.1. Research activities

The research work was performed in five distinct phases: literature review, preparation, testing, analysis and report writing. The literature review took a period of approximately six months. Books and other literature pertaining to Mocap and road cycling performance were first perused to obtain a thorough grounding in the topics. Next, published journal papers dealing with the MVN system, Mocap systems at large, road cycling kinematics and sports performance optimization were collected and reviewed to gain a deeper understanding of the research field. The preparation stage involved completing an application report for ethical approval for the study, which included (among other things) the formulation of an experimental protocol for the testing phase. Furthermore, signing up of participants for the study was also carried in the preparation stage, which lasted approximately one month.

The testing phase was comprised of an indoor and outdoor stage. The indoor testing was performed first and took place in one of the BERG laboratories at the Department of Mechatronic and Mechanical Engineering. The participants in the study were tested at different times of the day and in no specific order or schedule. Each subject came in for testing at their own convenience. The outdoor tests, which were conducted on an empty tar road outside Stellenbosch, were also performed at the discretion of the participants. The testing took approximately four months to complete. The data analysis phase also lasted approximately four months and consisted of pre-processing of the raw MVN sensor signals, post-processing of the MVN kinematics data as well as basic numerical and statistical analysis of the measurement results. This was carried out primarily in Matlab, although MVN studio and Microsoft Excel were used as well. Finally, the entire reporting process was completed in approximately three months in total. Therefore, the study spanned roughly 18 months in total.

1.4.2. Document outline

Besides the current information chapter, the main body of the report is made up of four chapters. The appendices section consists of a further three auxiliary chapters covering additional work.

Chapter 2 provides an overview of the literature study results. The bulk of the chapter is a comprehensive section on the working principles of the MVN system. There is also a review of the Mocap research conducted in sports performance and an overview of road cycling performance and bicycle fit.

Chapter 3 summarizes the experimental work. Herein are presented the details of the test methodology and protocols for the indoor and outdoor tests. There is also a short explanation as to the processing of the measurement data in MVN Studio and Matlab before the analysis.

Chapter 4 is the central chapter in the document covering the data analysis. It is divided into three sections, each corresponding to one of the research questions. The first section reports the findings from an evaluation of the feasibility of measuring outdoor road cycling kinematics using the MVN. This is followed by a comparison of the indoor and outdoor kinematics measurements to investigate the ecological validity of laboratory cycling. The chapter finishes with a demonstration of ways in which the MVN data can be used to analyze and improve road cycling kinematics.

Chapter 5 closes the study with a discussion of the research outcomes. It addresses the conclusions drawn from the experimental results in answer to the research questions, practical insights gained for future testing with the MVN system, recommendations for future road cycling research and the broader implications of the study in the fields of Mocap, sports science and road cycling research.

The appendices contain supplementary research reviews on secondary aspects of the study, as well as the bulk of the technical work. The appendix covering theoretical work consists of background information gathered on motion capture and road cycling. The experimental section covers details concerning the technical specifications of the MVN and other test apparatus. Finally, the appendix chapter on analysis presents details on the Matlab data management and programming.

2. LITERATURE STUDY

This chapter presents the results of a literature study performed on the two main focus areas of the study: the MVN BIOMECH Mocap (Mocap) system and road cycling kinematics. The first section contains a thorough description of the working principles of the MVN, from the raw sensor data through to full-body kinematics. The second section contains a review of the research conducted in sports with Mocap systems and in cycling kinematics.

2.1. The MVN BIOMECH System

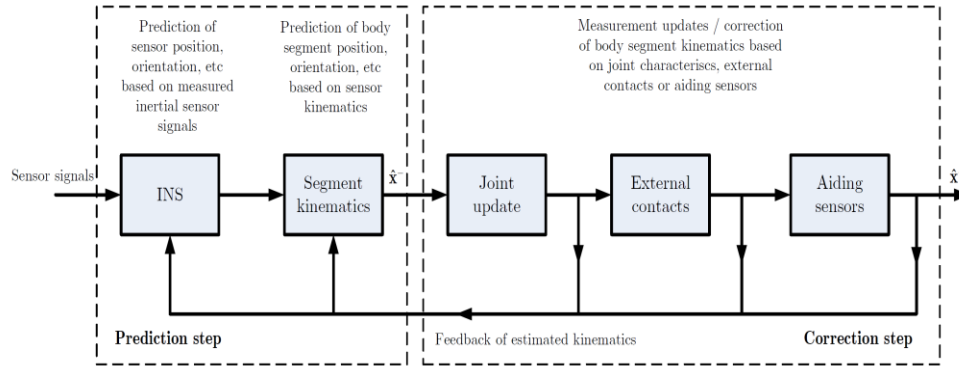
This section gives a detailed overview of the MVN BIOMECH, beginning with the overarching sensor fusion scheme. It then describes the signal inputs and mathematical background of the inertial navigation system used for marker tracking, the biomechanical model used to convert the sensor data to a digital full-body model and the various steps taken to eliminate errors in the measured kinematics.

2.1.1. Sensor fusion scheme overview

Sensor fusion is a technique used to combine sensor signals in such a way that measurements from one sensor are used to overcome the limitations of another. In other words, it is the synthesis of multiple data signals in order to obtain a more accurate or thorough model of an observed system (Welch, G and Bishop, G, 2001). The MVN BIOMECH system uses a sensor fusion scheme (Figure 2) to overcome the traditional weaknesses of inertial sensing (such as sensor drift) and combines the multiple sensor signals from each inertial unit to estimate full body kinematics. There are two main steps in the sensor fusion scheme: prediction and correction. In the prediction step, raw inertial sensor signals are received, interpreted eventually used to estimate the kinematics of the subject. This is followed by the correction step, where various measures are taken to identify and eliminate errors in the predicted kinematics.

The first part of the prediction step involves the tracking of individual inertial sensors that are placed as markers on the body. This is accomplished by means of an inertial navigation system (INS), which transforms the sensor signals into full three-degree-of-freedom (3DOF) motion data for each marker. The kinematics data of the sensors is then fed into the MVN biomechanical model to be converted into individual segment kinematics, which are then assembled together to form an anatomical model.

Once the prediction step is complete, the estimated body model is corrected for inaccuracies in joint centre location and global position using biomechanical constraints based on joint characteristics and external contacts. The third option shown in the correction step, namely aiding sensors (such as a GPS system), was not used during the research and will not be discussed.



(Source: (Roetenberg, D *et al.*, 2009))

Figure 2: MVN sensor fusion scheme

2.1.2. Inertial navigation system

The prediction step in the sensor fusion scheme begins with the sensor signals being input into an INS. An INS is a computer-controlled system which uses input from inertial sensors (accelerometers and gyroscopes), to continuously calculate the absolute position and orientation of an object in 3D space without external references. Usually, aiding systems are used to gain global measurements. In the MVN system, this is done with the magnetometers. INSs are used extensively to monitor and control moving vessels such as military aircraft, ballistic missiles and naval ships.

The sensor signals which are input to the INS come from small inertial measurement units (IMUs), called MTxs (see Figure 3), which are each placed on the most important segments of the test subject's body (one per segment). Each MTx contains integrated micro-electromechanical systems (MEMS) sensors that provide full 3DOF motion measurements. Each MTx contains a 3D accelerometer, gyroscope and magnetometer (Roetenberg, D, 2006) and the axes of these sensors are aligned to a common triaxial MTx coordinate system. For an overview of the three different types of MEMS inertial sensors used in the MVN MTxs and their working principles, see Appendix A.2.



(Source: MVN user's manual)

Figure 3: MVN MTx module containing MEMS sensors

The basic method used by an INS to predict position and orientation in the next time step is dead reckoning. Dead reckoning, in this context, refers to the prediction of current position and orientation using prior measurements and the laws of motion. This is done for each MTx on the body using its accelerometer and gyroscope signals. Linear position and velocity are obtained through double-integration and integration of the linear acceleration data. Similarly, angular position and acceleration are obtained by integration and differentiation of the angular velocity respectively. In this way, each MTx sensor can be used to calculate its own 3DOF kinematics at every time step. However, one of the problems with dead reckoning is the sensor drift error which occurs due to integration, leading to inaccurate orientation and position estimation. Positional drift due to accelerometer errors is corrected later in the segment kinematics correction step of the sensor fusion scheme (Section 2.1.4). However, gyroscope errors are dealt with in the INS using an error-state Kalman filter. The sensor input signals are described in the Kalman filter with Equations 1-3.

$$y_A = a_t - g_t + v_t \quad (1)$$

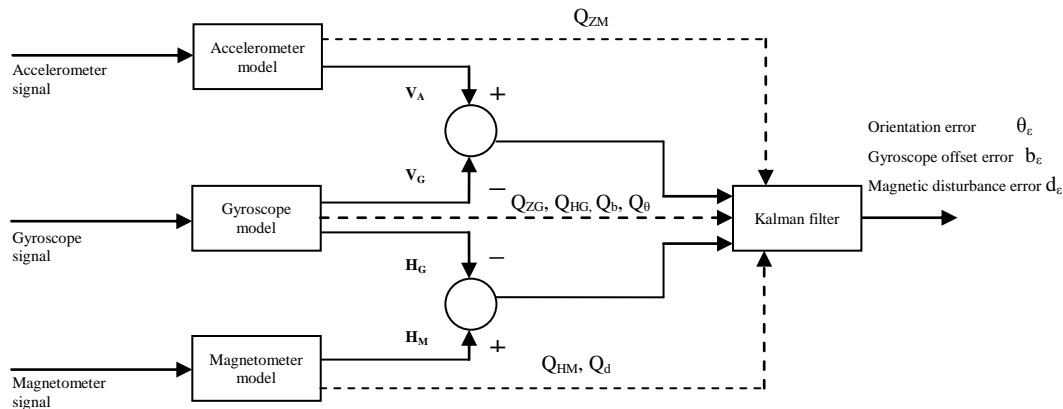
$$y_G = \omega_t + b_t + v_t \quad (2)$$

$$y_M = m_t + d_t + v_t \quad (3)$$

Where y_A , y_G and y_M are the accelerometer, gyroscope and magnetometer signals, a_t , ω_t and m_t are the measurable phenomena and v_t is a white noise term. The terms g_t , b_t and d_t represent gravitational acceleration, gyroscope error and magnetic disturbance error respectively. Even low values for b_t in the gyroscope measurements in Equation 2 due to temperature effects are compounded through integration and become extremely large after a few seconds. The error-state Kalman filter, also called a complementary filter, contains a gyroscope prediction model which estimates (using dead reckoning) the system state (angular data for the next time step), using

knowledge of the previous state (current time step) and state system properties (the angular laws of motion etc.). At the next time step, the estimated state is compared to the state measured by the sensor measurements. The filter then uses an error model to estimate the errors in the gyroscope measurement, as well as in the accelerometer and magnetometer, based on sensor signal characteristics and knowledge of their probable errors. It also estimates the errors in the prediction model and then makes a better estimate by weighting the trust it places in the measured and estimated state in the Kalman equations.

The errors in the angular data are also drastically reduced using sensor fusion. The Kalman filter compares the accelerometer and magnetometer sensor signals with the gyroscope signals for its estimation and then compensates for the orientation drift error. Due to its gravitational vector g_t , the accelerometer can be used as an inclinometer (finding down) to provide stability for rotations in the vertical plane. Furthermore, stability of the gyroscope orientation in the horizontal plane is improved by using the heading data from the magnetometer like a compass (finding north). In this way, accurate drift-free orientation can be obtained for the MTx inertial sensors.



(Source: (Roetenberg, D, 2006))

Figure 4: Kalman filter error model for eliminating gyroscope drift error

Figure 4 shows how the inclination estimate from the accelerometer, V_A , is used to correct drift error in the vertical plane of the gyroscope reading V_G . Similarly, the magnetometer heading estimate, H_M , compensates for drift in the horizontal plane of the gyroscope measurement, H_G . The error model also contains the error covariance matrices for these sensor readings, namely Q_{ZA} , Q_{ZG} , Q_{HM} and i . The differences

between the sensor estimates are output as a function of the orientation error θ_e , gyroscope offset b_e , and magnetic disturbance vector, d_e . These predictions are weighted using the related covariance matrices Q_θ , Q_b and Q_d .

The Kalman filter also needs to deal with errors occurring in the magnetometer signal y_M when ferrous materials distort the local Earth's magnetic field. There are three types of magnetic disturbances: permanent-constant distortion (for example attaching an MTx to a steel prosthesis), temporary-constant distortion (such as when passing by an audio speaker) and permanent-varying distortion (like when walking above steel underground piping). The magnetic disturbance vector, d_t (see Equation 3 as well as Figure 4), is used to quantify distortions relative to changes in the local magnetic flux and dip angle (Roetenberg, D *et al.*, 2003).

With permanent-constant distortions, the disturbance can be mapped *a priori* as a system error using initial values for d_t (Monaghan, C, 2010). During temporary-constant distortions, when the disturbance d_t is large, the Kalman filter lowers the weighting on the magnetometer signal and relies more on the gyroscope and accelerometer signals for estimating orientation, thus rejecting the disturbance. However, this can only be sustained for short periods (<30s). Tests have shown that this compensation technique can reduce body segment orientation errors from up to 50° (uncompensated) to 3.6° RMS (Roetenberg, D *et al.*, 2007). Permanent-varying distortions are the most difficult disturbance to deal with and cannot be handled with sensor fusion. Rather, the segment kinematics is calculated with a technique called Kinematic Coupling (KiC). KiC relies on the fact that certain adjacent joints have similar planes of rotation and a predictable relationship due to their sharing of body segments. Therefore, joint rotations can be calculated without magnetometers, although Kinetic Coupling is only currently available for the lower limbs in the MVN BIOMECH (Monaghan, C, 2010). This is a significant point which was central to the kinematic analysis in Chapter 4.

It should also be noted that the filter utilizes quaternion vector mathematics to describe the sensor signals in the Kalman equations. Unit quaternion matrices provide a convenient notation for representing the translation and rotation of rigid bodies in 3D space. A quaternion vector contains a real number and an expansion of the complex component into three dimensions such that,

$$q = w + xi + yj + zk \quad (4)$$

Where q is a quaternion vector, w is the real component and x, y and z are the imaginary components. Although difficult to visualize due to the fourth dimension, quaternion representations have an advantage over traditional Euler notation in that they avoid the singularity points associated with having only three degrees of freedom. These singularities cause what is called gimbal lock, which is effectively the loss of one degree of freedom in the system, resulting in mathematical anomalies near 90° . Since quaternion notation removes this potential problem in tracking the sensors, and offers faster transformations than other methods, this form of notation was chosen by the MVN developers over Euler angles for describing the MTx kinematics.

As mentioned previously, the 3D rate gyroscope on each MTx measures angular velocity ω , which can be integrated over time to provide the change of angle from an initially known angle in the global frame (G). Therefore, the rate of change in orientation of a sensor (S) with respect to G can be represented in quaternion form such as in Equation 5.

$${}^{GS}\dot{q}_t = \frac{1}{2} {}^{GS}q_t \otimes \Omega_t \quad (5)$$

where ${}^{GS}q_t$ is the quaternion describing the rotation from S to G at time t , $\Omega_t = (0, \omega_x, \omega_y, \omega_z)^T$ is the quaternion of the angular velocity ω_t and \otimes is a quaternion multiplication. In the case of the accelerometer data, which contains vectors for linear acceleration a_t and gravitation acceleration g in sensor coordinates, the sensor signals can be expressed in the global frame as in Equation 6.

$${}^G a_t - {}^G g = {}^{GS}q_t \otimes ({}^S a_t - {}^S g) \otimes {}^{GS}q_t^* \quad (6)$$

where q_t^* is the complex conjugate of q_t . Once the gravitational component has been removed the acceleration a_t can be integrated once to get the velocity v_t and twice to get the position p_t (Equation 7).

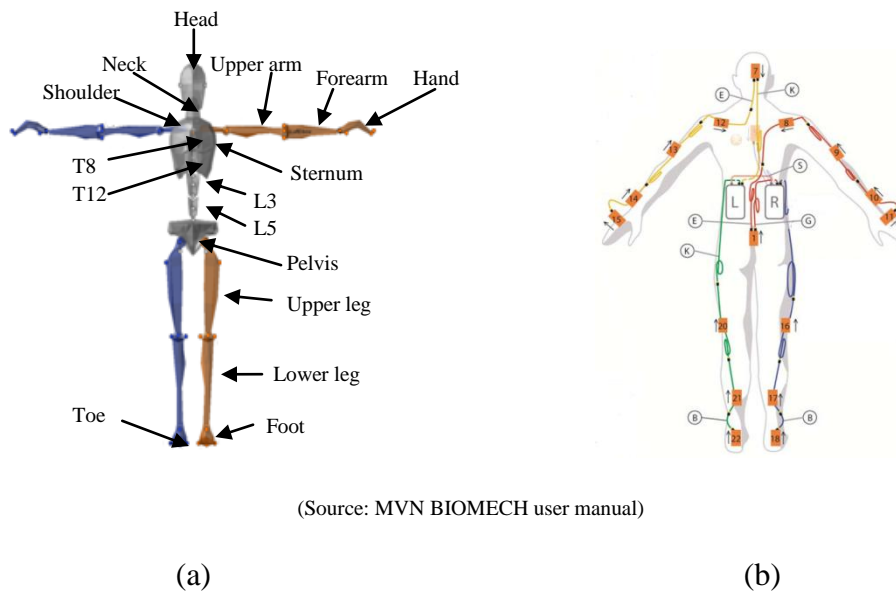
$${}^G \ddot{p}_t = {}^G a_t \quad (7)$$

In conclusion, the INS in the prediction step of the sensor fusion scheme transforms the raw accelerometer, gyroscope and magnetometer signals into full 3DOF kinematics for each MTx sensor module placed on the subject's body. The Kalman filter uses the accelerometers and magnetometers to overcome drift error in the gyroscope measurements, and the accelerometer and gyroscope signals to compensate

for short magnetic disturbance errors in the magnetometers. However, for longer term disturbances, the KiC algorithm can be used, although it is still limited to hip, knee and ankle flexion. The following step is to predict segment kinematics using the MTx tracking data.

2.1.3. Segment kinematics

This section describes the second part of the prediction step in the MVN sensor fusion scheme: the estimation of body segment kinematics from the sensor data. The INS tracking data contains the 3 degrees of freedom (DOF) kinematics of each MTx, which represents the kinematics of the segment to which it is attached. The MVN system uses a biomechanical model to define individual segment motion, assemble the body segments and then accurately perform tracking of the subject. The following subsection contains further information regarding the body segments, joints and joint angle conventions, set-up calibrations and calculations used for the data transformations.



(Source: MVN BIOMECH user manual)

Figure 5: MVN model consisting of (a) 23 segments tracked by (b) 17 MTxs

The biomechanical model consists of 23 body segments, although only 17 MTxs are placed on the body. Each MTx is assigned and fixed to a strategic body segment as shown in Figure 5b. Kinematics of those segments that do not have a sensor attached, primarily along the spine (T8, T12, L3, L5 as well as the shoulders, Figure 5a), are computed with an advanced spine and shoulders model using the kinematics from the

rest of the biomechanical model and known stiffness parameters between connecting segments (Roetenberg, D *et al.*, 2009). The biomechanical model also consists of 22 joints which connect the 23 body segments together. It is important for the interpretation of the Mocap output data to understand the way in which these joint angles are defined. Therefore, the conventions that were followed for the anatomical position of joint centres and the definition of coordinate systems used for the different joint axes are discussed below.

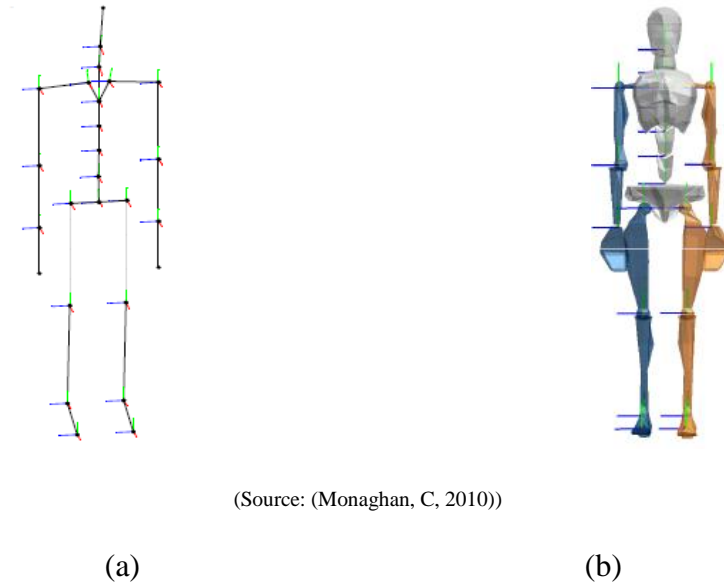
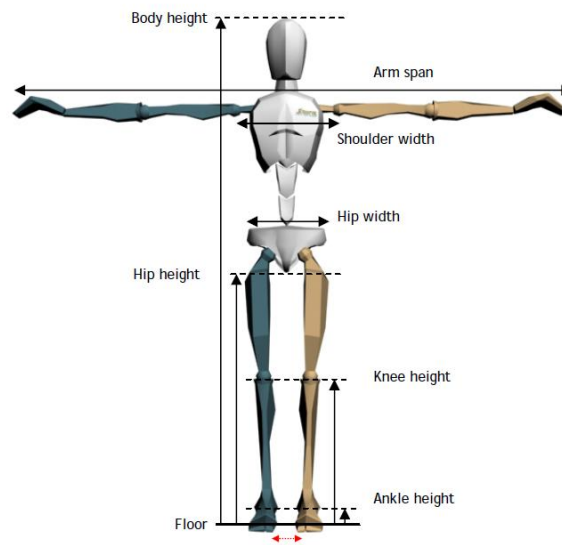


Figure 6: The (a) rigged skeleton and (b) XYZ coordinate system conventions

The MVN biomechanical model is based on the standards for joint rotations sequences as set out by the International Society for Biomechanics (ISB) (Monaghan, C, 2010). However, there are differences in some conventions due to various inconvenient ISB definitions. For instance, the ISB standards prescribe joint centres with segment origins that are sometimes defined proximally and other times distally, which is less suitable for IMCT than for optical Mocap. Furthermore, ISB standards stipulate some axes of rotation (such as the ankle joints), which do not run along the bone of the segment. This causes difficulties for inertial systems that predict joint centres from segment position. Moreover, the sequence of the x-, y- and z-axes is not the same for all joints. These issues have been resolved by choosing joint conventions which suit IMC calculations, as described below.

For simplicity, the same conventions have been chosen for all segments and joints. Origins of rotation are defined as being in the proximal joint centre for all segments, such that the biomechanical model is in the form of a rigged skeleton (Figure 6a). Furthermore, a right-hand coordinate system has been preferred to the ISB recommendation of a left-hand convention for the left side. The X-axis is positive in the posterior direction, the positive Y-axis is chosen as up and the Z-axis is positive laterally for the right side and medially for the left side (Figure 6b). An XYZ Euler extraction (from the quaternion matrices) for the lower body joints is used when Y is up, whereas this varies for the upper body. This is due to mathematical formulations, especially in the shoulder, relating to gimbal lock errors. The solution is to provide XZY and ZXY extractions, although some complex movements will still present problems (Monaghan, C, 2010).

In order to track the motion of a specific subject accurately, the model needs to be calibrated. This includes scaling the anatomical dimensions of the model to represent the subject and performing calibration poses to determine the initial sensor-to-segment orientation. The dimensions of the body model are defined by anthropometrical values for each segment. The scaling values which can be inputted are shown in Figure 7.

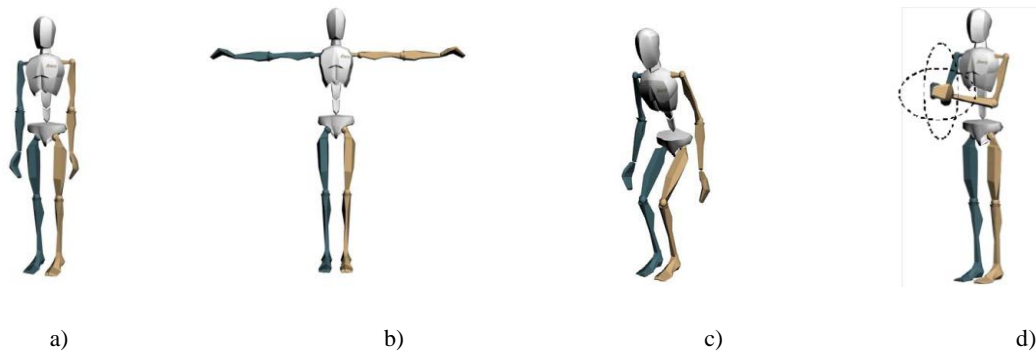


(Source: MVN user's manual)

Figure 7: Anthropometry values used for MVN biomechanical model

These dimensions can be measured and then entered individually for a test subject if high accuracy is required. However, only the subject's height and foot-size are mandatory inputs. If the others are left out, they are approximated by anthropometrical models and regression equations (Roetenberg, D *et al.*, 2009).

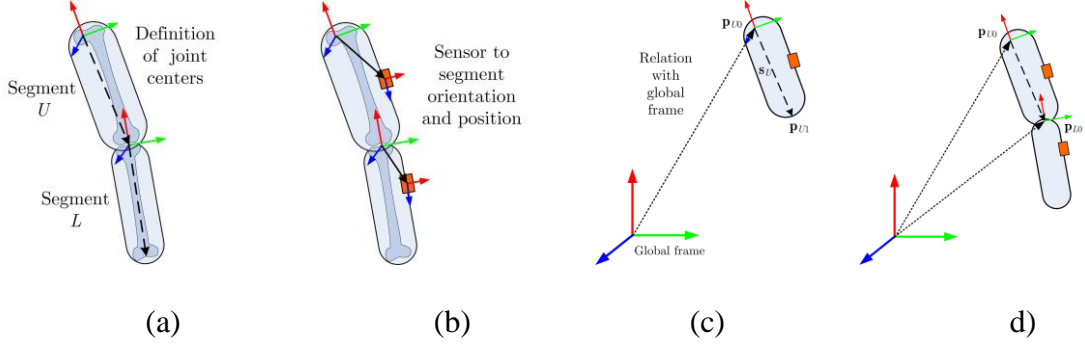
Once the MVN system is running, a calibration procedure must be performed before recording. The calibration phase involves the subject taking at least one of four predetermined poses. These are illustrated in Figure 8. Two are stationary; the neutral (N) pose and the T-position (T) pose, and two require a standard motion; squat and rotating hand-touch. The stationary calibrations are used to determine the orientation of the MTxs relative to known body segments orientations so that the biomechanical model can be accurately rendered from the INS data. The moving poses are used to improve accuracy around the functional axes of the legs and arms (Roetenberg, D *et al.*, 2009).



(Source: MVN user's manual)

Figure 8: a) Neutral b) T-position- c) squat and d) hand-touch calibrations

The conversion of MTx INS data to body segment kinematics for the biomechanical model is illustrated in Figure 9. The first step (Figure 9a), relates to the estimation of segment lengths based on anthropometrical values input into the MVN software during calibration. Next, the joint centres are estimated, as previously mentioned, at the proximal end of each segment. After this, the biomechanical model is functional but as yet not accurate. The following step involves the calibration poses described earlier.



(Source: (Roetenberg, D *et al.*, 2009))

Figure 9: Calculation sequence for estimation of segment kinematics

It has been mentioned that the calibration poses are used to determine the unknown orientation of the sensors relative to the known orientation of the body segments in the poses. Figure 9b shows how the sensor-to-segment alignment ${}^{BS}q_t$ can be determined by the global position of the sensor ${}^{GS}q_t$ relative to body segments that are at a known position or orientation ${}^{GB}q_t$ (as in Figure 8). The following quaternion multiplication in Equation 8 is used.

$${}^{GB}\dot{q}_t = {}^{GS}q_t \otimes {}^{BS}q_t^* \quad (8)$$

Once the calibration is completed a Mocap recording may be taken. This requires the now accurate biomechanical model to be continuously updated using the MTx tracking data from the INS. The conversion of the INS data to segment kinematics is carried out in the global frame as shown in Figure 9c. When the position p_{U0} of the joint origin, the orientation ${}^{GB}q_U$ and the length s_U of segment U are known, the position ${}^G p_{U1}$ can be calculated using the Equation 9.

$${}^G p_{U1} = {}^G p_{U0} + {}^{GB}q_U \otimes {}^B s_U \otimes {}^{GB}q_U^* \quad (9)$$

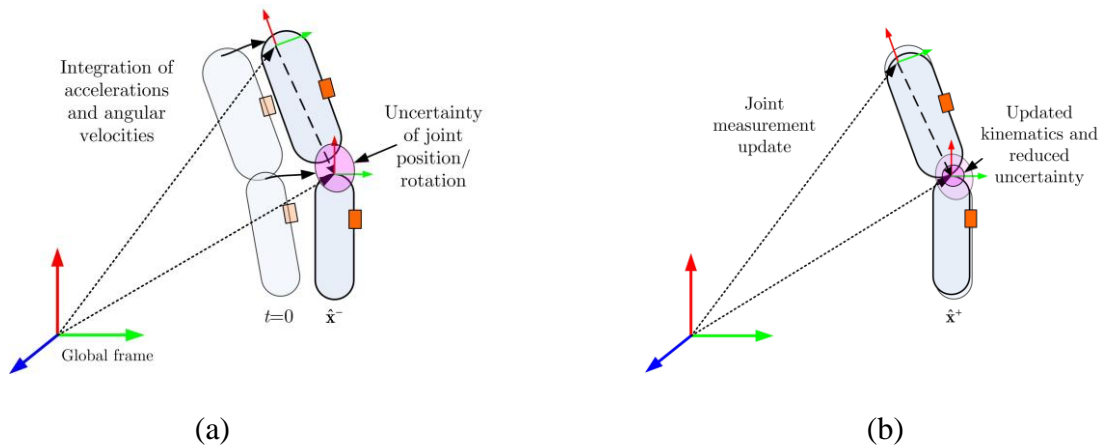
The segment lengths ${}^B s_U$ are derived from the anthropometric database using regression equations and calibration values. Original global positions ${}^G p_{U0}$ are assumed at the initial assumed contact points. Finally, magnetometers measure the segment orientation ${}^{GB}q_U^*$ relative to the global magnetic field. Accurately determining the position of the joint centres and the orientation of the connecting segments about them is critical to the accuracy of the biomechanical model. The calibration ensures that the segments are linked at the joint centres with the correct

orientation and with the position in the global frame defined accurately. Thus, a realistic model of the body motion can be assembled, complete with segment and joint kinematics, using the INS tracking data.

2.1.4. Joint updates and contact points

The major measurement challenges in the MVN system are accelerometer and gyroscope drift and magnetic interference. It was shown in Section 2.1.2 how the INS Kalman filter deals with orientation drift and magnetic disturbances using sensor fusion. However, the MTxs, and therefore the individual body segments, also experience drift errors in linear position which causes uncertainty about the joint centre position (Figure 10). Furthermore, the biomechanical model as a whole also experiences translational drift in the global frame due to a lack of external references. These two problems are compensated for in the correction step of the MVN sensor fusion scheme using methods called joint updates, and contact points, respectively.

Joint updates form an integral part of correcting each prediction step by reducing kinematic errors between segments. The position and rotation of joints become less and less certain with each time step due to cumulative sensor noise and movement related uncertainties such as skin artifacts.



(Source: (Roetenberg, D *et al.*, 2009))

Figure 10: Joint centre uncertainty (a) before and (b) after joint updates

It is therefore necessary to continuously update joint positions and orientations to limit the uncertainty. As with the gyroscope drift, a Kalman filter is used for the joint update algorithm. However, instead of using sensor fusion, the filter makes use of

biomechanical constraints in the body model to compensate for measurement inaccuracy. Although the methods employed to achieve this are beyond the scope of this thesis, a brief overview of the joint position update will be presented. For example, a linearized function can be used to define the joint position measurement y_t in terms of a joint state x_t , a measurement matrix C and a noise component w_t , as shown in Equation 10 below.

$$y_t = Cx_t + w_t \quad (10)$$

The Kalman filter prevents the joint position measurement from accumulating noise and errors by predicting the state for the next time step and then updating it after the measurement. The Kalman gain K , as shown in Equation 11, is used to weight the likelihoods of the predicted and measured joint position. This is achieved using stochastic parameters associated with the propagation of errors caused by integration errors and sensor noise as well as known joint position constraints respectively. In this way, the filter corrects unrealistic measurements (caused by positional drift) at each time step. Thus, with the Kalman filter update, cumulative sensor drift and joint position uncertainty are greatly reduced.

$$x_t^+ = Cx_t + K(y_t - Cx_t^-) \quad (11)$$

As with all skin-based marker systems, skin and soft-tissue artifacts do influence the accuracy of the measurements. This is because the MTx sensors are assumed to be in fixed positions relative to bony landmarks on the body. To overcome this, the fusion scheme rejects unlikely joint angles and position, such as unreasonably large abduction of the knee joint, based on known statistical uncertainties. Each joint is specified by statistical parameters for six-degrees-of-freedom joint laxity.

Secondly, since all the segments experience some drift in the same direction, the assembled model is also subject to boundless integration errors in the global frame. Therefore, the global position of the human model also requires correction. This is accomplished in the correction step of the sensor fusion scheme by the detection of the contact points of the test subject with the external world (for example feet on the ground). The sensor fusion scheme assumes that the body is in contact with the external world and subject to gravity. The probability of the location of these contact points is computed from the kinematics (in this case velocity and position) of various critical body parts. The default contact point setting in the MVN software is based on the assumption that the lowest contact points are the floor. Therefore, as the person in

the suit moves the contact points are constantly recalculated and updated. All segment corrections in the sensor fusion scheme implicitly make use of the contact points to render realistic motion and limit positional drift error. There are also other settings for seated testing where the pelvis is assumed to be fixed, which was used for the cycling tests presented in this thesis.

2.2. Research Review

This section reviews the published validation work performed with the MVN, implementations of Mocap technology in the field of sports research and an overview of bicycle fit and studies in the ecological validity of laboratory cycling.

2.2.1. Validations of Xsens Mocap technology

Although IMCT is still a relatively adolescent technology, successful validations of these systems are now emerging. Significantly, some of these studies have compared the performance of the MVN system used in this study to that of the “golden standard” Vicon (Oxford Metrics Ltd.) optical system. For example, the accuracy of Xsens accelerometers has been investigated for simplified movements of individual body segments (Thies, S.B *et al.*, 2007). The results of these linear acceleration tests for the upper and lower arm segments showed strong correlations between the optical and inertial measurements. Correlation coefficients of 0.988, 0.997 and 0.947 (upper arm) and 0.999, 0.991 and 0.988 (lower arm) were reported for predefined X, Y and Z directions respectively. This shows that Xsens inertial sensors can be substituted for Vicon cameras when used to measure segmental linear accelerations, which are a crucial aspect of full body IMC systems.

However, in order to validate the Xsens biomechanical model, the correlation between multi-segment measurements such as joint angles is needed. Significantly, a recent study has suggested that Xsens IMC in fact outperforms the Vicon in terms of reliability in measurements of thorax-pelvis and lower-limb 3D kinematics (Cutti, A *et al.*, 2010). A complementary study (Ferrari, A *et al.*, 2010) also reported very good interchangeability between the joint angle measurements of both systems (coefficient of multiple correlation > 0.85 for all joints). The results of these studies confirm that Xsens Mocap is both accurate and reliable enough for clinical studies, as well as on par with the “golden standard” Vicon system. Although these studies were conducted specifically to validate Xsens IMCT for clinical gait analysis, they do suggest that

kinematics data measured using inertial systems such as the MVN BIOMECH used in this study could be as valid for sports performance analysis.

2.2.2. Sports performance research using Mocap

Mocap assessment of individual athletes has significant benefits for the analysis and optimization of sports performance. It provides kinematic measurements of the whole athlete's body more quickly, thoroughly and objectively than traditional methods. Manual observations are highly subjective and can only be carried out from a single perspective at a time. Similarly, goniometer measurements are subject to significant errors and also often require the athlete to be stationary which is, of course, unrealistic. Mocap data, on the other hand, is captured dynamically in 3D and can be represented visually with a digital avatar for reviews. Unlike video analysis, the data is accurate and inherently quantitative which also allows for further objective and in-depth analysis. Therefore, Mocap offers deeper insight into an athlete's technique and how it can be changed to improve performance and reduce injuries. Furthermore, Mocap systems can be synchronized with other measurement devices such as force sensors and electromyography instruments. In this way, the athlete's kinetics and muscle activation patterns can be analyzed relative to body position more accurately.

Numerous sports-related studies have been conducted using the optical Vicon Mocap systems. These include analysis of high-speed sports movements such as side-stepping (Lloyd, D and Rubenson, J, 2008) and jumping (Tokuyamaa, M *et al.*, 2005), as well as slow repetitive motions such as running on a treadmill (Schache, A *et al.*, 2002). Research has also been conducted on sport-specific movements such as cricket bowling (Elliot, B *et al.*, 2007), tennis serving (Ahmad, A *et al.*, 2009) and handbike pedalling (Faupin, A and Gorce, P, 2008). Furthermore, Vicon systems have been used to investigate sports technique in order to reduce injuries, such as to the knee joint in basketball (Louw, Q *et al.*, 2006).

Sports performance research has also been conducted using other optical Mocap systems. Volleyball spike jumps (Chung, C.S, 1989) and standing long jump (Ashby, B and Heegaard, J, 2002) were analyzed using video data and 3D motion analysis respectively in order to understand the effect of arm motion on performance. Furthermore, optimization of segment-interaction in sprint starts was carried out using opto-electronic motion analysis (Slawinski, J *et al.*, 2010). However, the current research is limited to analysis of quasi-stationary or isolated sports movements. This is due to the relatively small capture area of optical systems since the cameras need to

be placed all around the subject and have fixed positions. This also means that optical Mocap is constrained to laboratory testing. Therefore, the opportunities for realistic field-testing of numerous sports using optical Mocap are restricted.

In fact, the lack of portability and insufficient capture area are two of the main reasons why alternative technologies such as IMCT have emerged strongly in the Mocap industry, providing mobile Mocap that can be used almost anywhere. This is illustrated by the fact that inertial sensors have been used in non-commercial IMCT setups for research in the biomechanics of alpine skiing (Brodie, M *et al.*, 2008), something which would be impossible using optical Mocap. The inertial data was used to improve race performance by optimizing skiing technique. Other successful sports performance research using IMCT has also included analysis of high-speed limb movements in baseball pitching (Lapinski, M *et al.*, 2009) and wrist rotation in golf swinging (Ghasemzadeh, H *et al.*, 2009), as well of ankle joint kinematics for the prevention of ankle sprain injuries (Chan, Y *et al.*, 2010). It can therefore be seen that setups with a few inertial sensors attached to the body have been successfully implemented in a number of sports analysis studies. Therefore, IMCT is emerging as a viable alternative to optical Mocap systems in sports performance analysis, especially since it can be used outdoors for field testing. However, there is currently no published work available documenting the use of full-body IMCT, of which the MVN BIOMECH is the only current system, for sports analysis.

2.2.3. The ecological validity of laboratory cycling

Researchers in the applied sports sciences often make recommendations to athletes based on studies conducted in laboratories. Therefore, the authority of these research findings is based upon the ecological validity of laboratory testing. However, due to differences in field and laboratory environments, the assumption of ecological validity is not always valid. An example of this is found in assessments of running using a treadmill. It was found that due to the lack of wind resistance, a 1% treadmill incline most accurately reflected the energetic cost of outdoor running (Jones, A and Doust, J, 1996). Similarly, studies in road cycling have found significant differences in time-trial performance of up to 8% when testing in laboratories and on the road (Jobson, S.A *et al.*, 2008). The need for understanding the factors causing these differences is highlighted in the following comment made in a recent review of cycling research:

“The relationship between performance in tests and performance in cycling competition has not been explored adequately. The question remains, how a change in performance in a cycling laboratory test translates into a change in performance in the actual competitive setting” (Faria, E.W et al., 2005a)

The simulated testing environment of a laboratory and indoor stationary trainer results in certain limitations in terms of realism. Most significantly, there is no air resistance or physical inertia when testing indoors. Moreover, lateral motion of the bicycle and athlete are also reduced due to the rigid wheel fixtures which may potentially affect the cyclist’s technique. Furthermore, it is possible that even the psychological effect of these factors on the athlete may alter performance. However, as previously mentioned, further research is still required to understand these effects. Two recent studies by Jobson investigated the effect of body size (Jobson, S.A *et al.*, 2007) and position (Jobson, S.A *et al.*, 2008) on the ecological validity of laboratory cycling. The results suggest that body size is a factor in the ecological validity of indoor testing, while body position is not. However, due to the absence of outdoor measurements of cycling kinematics, the correlation between pedalling technique on a trainer and on the road has not been scientifically established. For these reasons the comparison of indoor and outdoor body position is relevant to studies on the ecological validity of laboratory cycling.

2.2.4. Cycling kinematics and bicycle fit

Road cycling kinematics are optimal when the aerodynamic and biomechanical efficiency of the body position and pedalling technique are at a maximum and risk of injury and discomfort are at a minimum (details on optimal cycling kinematics are given in Appendix A.3.1). Therefore, as far as is possible the optimal body position of the cyclist should be accommodated by the bicycle geometry (Figure 11). This is called bicycle fit. Bicycle fit is primarily concerned with the three points of contact between the cyclist and the bicycle: the shoe-cleat-pedals, the pelvis-saddle and hands-handlebars interfaces (Silberman, M.R *et al.*, 2005). The correct spacing of these interfaces results in the optimal combination of comfort and performance, simultaneously reducing overuse injuries (Burke, E.R, 2003).

In his review of current bicycle fit methodology, Silberman (2005) describes two evaluations: static fit and dynamic fit. Static bicycle fitting is the easiest and most common approach to bicycle fit and has been practised for many decades. It is typically conducted using basic anthropometrical measurements of the cyclist and

mathematic formulas to estimate bicycle fit parameters such as seat height. Other guidelines are also often prescribed for the athlete when seated in specific stationary positions on the bicycle, such as the alignment of certain body parts and points on the bicycle at specific crank angles. A static fit is a useful tool for road cyclists. It is a good way to obtain “ball park” figures for the geometry of the bicycle and is often used as the first step in bicycle fitting. However, it is also a very limited tool due to the inadequate information which is considered (only body dimensions). Predicting optimal bicycle fit using anthropometry ignores the complex interdependencies between the cyclists physiology and suggests that all cyclists with the same basic anthropometry produce cycling power in the exactly the same way. In other words, static fits assume that optimal kinematics occurs at specific joint angles, which is debatable (Appendix A.3.2 gives details on common bicycle fit principles).

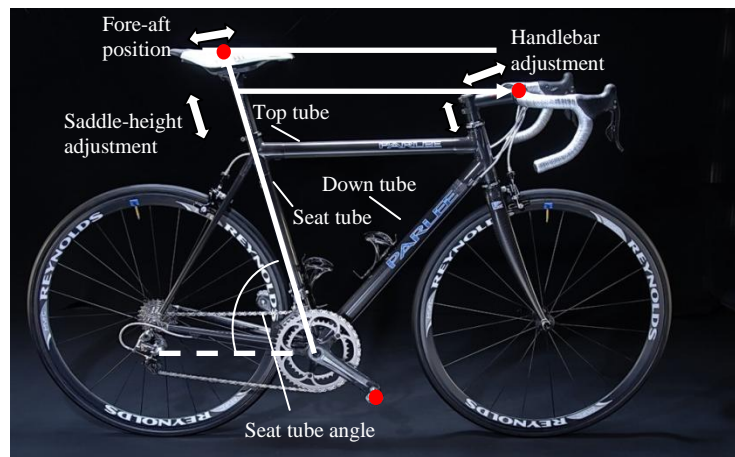


Figure 11: Basic bicycle fit parameters

For instance, it has been suggested by various authors that muscle activation patterns should be taken into consideration during bicycle fitting when optimizing trends in power delivery and fatigue (Chapman, A.R *et al.*, 2008; Egana, M *et al.*, 2009). Therefore, it is necessary to take the role of muscle activity around the pedal stroke into account. The bulk of the cycling power is generated during hip and knee extension (on the downstroke), and primarily by the gluteus maximus and quadriceps respectively. The muscles involved in the upstroke include the hip flexors, particularly those from the anterior thigh and inner hip, and the hamstrings, which act as knee flexors. These leg muscles activate at specific points on the pedal stroke, and their length-tension relationships determine the amount of power exerted at specific

joint angles. Since muscle fibre composition, size and length are highly subject specific, it is highly improbable that power delivery can be optimized by generalized static fit methods which specify joint angles. Furthermore, although some of these static fit principles are sound and universally accepted, there remains a measure of contention around how to calculate the bicycle fit parameters which is caused by the complexity and diversity of performance factors and cyclist physiology.

Another weakness of static fits is that they do not take the effect of the dynamics of pedalling on cycling kinematics and performance into account. However, one study conducted on the effect of force on knee kinetics and kinematics during cycling found that knee flexion was 5-6° higher during dynamic measurement than the static calibration values used for determining seat height (Farrell, K.C *et al.*, 2003). This considerable difference in joint angle was found to be due to lateral pelvic tilt during pedalling. Therefore, static fit methods are also ineffective in that they are unable to compensate for the variable changes in cycling kinematics from static measurements due to the diversity in joint ligament stiffness, ankle movement and misalignment.

Therefore, elite and competition level cyclists require more sophisticated bicycle fits which are conducted dynamically and which take more measurement data into account. After the static fit, a dynamic fit performed to fine-tune the bicycle parameters for metabolic, biomechanical and aerodynamic performance. This includes the measurement of wattage, heart rate, pedalling forces and kinematics (usually using video analysis) while the cyclist is pedalling on his bicycle on a trainer. There are many benefits to be gained from the integration of these measurements. For instance, the analysis of crank torque during pedalling aims to adjust the bicycle fit in order to minimize ineffective pedal forces which are out-of-plane and maximize efficiency during different phases of the pedal stroke (for example) reducing negative forces on the upstroke. Similarly, the effects of bicycle fit changes on aerobic economy, cycling power and frontal surface area can all be evaluated while the cyclist is on their bicycle in a simulated racing environment.

In conclusion, dynamic bicycle fit is perhaps the most obvious application of Mocap technologies for road cycling analysis. Although technological breakthroughs in advanced measurement devices already allow for precise kinetic and metabolic analysis during dynamic bicycle fit, high-tech Mocap systems such as the MVN offer the kind of clinical kinematic data that is still lacking.

3. DATA COLLECTION

This chapter documents the testing phase of the study. This includes details on the experimental setup and the test protocol used for the measurements of cycling kinematics using the MVN. The chapter concludes with the pre-processing of the MVN data and lessons learned from data collection.

3.1. Background Information

This section documents the test preparation procedure for the MVN system as well as the indoor and outdoor recordings.

3.1.1. Scope of testing

Road cycling is performed on diverse topographies, surfaces and types of routes. Therefore, it was decided that the testing would only be performed on flat, open and straight roads, thus eliminating changes in technique due to inclination, traffic and cornering respectively. Furthermore, although the racing position employed by cyclists may change at strategic points in a race, this study only considered the normal upright sitting position, as opposed to the more aerodynamic time trial position or the standing position used for sprinting and climbing. There were also boundaries for the test subjects. Due to the focus on cycling performance and the need for non-ferrous bikes during testing, only sub-elite (semi- or professional) athletes were accepted for participation. In addition, only male cyclists were tested to reduce the required sample size and avoid gender related differences in biomechanics.

3.1.2. Test subjects

The test group consisted of ten cyclists chosen from four different cycling teams. This selection intended to reduce the possibility of trends in the data caused by common coaching or bicycle fit appearing in the data. The cyclists were chosen based on their availability for testing, and were aware of the minor risk of road accidents or injury. Each test subject voluntarily agreed to participate and gave informed consent before participating in the study. Ethical approval for the study was obtained from the Committee for Human Research of Stellenbosch University's Faculty of Life Sciences. The participants were aged between 19 and 35, with a mean of 25.1 (± 5.6) years. Furthermore, their average height and weight were 176 cm (± 9.8 cm) and 74.2kg (± 5.4 kg) respectively.

3.1.1. Instrumentation

Besides the MVN system, a CycleOps Powerbeam Pro stationary trainer was used for the indoor testing. However, an aluminium version of the steel trainer frame was made to reduce the magnetic interference to the MVN system. Technical details of the Powerbeam and other miscellaneous testing instrumentation are supplied in Appendix B.2. The technical specifications of the MVN MTxs, XBus Masters and receivers, as well as a description of the how the MVN system exceeds the measurement requirements for the tests, is given in Appendix B.1.

3.2. Experimental Setup

3.2.1. MVN suit

The first step in setting up the MVN suit was preparing the suit for the subject. Furthermore, it was necessary to determine the suit size required for the test subject before testing. The Lycra suits come in various sizes ranging from small to double extra-large. Subject height and weight were used to choose the suit size according to Xsens recommendations. Since the Lycra suit needed to be washed after every session, the suit had to be rewired for each test. This involved placing the MTxs in the correct positions, connecting MTxs with the correct cables and folding the cables into the cable gutters, which is unfortunately a very tedious and time consuming process.

Before testing, the MVN Studio software required the setup of a recording session including settings for the sensor fusion scheme and biomechanical model. Regarding the fusion scheme, the User Scenario was set to a ‘fixed pelvis’ contact point to simulate the seated cycling position. Moreover, the Kinetic Coupling (KiC) algorithm was chosen as the Fusion Engine setting (this is discussed in Section 5.2.1). MVN Studio requires anthropometrical measurements of the subject (at least height and foot size) to scale the biomechanical model. Along with the option of inputting more body dimensions, the software also allows for adjustments to the assumed distances between each MTx and a proximal bony landmark (joint centre), on the leg segments. However, these extra measurements were not used in this study due to a lack of the required measurement instrumentation and expertise to perform such measurements.

After the wiring of the suit and the setup of the MVN Studio settings, which was performed before the session, the subject was instructed to put the MVN suit on over their regular cycling shorts. Then, it was necessary to inspect the placement of the

MTxs on the body. If the sensors are not placed correctly, the accuracy of the measurements is adversely affected. Firstly, the sensor units should be fixed firmly against the body, which requires the suit to fit tightly around each segment. Secondly, the position of the MTxs on the segments should correspond to the illustration given in the manual since the biomechanical model assumes correct sensor placement. This relates to the linear distance of the MTxs from adjacent joints, their orientation about the segment surface and symmetry between corresponding limbs. Once the suit had been correctly mounted and the system was running, the biomechanical model was inspected on the computer screen in Live Preview mode for anomalies. This was done in order to ensure that the sensors were attached correctly to the body and that the subject was standing in a magnetically undisturbed area that would be suitable for calibration.

Next, the calibration poses described in Section 2.1.3 were conducted. The minimum requirement for calibration is an N-pose or T-pose, although a weighted average is taken if both are performed. Both calibration poses were conducted in this study to minimize the effect of incorrect poses and increase accuracy. The hand-touch calibration was also performed in order to improve the accuracy of the upper body in the biomechanical model, especially the arms. Unfortunately, the squat pose was not used due to difficulties in executing the movement wearing cycling shoes with cleats. It was also not possible to perform the calibration with the shoes off and then put them back on since the foot sensors are fixed to the shoe and cannot be moved after calibration. The last step in setting up the MVN was to ensure that the live preview of the biomechanical model in the MVN Studio interface corresponded satisfactorily to the actual motion of the subject in the suit. This step is important in validating the calibrations and ensuring that the MTxs are placed correctly on the body.

3.2.2. Laboratory test

The indoor testing was conducted on the Powerbeam Pro trainer in the Department of Mechanical and Mechatronic Engineering at Stellenbosch University. Each cyclist was tested on their own bicycle and in their own cycling apparel.

Figure 12 shows a representative indoor test setup. The laboratory contained a desk with the desktop computer and MVN USB wireless receivers, a space for the bicycle and trainer and another space for putting on the MVN suit and conducting the calibrations. The trainer and mounting block for the front wheel were aligned with the MVN camera, which was fixed to the wall faced by the cyclist during the test. This

was to record the frontal view of the cyclist during the test in order to compare to the biomechanical model during the analysis. The positions and alignment of the trainer, mounting block and camera were marked off on the floor to ensure repeatability between tests. As mentioned earlier, a fan was also used for the indoor tests to increase the interior ventilation since the subject in the Lycra suit can become quite hot performing prolonged high intensity tests. The laboratory in which indoor testing was performed was emptied of all ferrous materials since the calibration steps should be carried out in the least magnetically affected area to ensure accurate results.

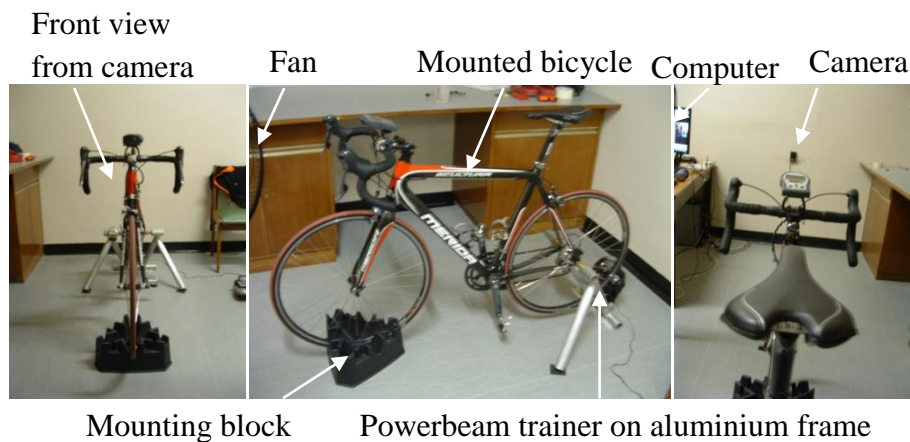


Figure 12: Laboratory setup for indoor tests

Before commencing the indoor test the cyclist's bicycle was mounted onto the Powerbeam trainer. The following steps were taken to mount the bicycle:

- The bicycle skewer was replaced with the Powerbeam trainer skewer
- The bicycle was straightened and the rear wheel clamped firmly into the trainer
- The contact pressure between the tyre and roller was adjusted and roller was locked into position
- The front wheel was placed onto the mounting block and the bicycle was aligned with the floor markers and camera correctly

Due to varying factors affecting wheel clamping conditions on the trainer such as tyre pressure and cyclist mass the rolling resistance for each test session differed considerably. It was therefore necessary to complete a roll-down calibration before each test to determine the rolling resistance. This is a significant component of power

measurement and was thus important for the integrity of the test protocol since the tests were performed with the power to weight ratio controlled. The procedure for the rolling resistance calibration was taken from the Powerbeam user's manual. The following steps were taken to complete the Powerbeam power-meter calibration:

- After mounting the bicycle on the trainer the cyclist climbed on the bicycle
- The roll down calibration option was selected on the wireless handlebar unit
- A speed of 18 mph ($\sim 29 \text{ km}\cdot\text{h}^{-1}$) was maintained for 2 minutes
- The cyclist immediately stopped pedalling and the system coasted to a stop

3.2.3. Field test

The outdoor tests were conducted on the Blaauklippen Road in Paradyskloof, Stellenbosch. The MVN data was collected on a straight and flat stretch as the pursuit vehicle followed the cyclist within wireless range with the MVN laptop. The only preparation that was required was the setup of the MVN wireless receivers on the pursuit vehicle. As mentioned earlier, the signal range of the MVN system outdoors is affected by the relative position of the two receivers. The MVN user manual suggests that they be at least a meter apart and preferably a meter apart both vertically and horizontally. Therefore, USB extensions were used to fix the receivers onto the bonnet and roof of the pursuit vehicle.

3.3. Test Procedure

It was decided that the tests would be conducted primarily to obtain the cycling kinematics prior to the onset of fatigue. This method was chosen for its convenience, so as to shorten the testing time and minimize disturbances to the training schedule of the test cyclists. Therefore, due to the uniformity of cycling kinematics, the MVN recordings were carried out over a short period of one minute (although this already amounted to almost 100 pedal strokes). It was also decided to measure and compare the kinematics at different power outputs. These were divided into the categories of low, medium and high power (more detail will be given on these test intensities in Section 3.3.1). Therefore, six one-minute recordings were taken with each subject in the MVN; three indoor and three outdoor.

3.3.1. Indoor protocol

The indoor testing was facilitated by the Powerbeam Pro software package, which was used to set up workouts on the trainer. The Powerbeam workout was loaded onto

the memory of the wireless handlebar unit before the test session and run parallel to the MVN recording. The workout consisted of six stages, including a warm up, three recording periods and two readjustment periods. Table 1 shows a summary of the workout stages.

Table 1: Summary of Powerbeam workout for data collection

Step	Description	Power-to-weight ratio [W.kg ⁻¹]	Time taken [min]
Warm up	Warm up at low power output	2	3
Low power	Maintain low power target	2	1
Readjustment	Adjust power to next target	3.5	0.5
Medium power	Maintain medium power target	3.5	1
Readjustment	Adjust power to next target	5.5	0.5
High power	Maintain high power target	5.5	1

The warm up and recording periods each had a target power to be maintained for the full duration of the stage, and the readjustment periods allowed for the transient shift in power output between the two targets. The power targets were derived from fixed power-mass ratios, measured in Watts per kilogram of body weight. The three power-to-weight ratios were 2, 3.5 and 5.5 W.kg⁻¹ and corresponded to low, medium and high cycling power outputs respectively. These values were taken from another road cycling study (Garcia-Lopez, J *et al.*, 2009). The workouts were programmed in the software according to the test cyclist's weight and then loaded onto the handlebar unit before each session.

Following the completion of a test, the subject would take off the suit and the recordings were inspected for anomalies. This was especially relevant in terms of magnetic disturbances associated with the different bicycles, although this was also done before the test in the live MVN preview. Table 2 summarizes the sequence of the test protocol and shows the estimated times for each phase. In total, the test sessions took 45 minutes to prepare and another 45 minutes to conduct.

Table 2: Entire indoor test protocol

Phase	Activity	Total time
Before test	Choose suit size and rewire MTxs Set up Powerbeam workout	±45 min
Test setup	Mount bicycle on trainer Put on MVN suit Calibrate biomechanical model Perform Powerbeam roll-down test	±30 min
Data collection	Warm up Low power Medium power High power	±10min
Conclude session	Take off MVN suit Run through recordings	±5min

3.3.2. Outdoor protocol

The outdoor procedure was similar to that of the indoor testing. However, built-in power meters (such as PowerTap or SRM technologies) were not used by some of the cyclists. In these cases, the low, medium and high intensity recordings were defined by bicycle speed and not power-to-weight ratios. Therefore, speed-to-power correlations were obtained using a bicycle with a built-in power meter and speedometer and used to simulate the power-to-weight ratios used in the indoor testing. Speeds of 25, 35 and 40 km.h⁻¹ were specified to approximate power-to-weight ratios of 2, 3.5 and 5.5 W.kg⁻¹. Although this was a slightly crude estimation, it was sufficient for the purposes of recording the different levels of effort considering the low sensitivity of body position to small changes in power output.

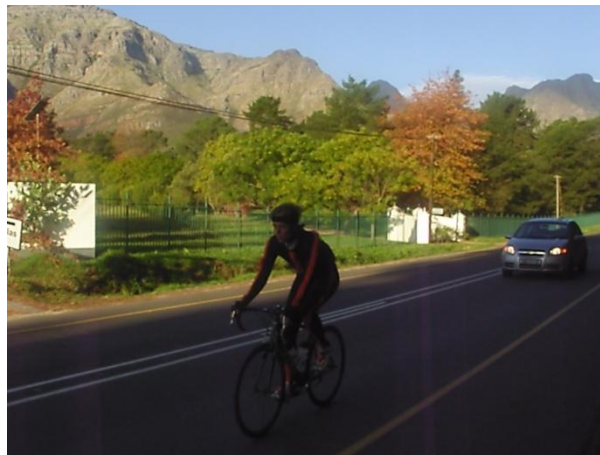


Figure 13: Road test with pursuit car transporting laptop and wireless receivers

Figure 13 shows the setting for the road tests along with the pursuit car remaining within a following distance of 30 m. Calibrations were conducted on the road side. The cyclist was given a stretch of road approximately 200 m long to reach the desired speed, and then had to maintain this (by visual feedback from their power meter or speedometer) for one minute. This was repeated three times in succession (with a rest period in between) for low, medium and high power along the same stretch of road.

3.4. Data Pre-processing

After recording, the MVN software interface displays a 3D visual representation of the biomechanical model. Multiple virtual views can be displayed simultaneously during a replay of a Mocap recording, along with the video of the test subject captured by the MVN camera. The avatar can be viewed from any angle or distance in the virtual 3D space and the recording can be played at various speeds. Furthermore, a preliminary review all the kinematic measurements (joint angles, segment kinematics, sensor data) in the recording can be done using the MVN Studio plotting tool. An example of the post-test MVN interface can be seen in Figure 14.

The joint angle data was retrieved from MVN studio in order to import the measurements to Matlab for analysis. The kinematics from the three one-minute long constant-power phases of the test protocol was separated from the single MVN recording of the entire test protocol. This was done by selecting the appropriate sections of the original single MVN files and exporting them from MVN Studio as open source files. It is important to select the desired output variables for export in the MVN Studio settings to prevent oversized files. In this study, data for the joint angles, magnetometer signals and segment positions were exported.

MVN motion data files can be exported in four formats: Coordinate 3D (C3D file extension), BioVision Hierarchical (BVH), Filmbox (FBX) or MVN open XML (MVNX) format. XML (Extensible Markup Language) is a simple and popular format for encoding electronic documents. It is widely used over the Internet and is compatible with most major commercial software packages such as Matlab and Microsoft Excel. Therefore, MVNX format was used since it could be imported into a Matlab workspace. In total, from the two tests (indoor and outdoor) each consisting of three different power phases, six MVNX files were exported for each cyclist. Therefore, from the original 20 test recordings (MVN files) for the 10 test subjects, a total of 60 MVNX files were exported from MVN Studio.

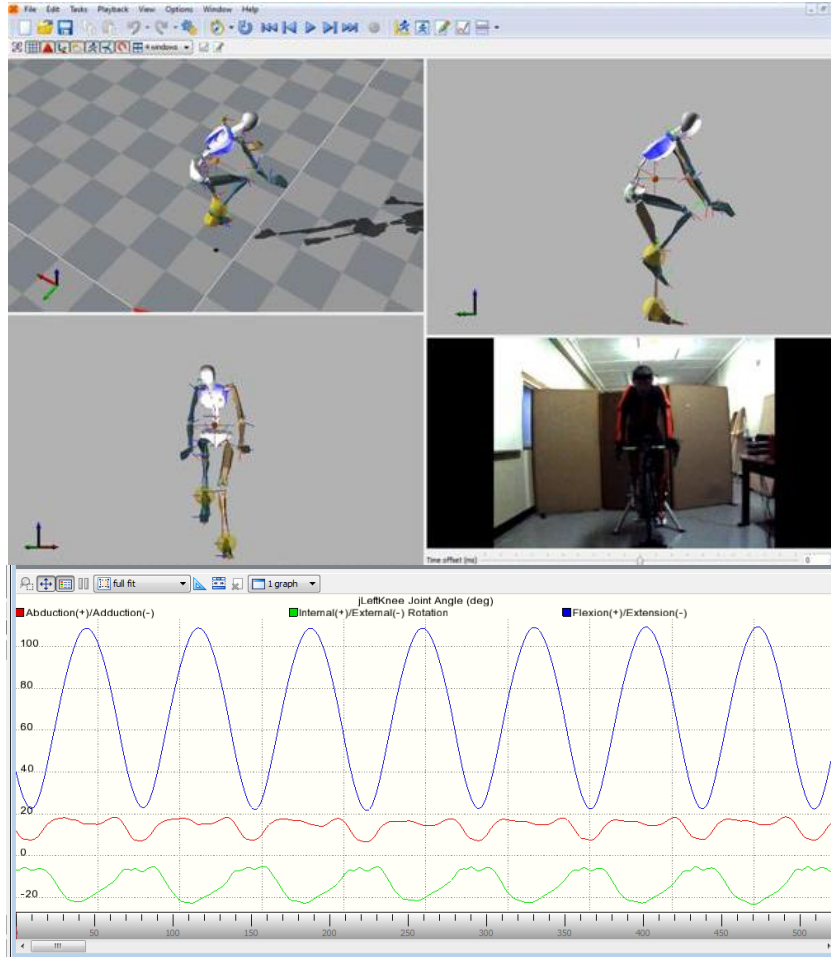


Figure 14: MVN interface containing test recording

Although MVN Studio runs relatively smoothly and efficiently, extracting the MVN data is still not very user friendly. There is no way to extract specific kinematic variables for selected joints, meaning that the MVN files can be unnecessarily large. There is also no way to directly export the kinematic data into Matlab, and therefore an online toolbox is required to import the MVNX files. Even when run on a new and powerful computer, the import function is still relatively clumsy and took approximately five minutes to load each 60 second MVNX recording. Furthermore, the format of the MVN data in the MVNX files is also not clearly indicated in the MVN documentation or labelled in the MVNX data and can be confusing. Therefore, care needs to be taken when selecting data from extracted MVNX data for analysis. For more information regarding the data management, refer to section C.1 of the Appendices.

4. DATA ANALYSIS

This chapter presents the research analysis and results. It contains three sections corresponding to the analysis conducted to answer the three research questions stated in Chapter 1. The first section describes the validation of the outdoor measurements. The second section contains a comparison of the indoor and outdoor data. The last section investigates the usefulness of the MVN data for application in dynamic bicycle fit. The chapter closes with conclusions from the data analysis.

4.1. Validation of MVN Measurements

The first research question to be addressed was: Can the MVN be used to conduct field measurements of cycling kinematics? This involved assessing the magnetic interference in the MVN data, performing a benchmark test against the Vicon optical system and comparing the outdoor measurements to typical values presented in previous studies.

4.1.1. Magnetic interference

As explained in Section 2.1.2, the MVN system's Kalman filter utilizes the heading data of the magnetometers to correct gyroscope drift in the horizontal plane. This prevents misalignment of the body segments in the biomechanical model, provided that the local magnetic field is homogenous. Therefore, assessing the state of the local magnetic field during a MVN recording can give an indication of the magnetic interference experienced by the system, and hence the associated measurement uncertainty. This is accomplished by extracting the raw magnetometer data from each MTx sensor on the subject's body and analyzing certain magnetic field parameters. A magnetic field can be parameterized by calculating the field strength and field inclination angle. The magnetic field strength is related to the flux density of the field, while the inclination angle is the angle that the field makes with the Earth horizontal. Therefore, the closer the local magnetometer readings are to the reference (undisturbed) inclination and intensity values, and to each other, the more confident the Kalman filter is of the integrity of heading data and thus the kinematic data.

Therefore, by considering the MTx signals individually it was possible to sample the magnetic field at 17 different points around the cyclist's body. The specific areas on the bicycle and in test environment where distortions in the magnetic field occurred could then be found by correlating them to the sensors on the body model. One of the

challenges in comparing MTx data was that their measurement coordinate systems were oriented differently to each other in the global frame. Therefore, since the magnetic inclination angle being measured was in the global frame, the local measurements for each magnetometer needed to be rotated and aligned in the global frame. This was complicated by the fact that the rotation data used in the sensor fusion scheme is not made available in MVN Studio. Therefore, manual methods were required in order to calculate the inclination angle around each MTx.

The problem of translating the sensor data to the global frame was solved by using the accelerometer as an inclinometer to approximate the downward direction in the global frame. However, this was not possible for the moving sensors because of the extra acceleration components in the accelerometer signal. Therefore, only the magnitude of the field intensity was considered for these segments. The magnetic field strength, on the other hand, is constant at all positions in a homogenous field. Therefore, although the inclination angle cannot be calculated using the accelerometer data from MTxs on moving segments, the magnetic field around these sensors can still be evaluated using the magnitude of the magnetic field strength. This value is the scalar magnitude of the three dimensional vector measurements taken locally by each magnetometer. Since the motion of the sensor is irrelevant to this scalar measurement, it was not necessary to translate the sensor coordinates to the global frame. For more detail about the magnetic analysis calculations, and an example of a similar study by XSENS where magnetic intensity analysis was done with the MVN magnetometers, refer to Appendix C.2.1.

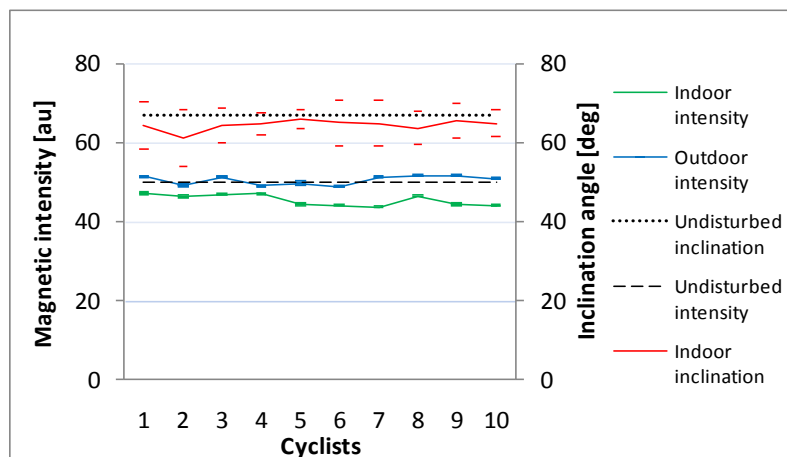


Figure 15: Inclination angle and intensity near head segment sensor

There are eleven stationary sensors in the MVN suit: those attached to the head, torso (shoulders, sternum and pelvis) and arms (upper arm, forearm and hand). Beginning with the torso sensors, Figure 15 shows the orientation and density of the magnetic field around the head sensor for all 10 cyclists. For the sake of brevity, only the measurements for the low power sessions are shown since there was no notable difference in magnetic field between recordings. Undisturbed values were taken as the Earth’s magnetic field measured in a calibration test near the outdoor test venue.

As may be expected from the unsophisticated method of calculating inclination, the variance in the readings was high (upper and lower limits specify standard deviation). This was probably due to the noise on the accelerometer signal caused by vibrations and slight movements. However, since the mean values were still close to the undisturbed value of 67° , the MTx rotation method seems to work, and the noise is assumed to be approximately Gaussian. Therefore, despite the uncertainty on the measurement, the inclination angles can still be used to give an indication of distortions in the magnetic field. Predictably, the red line is relatively flat for the head sensor since the head sensor is furthest from the bicycle and is not likely to be affected by ferrous materials. The intensity for each cyclist in Figure 16 was far more consistent, as can be noted from the very small deviations (magnetometer unit of measurement is arbitrary and values were scaled to fit the graph). As can be seen from the green curve, the indoor intensity was lower than the undisturbed outdoor value. This is thought to be due to distortions caused by ferrous metals in the building, such as steel support beams in the floor and ceiling. The outdoor intensity, on the other hand, was consistently close to the undisturbed value.

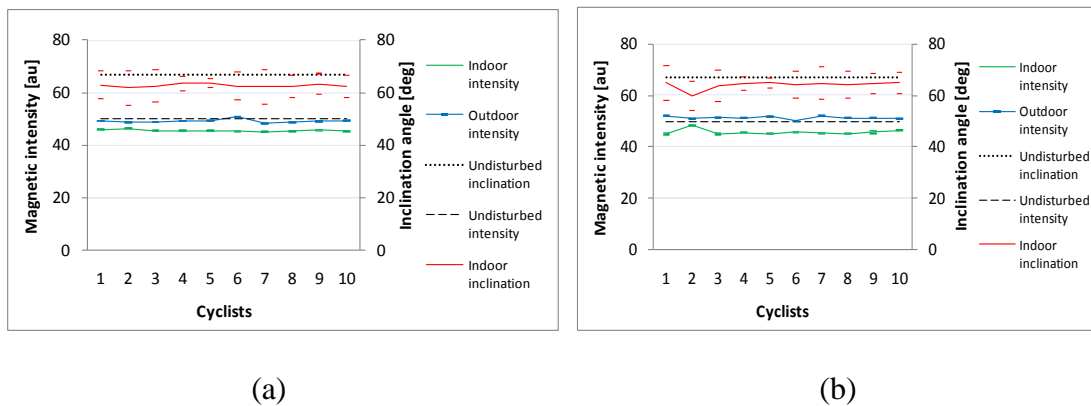
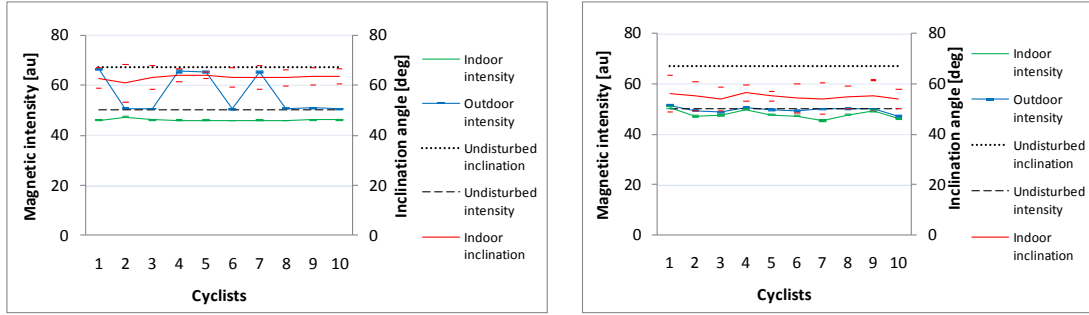


Figure 16: Magnetic readings for (a) sternum and (b) pelvis sensors

Figure 16 shows the inclination angle of the magnetic field near the sternum and pelvis MTxs. Both demonstrated a strong similarity in inclination and intensity measurements. The indoor inclination was again noisy and slightly lower than the undisturbed value, but the values were relatively constant for all the tests. Surprisingly, the pelvic sensor which was located close to the saddle (and possibly ferrous materials), measured a less disturbed inclination than that which was measured near the sternum. This could possibly be explained by the fact that the sternum sensor experienced movement due to the breathing of the cyclist, which distorted the gravity vector values in the accelerometer. The indoor intensity was offset by approximately 10% on average from the undisturbed value, which indicates that there were common and significant environmental disturbances. However, both the indoor and outdoor intensities were surprisingly consistent, implying negligible bicycle-related disturbances near the sternum and pelvis. Cyclist 2 is the only one with a disturbed pelvic sensor. However, Cyclist 2's sternum values were unaffected indicating that there may have been ferrous metals near the saddle. However, all in all Figure 16 indicates that the sternum and pelvic sensors were generally undisturbed.

The final torso measurements are for the two shoulder sensors, shown in Figure 17 below. As expected, the left shoulder sensor measured a magnetic field inclination angle almost identical to the ones shown in Figure 16a for the sternum since they were in close proximity to each other and both moving during breathing. Similarly, the indoor intensity remained essentially unchanged from the sternum indoor intensity. However, the outdoor intensity values for Cyclist 1, 4, 5 and 7 were significantly disturbed. It is suspected that these disturbed values, which are for the last four tests conducted, are due to an error in the MTx. Analysis of a later recording taken with the MVN suit confirmed that the left shoulder magnetometer was damaged. In terms of the right shoulder sensor, the indoor intensity and inclination angles contained a significantly higher bias error, although relatively consistent. There is no obvious cause related to the bicycle material or environment for this large discrepancy between the shoulder sensors for the indoor intensity. The sensor is fully functional, having taken accurate measurements in the subsequent outdoor tests, and it seems unlikely that right side of the cyclists was disturbed in general since the right upper arm is not affected. However, it is the change in indoor intensity that is responsible for error in the inclination calculation (refer to Equation 21 and Figure 51 in Appendix C.2.1 for use of intensity components to calculate inclination).

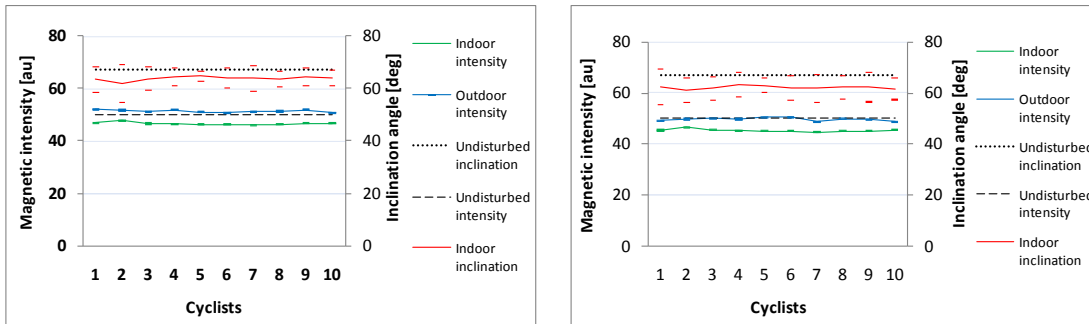


(a)

(b)

Figure 17: Magnetic readings for (a) left and (b) right shoulder sensors

Following the trend for the torso, the upper arm segment sensors (Figure 18) measured essentially no bicycle-related interference. The strong correlation to the sternum and pelvic measurements seems to indicate that the magnetic field around the upper body region was fairly uniform. It can, therefore, be concluded that the road bicycles caused minimal magnetic interference to the measurements from sensors on these body segments during the testing.



(a)

(b)

Figure 18: Magnetic readings for (a) left and (b) right upper arm sensors

However, when considering the magnetometer readings around the forearm and hand segments it becomes apparent that there was less uniformity with previous segments as well as between cyclists. The results in Figure 19 show that the magnetic field was significantly distorted on both the left and right arms, although interestingly the interference was not the same. The uneven left forearm results suggest that there were more bicycle-related disturbances (ferrous metals) on this side, although the right

hand side was also slightly affected. The reason for these disturbances is almost certainly the proximity to the handlebar interface.

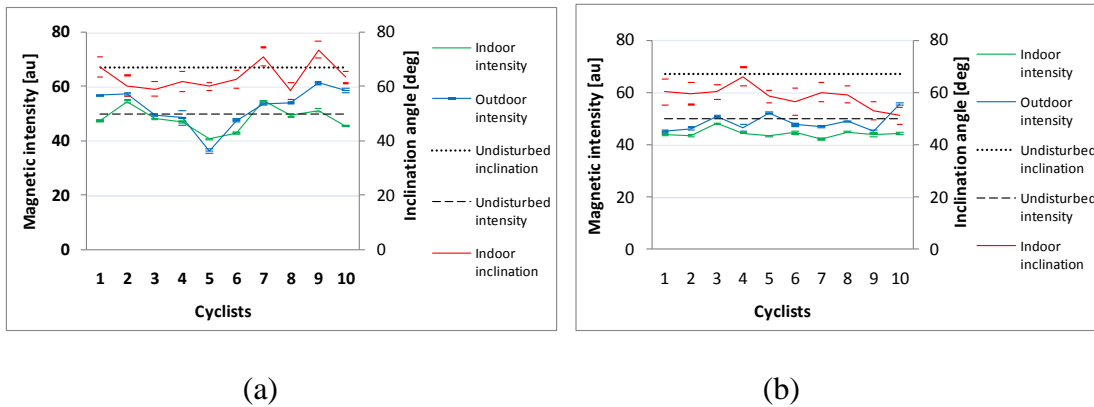


Figure 19: Magnetic readings for (a) left and (b) right forearm sensors

This is demonstrated even more clearly in the inclination angle measurements around the hand segments, shown in Figure 20. The disturbances shown in Figure 19 were more pronounced, especially for Cyclist 2, 7, 9 and 10. There were also differences for some cyclists between the amounts of interference in the indoor and outdoor tests. This may have been due to the fact that these cyclists placed their hands closer to the brakehoods (containing steel components) in some tests.

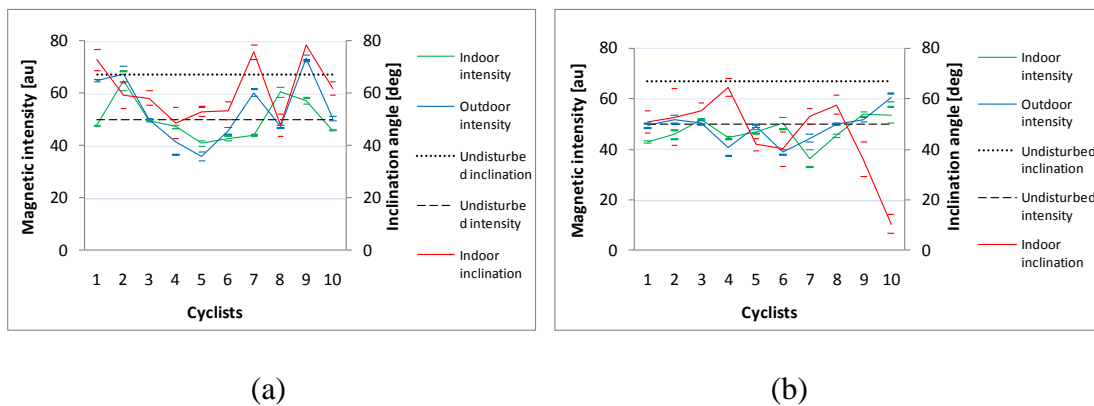


Figure 20: Magnetic readings for (a) left and (b) right hand sensors

Unlike the upper body, which is for the most part slightly above the bicycle, the legs are situated much closer to the majority of the bicycle components. However, as previously mentioned, analysis of the magnetometer data from the MTxs on the moving lower limb segments did not include inclination. Nevertheless, the magnetic

intensity around the thigh, shank and foot sensors still provided adequate insight into the homogeneity of the local magnetic field.

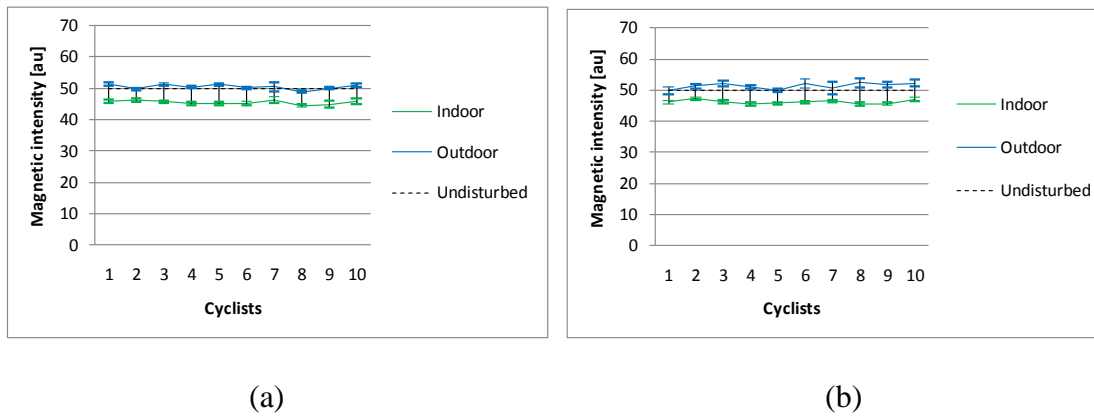


Figure 21: Magnetic readings for (a) left and (b) right upper leg sensors

As shown in Figure 21, the intensity near the upper leg sensors bears a strong resemblance to the nearby pelvic sensor. The indoor readings were again lower than the outdoor readings, but there were no signs of bicycle-related distortions in the field. The upper legs were seemingly undisturbed by the drivetrain (chain, sprockets etc.). However, the bicycle drivetrain did affect the lower leg sensors (Figure 22).

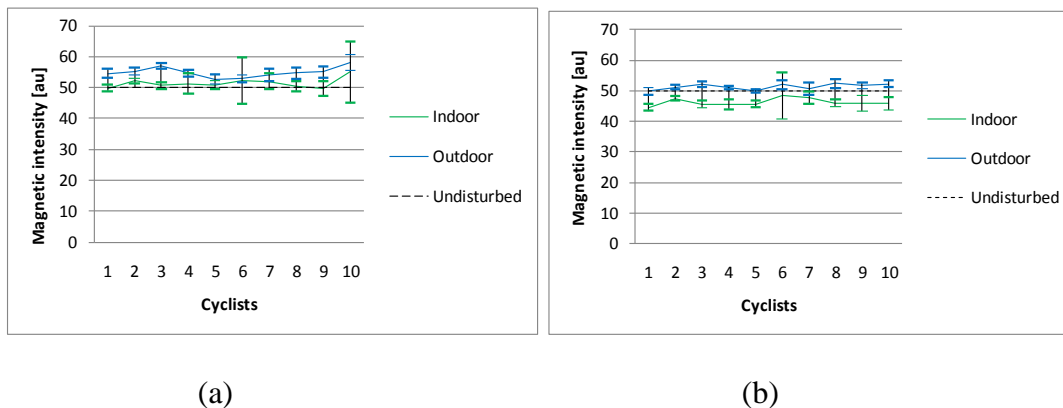


Figure 22: Magnetic readings for (a) left and (b) right lower leg sensors

Both the indoor and outdoor intensity were approximately 10% higher for the lower left leg than the upper left leg, although the right upper and lower leg were much more similar. This seems to indicate that the left lower leg was affected by a common bicycle-related disturbance which had less influence on the right lower leg. This was

most likely the effect of the chain and sprockets, since bicycle drivetrains are not bilaterally symmetrical. Furthermore, both left and right lower legs showed less uniformity between cyclists, which indicates the presence of some differences in the magnetic disturbance around the lower leg area. This suggests that the components in different road bicycle drivetrains contained different quantities of ferrous material. The measurements for Cyclists 6 and 10 also deviated considerably, indicating large but inconsistent deformations in the magnetic field during the pedal stroke.

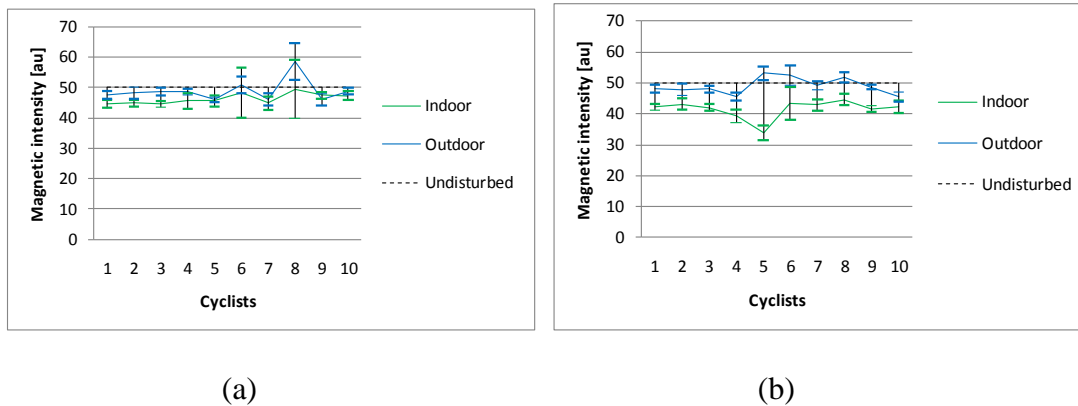


Figure 23: Magnetic readings for (a) left and (b) right foot sensors

As may be suspected, the foot sensors experienced the greatest disturbances being closest to the drivetrain of the bicycle. However, the changes in the magnetic intensity were not systematic. In fact, while some cyclists experienced extremely large disturbances, for example Cyclist 6 and 8, many simply experienced less consistency in intensity. This seems to indicate that the magnetic field around the legs was highly deformed. Interestingly, the increased variance in intensity around some foot sensors means that the magnetic disturbances vary anteriorly and posteriorly as the foot moves along the pedal revolution. This leads to the deduction that the primary source of interference in these cases was not from the pedals or the crank hub, which remain at a fixed relative distance from the foot during pedalling, but may have been caused by the ferrous materials in the chain, derailleur or chain sprockets in the rear wheel. However, in the cases where there were large differences in the mean value, such as with Cyclist 5 or 8, it is highly likely that materials either in the pedals, crank hub or cleats in the shoes disturbed the magnetic field.

It has been shown thus far in the magnetic analysis that the field deformations were worst at the handlebar-hand and pedal-shoe interfaces. To summarize the magnetic analysis and present the major interference more quantitatively, the increase in

magnetic interference when moving down the arms and legs is illustrated in Figure 24 and Figure 25 respectively.

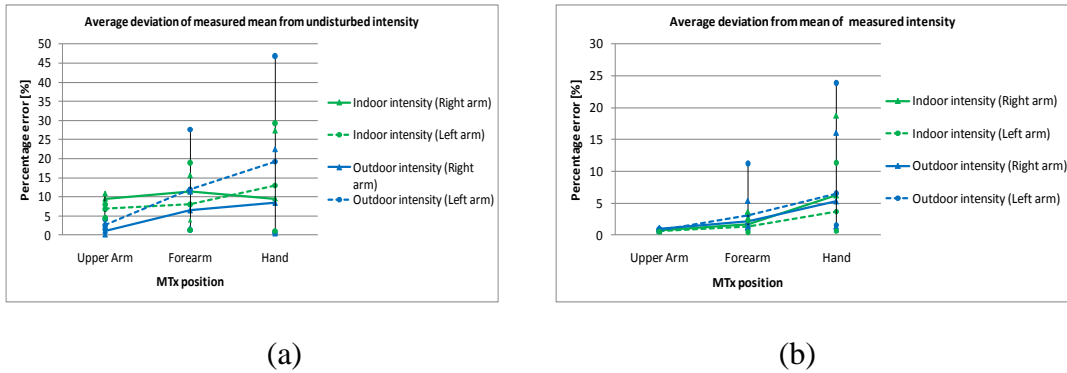


Figure 24: Increasing magnetic interference toward hands

Figure 24a is a plot of the percentage error of the average difference between the undisturbed and measured intensity for the left and right arm sensors in the indoor and outdoor tests. Here it can be clearly seen how the intensity became more and more disturbed when moving from the upper arms to the hands on the handlebar. The intensities for the upper arm sensors, furthest from the bicycle, were fairly consistent (no outliers) for both indoor and outdoor tests and almost totally undisturbed (low deviation) for the outdoor tests. However, as shown previously, the indoor deviation from undisturbed intensity for the upper arm was on average 8% and 10% for the left and right sides respectively. As can be seen from the relatively flat green lines, the indoor environmental disturbances masked the bicycle related disturbances. However, the outdoor intensities showed an approximately linear increase in average error towards the hands. Interestingly, the left arm sensors experienced roughly double the magnetic disturbance (4%, 11.5% and 19%) that of the right arm sensors (1.5%, 6.5% and 8.5%). Although some of the cyclists were relatively undisturbed, as can be seen by the near-zero minimum disturbances, some of tests showed errors of up to 47% for the left hand and 22.5% for the right hand.

Figure 24b illustrates how the amount of variation in the intensity measurement also increased closer to the handlebars. Whereas the upper arm sensor was extremely stable for laboratory and road tests (percentage deviation of 0.5% with essentially no outliers), there was again an almost linear increase in instability towards the hand sensor. Similarly to Figure 24a, the left arm outdoor values were more pronounced,

with the intensity varying up to 24% during a test. This suggests the magnetic field around the handlebars was heterogeneous, and that there were concentrated areas of distortion (such as the gear shifters and brakehoods). Other tests showed very little variation for any of the arm sensors, indicating that the disturbances are not constant.

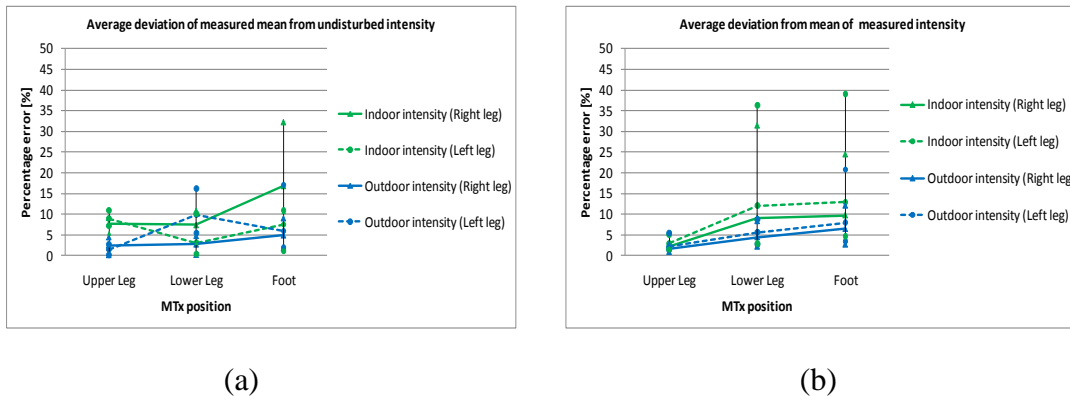


Figure 25: Increasing magnetic interference towards feet

The progressive increase in magnetic interference down the legs can also be seen in Figure 25a. However, it is interesting to note that the sensors for the lower leg and foot showed a more similar average error in intensity than the forearm and hand sensors. This may be due to the fact that at the bottom of the pedal stroke the lower leg passes through the same magnetic field that the foot passes through at the top of the pedal stroke relative to the bicycle. The average indoor disturbances increased from the environmental average of 8-10% for the upper leg to 17% near the foot (the highest disturbance error was a 32% offset from the undisturbed intensity). Interestingly, the disturbances were notably lower for the outdoor leg measurements. With the exception of the lower left leg sensor, which had a 10% average error, all the lower limb sensors for the outdoor tests showed errors of 2.5-5%. This suggests two things: firstly, the lower left leg appears to have been by far the worst affected of the leg sensors and further investigation is required to determine the reasons for this. Secondly, it appears that the foot sensors experienced much higher disturbances during the indoor tests. Therefore it is presumed that the indoor magnetic field near the feet was also affected by the metal in the laboratory floor and the stationary bicycle trainer’s magnetic brake which generated a field of unknown size.

This deduction is supported by the fact that the variation in the lower leg and foot sensor intensity measurements was significantly higher in the laboratory tests (Figure 25b). A complicating factor in understanding the interference for the lower body was

the motion of the lower limb sensors compared to the relatively stationary arm sensors. This is highlighted by an increase in variation as the segments moved back and forth and up and down past different bicycle components during the pedal stroke. Whereas the upper leg sensors were largely stable, the intensity measurements near the feet varied on average during each test by ~12% in the laboratory and ~7% on the road. However, some cyclists had disturbances of up to 39% for the left foot sensor.

The interference to the magnetometer readings during the testing reduced the MVN Kalman filter's ability to compensate for gyroscopic drift error using sensor fusion. The resulting instability in the horizontal plane led to varied levels of degradation to the biomechanical model. This was initially observed visually for the lower body in MVN Studio as an exaggerated hip abduction/adduction (due to drifting of the lower leg segment in the horizontal plane relative to the upper leg segment) and unrealistic ankle inversion/aversion (due to drifting of the foot segment relative to the lower leg segment). The disturbances to the arm sensors generally resulted in high uncertainties in the position of the shoulder joint centre and therefore also in the position of the hands and elbow and wrist joint angles. This is illustrated in Figure 26 by the difference between a less disturbed test and an extreme case of these errors in the biomechanical model. The reason the Kalman filter could not correct shoulder, hip and ankle errors (while the knee, for instance, remained unaffected) is that the constraints in the biomechanical model are based on the likelihood of joint centre position. Therefore, since the range of knee abduction/adduction is relatively small, the joint updates in the sensor fusion scheme refused high drift in the knee joint while allowing more biomechanically feasible drift elsewhere.

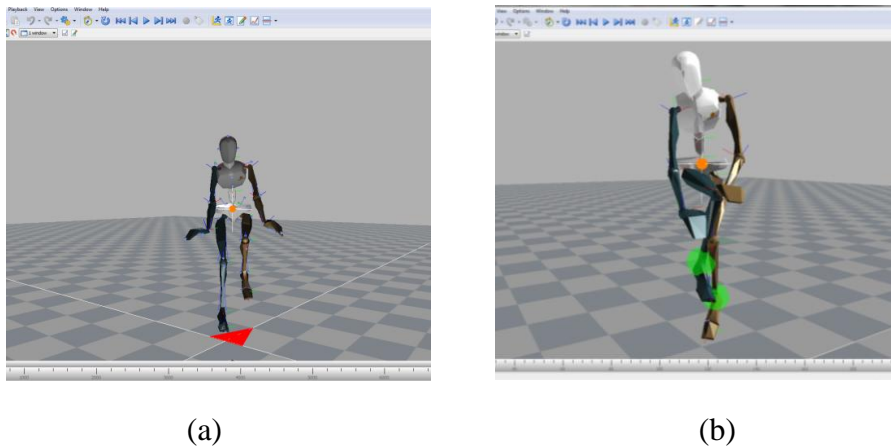


Figure 26: Example of (a) negligible and (b) severe interference

Therefore, it is clear that the MVN system was unacceptably disturbed during testing and that the kinematic data as a whole contained drift errors and could not be used. However, it was possible to extract accurate hip, knee and ankle flexion angles from the recordings. This was done using the KiC fusion engine, which determines the joint flexion angles based on the kinematics of connected segments in the lower body. Fortunately, these are the most important joint angles for analysis of cycling kinematics, which meant that meaningful analysis with the test data was still possible.

4.1.2. Background to kinematic analysis

The lower body joint flexion results shown in this section can be difficult to visualize, even in two dimensions. Therefore, it is first necessary to familiarize the reader with the terms and variables referred to in the analysis. Definitions of the bicycle crank angle (including key positions during the pedal stroke) as well as for the hip, knee and ankle flexion angles are shown in Figure 27.

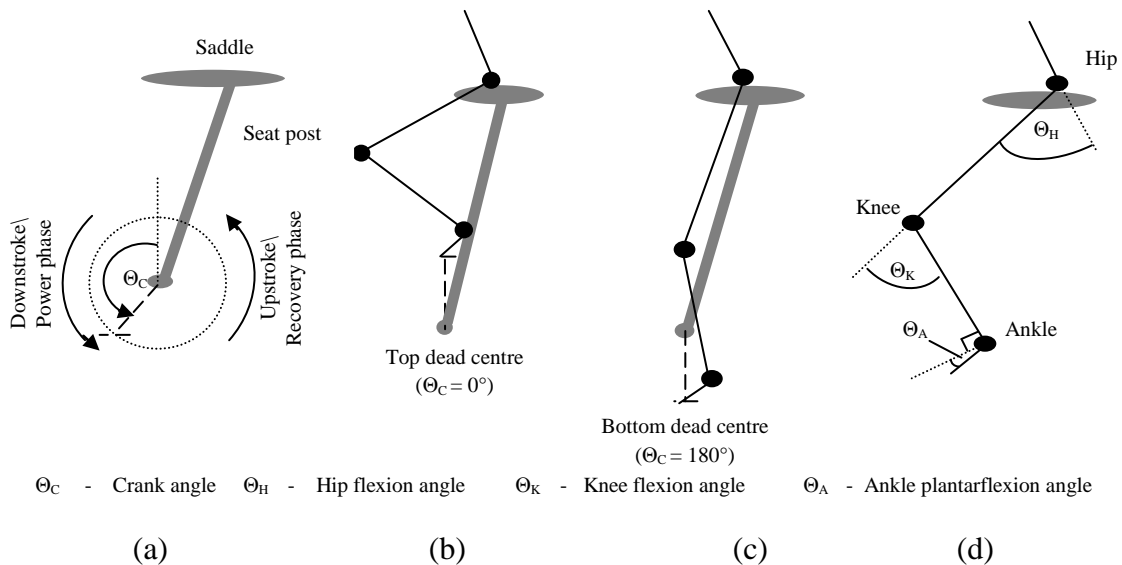


Figure 27: Definition of (a) crank, (b) joint angles, (c) TDC and (d) BDC

The crank angle (Figure 27a) is measured from the top dead centre (TDC) in the direction of crank rotation (Figure 27c). At the bottom dead centre (BDC) the downstroke ends and the upstroke begins (Figure 27a, c). Each pedal revolution is divided into the downstroke (from TDC to BDC), where power delivery occurs during hip and knee extension, and the upstroke (BDC to TDC) where the extended leg recovers to a “loaded” position for the next downstroke. The hip flexion angle is

external to the angle between the femur and the lumbar spine segments, or thigh and lower back (Figure 27d). The knee flexion angle is external to the angle between the femur and tibia (thigh and shank segments). Finally, the ankle plantarflexion is the angle of the foot segment greater than 90° to the shank. When $\Theta_A < 0^\circ$ it is referred to as dorsiflexion. Although the maxima and minima for Θ_A are less obvious, it can be seen from Figure 27b and Figure 27c that Θ_H and Θ_K are greatest when $\Theta_C \approx 0^\circ$ and smallest when $\Theta_C \approx 180^\circ$.

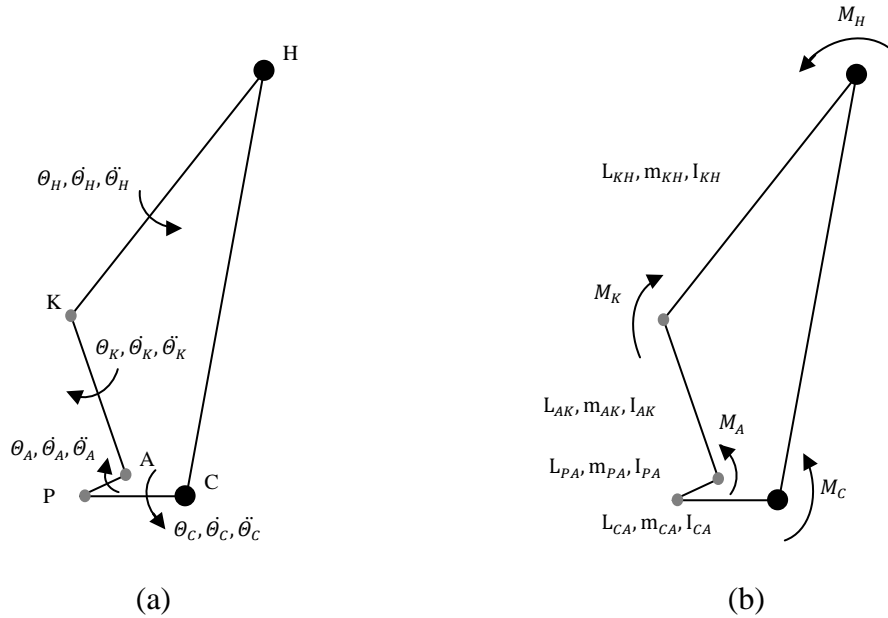


Figure 28: Five-bar linkage model for (a) kinematic and (b) kinetic analysis

Some attempts have been made to model pedalling motion mechanically (Redfield, R and Hull, M.L, 1986; Hull, M.L and Jorge, M, 1985). The traditional solution was to use a closed loop five-bar linkage system constrained to planar motion, such as in Figure 28. The crank arm (from the crank spindle (C) to the pedal (P)) is fixed at C and the hip joint is also assumed to be fixed at the hip joint centre (H). Therefore, the link between C and H is stationary. The foot (PA), shank (AK) and thigh (KH) segments can be analyzed kinematically using the angular position, velocity and acceleration of each linkage (Figure 28a). However, to understand factors responsible for the joint angles it is important to consider the kinetics of the system (Figure 28a). The leg muscles generate joint moments M_H , M_K and M_A at the hip, knee and ankle which result in an effective torque moment M_C in the bicycle drivetrain which propels the bicycle forwards. The cycling kinematics resulting from these joint moments are

related both to the spatial configuration of the links and the inertial effects of the linkages (due to aspects such as mass) and the resistance torque in the crank spindle caused by friction forces resisting the bicycle motion. It should also be noted that the ratios between the lengths of the linkages (cyclist anthropometry) affect both the static angles and dynamic forces involved in pedalling mechanics.

These planar linkage systems only model pedalling kinematics in 2D (flexion angles). However, they help to illustrate the interdependencies between Θ_H , Θ_K and Θ_A . All three joint angles are determinate at a given crank angle and angle between the foot and crank arm (pedal position relative to the heel and crank spindle). This is because only two constraints are required to specify the linkage configuration for five-bar linkage systems. The significance of this is that at any given point the joint angles are dependent upon both the kinematics and kinetics of all the other segments. For example, altering Θ_A almost always necessitates changes in Θ_H and Θ_K and vice versa. This should be kept in mind for the interpretation of the kinematic results presented later in this chapter.

4.1.3. Benchmark test with Vicon system

It was shown in Section 2.2.1 that the MVN measurements have been validated for undisturbed test environments. However, the author is not aware of previous research to validate joint angle measurements taken with the KiC algorithm for magnetically disturbed settings. Therefore, a benchmark test was conducted with the Vicon Mocap system at Tygerberg campus of Stellenbosch University to compare measurements of cycling kinematics between KiC and the gold-standard optical system. During the test Θ_H , Θ_K and Θ_A were measured simultaneously by the MVN and Vicon systems for a single cyclist while the subject pedalled at a constant power of 250 W for two minutes. The two sets of flexion data were synchronized by using a reference point in the data where the subject change position in his seat and then normalized and averaged over all the pedal strokes.

A comparison of the MVN and Vicon flexion curves for the hip, knee and ankle are shown in Figure 29. The MVN data was processed three times with different amounts of subject-specific anthropometric data. The red curves show the flexion measurements with the biomechanical model only scaled by the subjects height and foot size (“MVN” in legend), as was done in this study. The blue line represents the flexion measured with comprehensive anthropometry data obtained from a clinical approved anthropometry evaluation of the subject (“MVN+anthrop”). Finally, the

green line represents the most accurate KiC measurements, with the measured distance between the each MTx and bony landmarks of the joint centres for each segment on the left and right legs also included (“MVN+anthrop+KiC”).

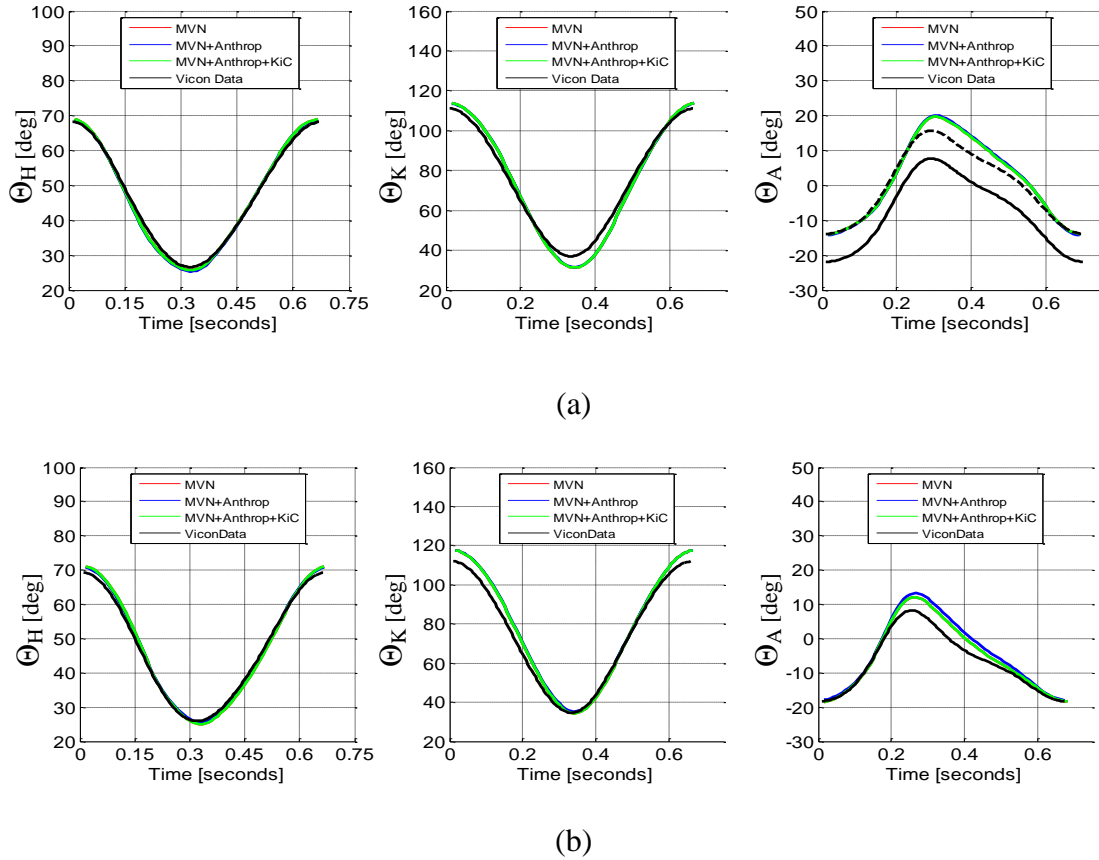


Figure 29: Comparison of Vicon and MVN (a) right and (b) left leg flexion

The correlations between the MVN and Vicon measurements were very high for all three joints (Table 3). The Θ_H values ($R^2 > 0.996$) were especially alike, with differences of only 2° and 1° for left and right hips. This is followed by Θ_K ($R^2 > 0.993$), which was still very similar to the Vicon although the MVN measured the Θ_{MAX} slightly high for the left and right knees (6° and 3° respectively). Furthermore, Θ_{MIN} was measured 5° lower for the right knee, while the left leg values were almost identical. One of the reasons for this may be leg length discrepancy, which is taken into account for the Vicon system by separate left and right leg segment measurements whereas the MVN model assumes bilateral asymmetry in the biomechanical model. Therefore, these errors in segment length could translate into

incorrect joint centre calculations and therefore ‘false’ or masked differences in left and right flexion. This is definitely one of the major limitations of taking clinical measurements with the MVN, since there is no way to compensate for bilateral asymmetry in the test subject’s anthropometry.

Table 3: Flexion measurements taken during Vicon validation test

	Θ_{MAX} [deg]		Θ_{MIN} [deg]		Θ_{RANGE} [deg]		R^2	RMSE
	MVN	Vicon	MVN	Vicon	MVN	Vicon	Both	Both
Θ_{H} [L/R]	104 ± 2	102 ± 1	58 ± 2	58 ± 1	46 ± 2	43 ± 1	0.996	0.9
	102 ± 2	101 ± 1	58 ± 2	59 ± 1	43 ± 1	43 ± 1	0.997	0.8
Θ_{K} [L/R]	118 ± 0	112 ± 0	34 ± 1	35 ± 2	83 ± 1	77 ± 1	0.998	3.4
	114 ± 0	111 ± 0	32 ± 1	37 ± 1	82 ± 1	74 ± 1	0.993	3.1
Θ_{A} [L/R]	12 ± 2	8 ± 2	19 ± 2	18 ± 1	31 ± 1	27 ± 2	0.956	2.8
	20 ± 2	8 ± 2	14 ± 1	22 ± 1	35 ± 2	30 ± 2	0.991	2.2

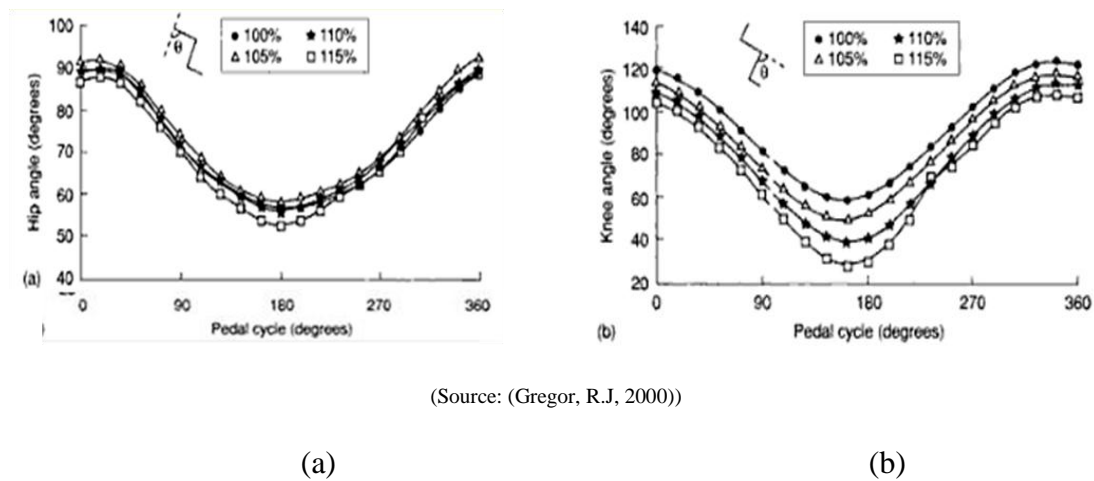
The correlations between measurements for Θ_{A} are slightly less high ($R^2 > 0.956$). The main reason for this is a significant offset of approximately 8° for the right ankle. The cause of this discrepancy is not known. It is assumed that the MVN data is incorrect since the Vicon measured left and right ankles in the same region. However, the dashed black line was plotted after adjusting the data for the offset and it can be seen by the similarity to the left ankle curves that it was a bias error related to the experimental setup. The flexion curves for Θ_{K} appear to have a very similar shape, especially during maximum dorsiflexion (Θ_{MIN}) at the beginning and end of the pedal stroke. However, as Θ_{K} increases into plantarflexion midway through the pedal stroke the Vicon curve is lower. Therefore, it can be said that the MVN appears to measure ankle flexion slightly high while measuring dorsiflexion very accurately. Furthermore, the similarity in general shape of the curves suggests that the differences in ankle measurements with Vicon, unlike the offset error for the right ankle, are related to differences in the processing of data for the biomechanical model for the two systems and not experimental error. It is the opinion of the author that the main cause of the problems in the ankle measurement is that the rotational axes of this joint are defined slightly differently in the MVN system to the Vicon system. This is discussed more fully in Section 2.1.3.

However, when considering the root-mean-square errors (RMSE), the MVN data measured using the KiC algorithm can be considered valid. Measurements for Θ_{H}

were very accurate ($RMSE < 1^\circ$). The Θ_K measurements were slightly higher, with Θ_{ROM} being 6-8° more than the Vicon values, and this is reflected in the RMSE value of roughly 3-4°. Lastly, although caution should be taken when interpreting Θ_A , the RMSE was still below 3° which is in fact very low.

4.1.4. Comparison of results with other studies

Since comparative field measurements are not possible with any other clinical Mocap system, the MVN outdoor data could not be directly validated. Therefore, although the benchmark test with the Vicon showed that the KiC algorithm performed well in the indoor test, it is also helpful to compare the field measurement taken during the road tests with other literature as well. This is especially important to compare normative values for larger test populations, since the Vicon benchmark test in this study was only performed with one cyclist. Although there is a shortage of official studies of sub-elite level cyclist kinematics the author did find a study where flexion measurements were taken for the hip and the knee at different seat heights by Gregor (2000). The flexion curves reported in Gregor's study correlate very strongly with the MVN measurements (compare Figure 30 with Figure 29).



(Source: (Gregor, R.J, 2000))

Figure 30: Flexion angles for (a) hip and (b) knee at different seat heights

Here it is interesting to note that Gregor found Θ_H to have a relatively low sensitivity to saddle height (Figure 30a) compared to Θ_K which changes significantly (Figure 30a). The curves for Θ_H show a uniform offset change of $\sim 8^\circ$ between saddle heights adjusted to 100-115% leg length. Surprisingly, the difference in flexion at different seat heights for Θ_K is effectively half as low for Θ_{MAX} (105-120°) as for Θ_{MIN} (30-

60°). Therefore, Θ_K does not simply shift down with increasing saddle height. Instead, the range of flexion Θ_{RANGE} increases the more the cyclist has to ‘reach’ at the BDC. This means that Θ_{MIN} for the knee is highly variable and dependent upon bicycle fit. However, the general sinusoidal shape for Θ_H and Θ_K remains unchanged with seat height. This is exactly the same pattern as measured with the MVN in Figure 29 and the rest of the outdoor results (compare Figure 33 on page 61).

A summary of the outdoor measurements for maximum, minimum and range of hip, knee and ankle flexion are given in Table 3 (mean and standard deviation). To avoid possible skewing of the data due to changes in kinematics between high, medium and low cycling power, only the mean and standard deviation in flexion for the medium power outdoor tests are given below. The medium power sessions were chosen to most accurately reflect conditions in a typical sub-elite race. Another study by Bini et al. (2008), in which only the range of motion was measured for hip, knee and ankle, is used as a comparison along with those reported by Gregor’s and in Figure 30.

Table 4: Summary of flexion outdoor cycling measurements

	Θ_{MAX} [deg]	Θ_{MIN} [deg]	Θ_{RANGE} [deg]
Θ_H	76 ± 10 (~90 ^{**})	24 ± 9 (54 ± 4 [*])	52 ± 5 (54 ± 4 [*] , 40 ^{**})
Θ_K	117 ± 8 (100-120 ^{**})	32 ± 8 (30-60 ^{**})	85 ± 7 (69 ± 4 [*] , 60-75 ^{**})
Θ_A	12 ± 9	-10 ± 9	22 ± 7 (19 ± 4 [*])

* (Bini, R et al., 2008)

** (Gregor, R.J, 2000)

The average hip values for Θ_{MAX} and Θ_{MIN} are notably lower than those in Gregor’s study. However, it should be kept in mind that Θ_H is measured as the open angle between the thigh and the pelvis. Therefore, Θ_{MAX} and Θ_{MIN} can be affected by the upper body position of the cyclist. In other words, Θ_H will be generally higher for an aerodynamic position than for an upright position. Therefore, when comparing studies it is better to consider Θ_{RANGE} for the hip since the orientation of the hip cannot always be normalized. The MVN outdoor hip Θ_{RANGE} is almost identical to that of Bini, although Gregor reports a significantly lower 40°. As in the validation study, the MVN reports realistic but slightly exaggerated Θ_{MAX} and Θ_{MIN} for Θ_K , resulting in a high Θ_{RANGE} value. However, this may be due to experimental factors

such as differences in ankling patterns (Θ_A curve) and crank length between the sample populations as well. Lastly, due to the high variability in Θ_A amongst cyclists there are no benchmark values for Θ_{MAX} and Θ_{MIN} . However, the Θ_{RANGE} documented by Bini is very close to the outdoor values measured by the MVN.

4.2. Comparison Between Indoor and Outdoor Data

After validating the outdoor data, the second research question was: Is there a significant difference between cycling kinematics measured on a trainer in a laboratory and on the road? Addressing this question involved comparing the indoor and outdoor measurements of Θ_H , Θ_K and Θ_A to investigate the ecological validity of lower leg flexion in the laboratory. This was carried out directly by contrasting indoor and outdoor data, as well as indirectly by evaluating the changes in flexion between high, medium and low power sessions in the laboratory and on the road.

4.2.1. Laboratory and field measurements during medium power test

For the sake of illustration, a comparison of Θ_{IN} and Θ_{OUT} is shown in Figure 31 for the right knee. Each of the ten cyclist's Θ_{MAX} and Θ_{MIN} values are given for each of the six tests (three indoor and three outdoor). The indoor tests are represented by the increasingly lighter shades of red, which signify the decreasing effort from high to low power. Similarly, the outdoor tests are shown in blue.

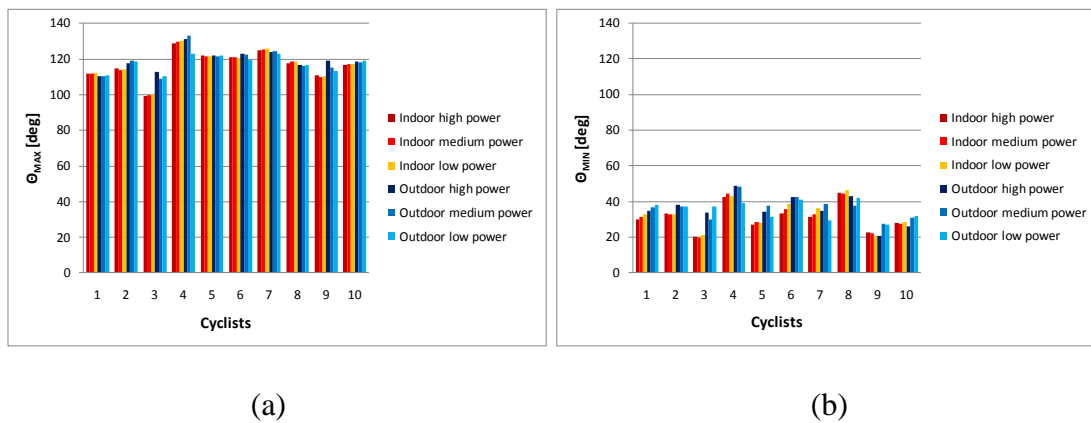


Figure 31: Indoor and outdoor (a) Θ_{MAX} (b) Θ_{MIN} right Θ_K

Observing the height difference between the red and blue columns for each cyclist gives an impression of the congruency between Θ_{IN} and Θ_{OUT} . At the same time, it should be kept in mind that any measurement of biomechanics cannot be expected to

be the same in different tests. However, Cyclist 3 demonstrates a noticeably lower indoor Θ_{MAX} and Θ_{MIN} and can be considered an outlier. Cyclist 3's Θ_{RANGE} appears to be the unchanged; suggesting that an unreported bicycle fit adjustment was made between the indoor and outdoor tests. The seat height was most probably increased after the indoor test, since it was shown that this leads to lower Θ_K values (Figure 30).

The summary comparison of the indoor and outdoor data for all three joints is shown in Table 5. The difference between indoor and outdoor measurements is defined by $\Delta\theta_{avg} = \frac{1}{j} \sum_j (\theta_{IN} - \theta_{OUT})$ where j refers to the ten cyclists. Highly significant differences were defined by a 95% confidence ($P < 0.05$) and are double-underlined. However, considering that the measurements were biomechanical in nature, differences within a confidence level of 80% ($P < 0.2$) were taken as moderately significant in this study and these are single-underlined. Most noticeably, there were highly significant changes in Θ_{MIN} for Θ_H , Θ_K and Θ_A of -6° ($P < 0.015$), -3° ($P < 0.03$) and 4° ($P < 0.04$) respectively. The differences between Θ_{MAX} of -4° ($P < 0.065$), -1° ($P < 0.2$) and 3° ($P < 0.025$) were moderately significant. This means that, on average, the Θ_H and Θ_K curves were statistically higher for the outdoor tests (sometimes over 10° and 5° respectively), whereas Θ_A was lower, sometimes by more than 8° . On the other hand, Θ_{RANGE} remained much more similar for Θ_H and Θ_A (especially), although Θ_K showed a moderately significant change between tests of 2° ($P < 0.09$).

Table 5: Comparison between indoor and outdoor flexion measurements

	Θ_{MAX}		Θ_{MIN}		Θ_{RANGE}	
	$\Delta \theta_{avg}$ [deg]	<u>P_{0.05}</u>	$\Delta \theta_{avg}$ [deg]	<u>P_{0.05}</u>	$\Delta \theta_{avg}$ [deg]	<u>P_{0.05}</u>
Θ_H	-4 ± 6	<u>0.062</u>	-6 ± 6	<u>0.013</u>	1 ± 3	0.234
Θ_K	-1 ± 4	<u>0.198</u>	-3 ± 5	<u>0.027</u>	2 ± 3	<u>0.085</u>
Θ_A	3 ± 5	<u>0.024</u>	4 ± 5	<u>0.039</u>	0 ± 6	0.969

4.2.2. Correlations between low and high power sessions

The indirect method of evaluating the effect of the laboratory testing on cycling kinematics involved an investigation into the way Θ_H , Θ_K and Θ_A changed between high, medium and low power during the indoor and outdoor tests. This was done to test the remarks made by Gregor in the well known book Exercise and Sports Science, which are based on the ecological validity of laboratory testing:

“One fact, however, remain relatively clear: Once the constrained cyclic movement of the lower extremity is established at a seat position and crank length comfortable to the rider, lower-extremity kinematic patterns remain relatively constant. Pushing extreme gears on high load may further modify rider kinematics, but for the most part, in a seated position across a range of loads, rider kinematics is relatively stable.” (Gregor, R.J, 2000)

Figure 32 shows the Θ_{MAX} , Θ_{MIN} and Θ_{RANGE} of Θ_H , Θ_K and Θ_A for increasing cyclist workload (2, 3.5 and 5.5 $W.kg^{-1}$) during the indoor and outdoor tests for all cyclists. As can be seen from the relatively flat lines, there are no drastic effects of power output on joint kinematics, with only minor gradients for some joints. However, upon closer inspection the laboratory results do remain more stable than the field results across different workloads; Θ_{RANGE} for differs Θ_A quite noticeably on the road, while Θ_{MAX} and Θ_{MIN} for Θ_H increase more with cycling power on the road even though Θ_{RANGE} remains relatively constant. The trend for indoor and outdoor Θ_K , however, is more similar and suggests less dependence upon cycling workload for the knee.

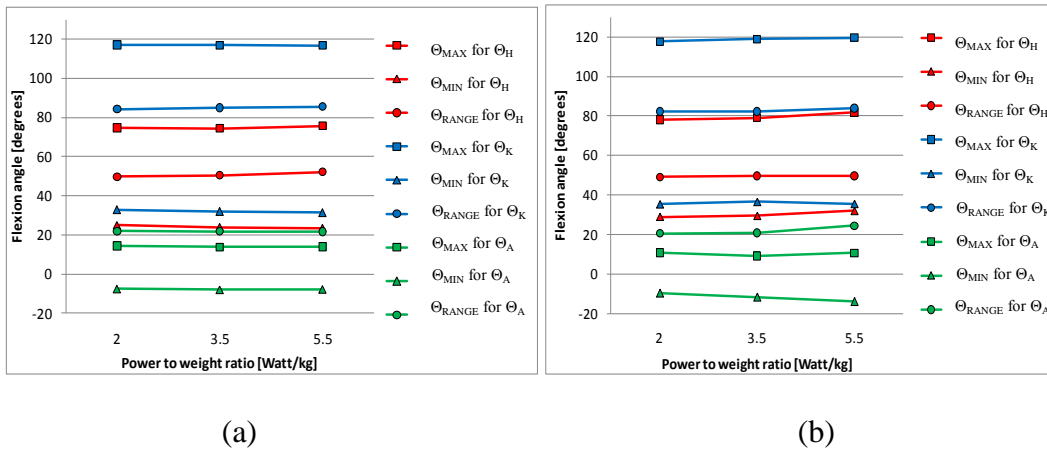


Figure 32: Θ_H , Θ_K and Θ_A in (a) indoor and (b) outdoor power sessions

A summary of the changes in Θ_{MAX} , Θ_{MIN} and Θ_{RANGE} with cycling power for Θ_H , Θ_K and Θ_A is given in Table 6. Correlations are given for each variable between high and low power. Again, highly significant differences are double-underlined and moderately significant differences are single-underlined. For the sake of simplicity, the medium power data is excluded from these values and the average difference in flexion is defined as $\Delta\theta_{avg} = \frac{1}{j} \sum_j (\theta_{high,j} - \theta_{low,j})$ where j refers to the ten cyclists.

It appears that the greatest changes in rider kinematics were for Θ_H with almost all differences being significant, followed by Θ_K with half of the variables showing significant changes and then finally Θ_A where only Θ_{MIN} and Θ_{RANGE} for Θ_{OUT} were moderately different. Interestingly, the indoor Θ_H contained highly significant changes for Θ_{MIN} ($P < 0.05$) and Θ_{RANGE} ($P < 0.001$), and moderate changes for Θ_{MAX} ($P < 0.15$) from low to high cycling power. On the other hand, the outdoor Θ_H contained larger but only moderately significant differences for Θ_{MAX} and Θ_{MIN} of 4° ($P < 0.06$) and 3° ($P < 0.16$) respectively. There were small but moderately significant changes for Θ_K in the laboratory tests; Θ_{MIN} was 1° higher in the indoor low power test, and Θ_{MAX} was 2° higher in the outdoor high power test. The only notable change in Θ_A was 4° increase in dorsiflexion during the outdoor high power test.

Table 6: Comparison of flexion measurements at high and low power

	Θ_{MAX} [indoor/outdoor]			Θ_{MIN} [indoor/outdoor]			Θ_{RANGE} [indoor/outdoor]		
	$\Delta \theta_{avg}$ [deg]	R^2	$P_{0.05}$	$\Delta \theta_{avg}$ [deg]	R^2	$P_{0.05}$	$\Delta \theta_{avg}$ [deg]	R^2	$P_{0.05}$
Θ_H	1 ± 2	0.977	<u>0.144</u>	-2 ± 2	0.955	<u>0.049</u>	3 ± 1	0.936	<u><0.001</u>
	4 ± 5	0.667	<u>0.057</u>	3 ± 6	0.368	<u>0.152</u>	1 ± 3	0.664	0.489
Θ_K	0 ± 1	0.993	0.330	-1 ± 2	0.936	<u>0.062</u>	1 ± 2	0.891	<u>0.104</u>
	2 ± 3	0.766	<u>0.085</u>	0 ± 5	0.644	0.896	2 ± 5	0.613	0.311
Θ_A	0 ± 5	0.827	0.756	0 ± 6	0.641	0.925	0 ± 6	0.560	0.890
	0 ± 7	0.411	0.943	-4 ± 10	<u>0.086</u>	0.249	4 ± 7	0.274	<u>0.121</u>

The superior indoor correlation values for Θ_H ($R^2 > 0.93$ vs. $R^2 > 0.36$), Θ_K ($R^2 > 0.89$ vs. $R^2 > 0.61$) and Θ_A ($R^2 > 0.56$ vs. $R^2 > 0.08$) also indicate that rider kinematics were much more consistent between high and low power during laboratory testing than during the road tests. The increased variability in joint angles during outdoor testing is also easily seen by noting that the standard deviation in $\Delta\theta_{avg}$ is two to three times greater outdoors than indoors for Θ_{MAX} , Θ_{MIN} and Θ_{RANGE} of Θ_H and Θ_K .

4.3. Applications of the MVN Data

This section deals with the last of the three research questions: How can the MVN be used for improving road cycling kinematics? As shown in Section 2.2.4, the best way of optimizing cycling kinematics is by improving bicycle fit. Therefore, three important aspects of cycling kinematics optimization are highlighted in relationship

to bicycle fit: dynamic measurement and analysis of body position, identification of bilateral asymmetry and prevention of overuse injuries.

4.3.1. Dynamic measurement and analysis

As previously discussed (Section 2.2.4), the MVN system is ideal for use in performing dynamic bicycle fits, which are greatly superior to static fits. The insufficiency of static fit methods is illustrated by the test data in this study. As can be seen in Table 3, the standard deviations in Θ_{MAX} and Θ_{MIN} are reasonably high (8-10°). This means that Θ_A , especially, has a standard deviation of almost a third of the Θ_{RANGE} . Together with the high deviations for Θ_H and Θ_K , this suggests that the ‘optimal’ bicycle fit adopted by the test subjects was not highly correlated with saddle position. This is an interesting point. Many static bicycle fit methods make use of anthropometrical measurements to approximate saddle position, which of course assumes certain ideal joint angles. However, these results show that many competitive cyclists with close-to-optimal bicycle fit are riding at very different joint angles.

Static fits have two main weaknesses; firstly they are mostly based on static measurements of parameters such as body dimensions instead of kinematics, and secondly this data is used to predict bicycle fit instead of to optimize bicycle fit. The key to dynamic bicycle fit, therefore, is dynamic and subject-specific measurement of performance indicators which can be used to optimize bicycle fit by monitoring performance before and after interventions. Changes to body position can then be evaluated by monitoring variables such as power output, volume of oxygen and heart rate. However, until recently, clinical Mocap technology had not been available for measuring cycling kinematics dynamically. Dynamic bicycle fits were typically performed by monitoring only the kinetic variables without insight into the kinematics. However, systems such as the MVN offer bicycle fitters detailed, objective and accurate measurements of joint angles while the cyclist is pedalling.

In order to illustrate the value of the MVN data for bicycle fit, the flexion over the crank angle Θ_C are shown in Figure 33 for Cyclist 1 and 7. Since each test session lasted one minute at a fixed cadence of between 90-110rpm the plots contain superimposed measurements of approximately 100 crank cycles, or pedal revolutions. Therefore, the thickness of each curve gives an indication of the consistency of the pedalling technique. Another valuable aspect of measurements taken with the MVN is the crank angles at which Θ_{MAX} and Θ_{MIN} occur. Evaluations of kinematics over Θ_C

give great insight into the points on the pedal stroke at which they occur and usually require some form of rotary encoder to measure. However, a method was developed in this study to estimate the crank angle using position data for the toe segment of the biomechanical model (see Appendix C.2.2 for details).

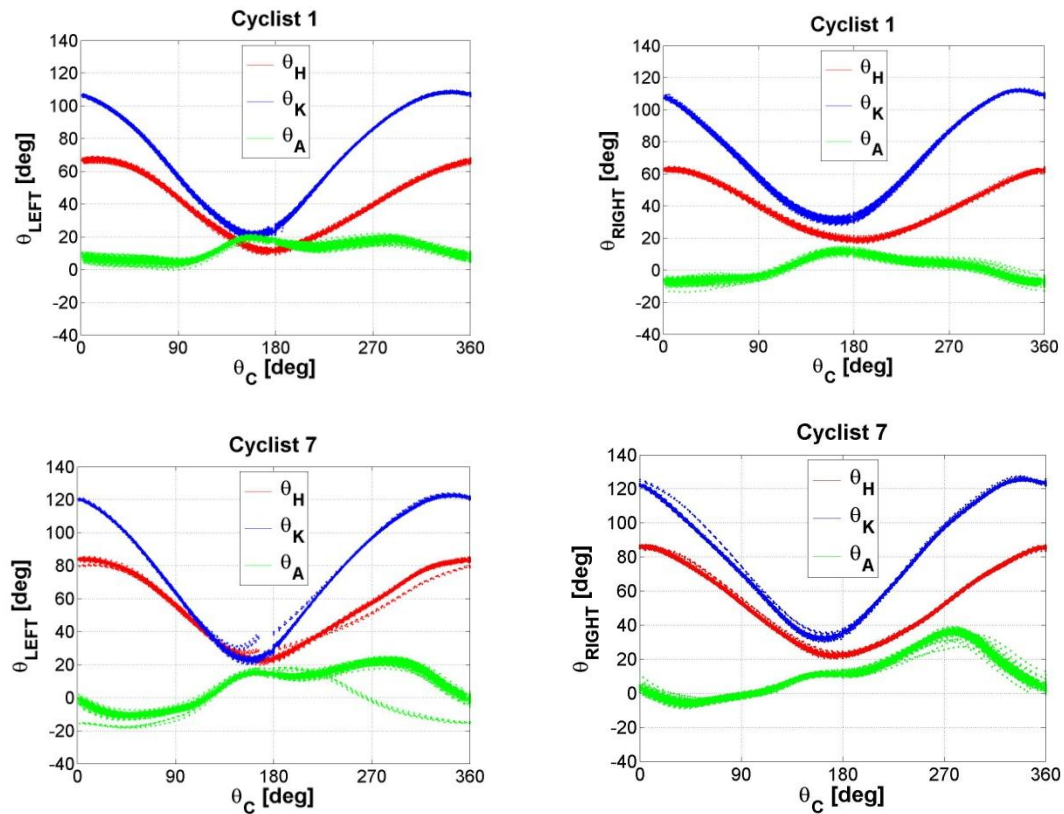


Figure 33: Examples of θ_H , θ_K and θ_A for left and right legs

The crank angle values for θ_{MAX} and θ_{MIN} in Figure 33 (and the rest of the collected data) correlate very well with those in previous studies and serve to validate the method for obtaining θ_C . Gregor’s book, “Road Cycling” (Gregor, R and Conconi, F, 2000), contains hip and knee flexion curves almost identical in relation to the crank angles determined in this study (compare hip and knee curves in Figure 30 to Figure 33). The crank angles in “Road Cycling” corresponding to θ_{MAX} and θ_{MIN} for θ_H ($\sim 20^\circ$ and $\sim 180^\circ$) and θ_K ($\sim 345^\circ$ and $\sim 165^\circ$) were also confirmed by other authors (Farrell, K.C *et al.*, 2003; Timmer, C, 1991). Furthermore, θ_A was evaluated in relation to crank angle in a study conducted by Cavanagh and Sanderson (1986) on elite cyclists. Peak dorsiflexion occurred at 90° , while the maximum plantarflexion was measured at 285° . As can be seen, these values are in line with those in Figure 33

(Cyclist 7 especially). The reason why the peak plantarflexion in the second quadrant is greater for some cyclists is due to less heel lift in the fourth quadrant, which could be associated with poor ankling technique.

Interestingly, Θ_K occurs earlier than would be intuitively expected in the pedal stroke (at the TDC and BDC). This is of course partly due to the fact that the seat post is not vertical but in fact $\sim 75^\circ$ from the horizontal, making the crank angles of 165° and 345° the actual longest and shortest distances from the saddle (and thus hip joint) respectively. However, Θ_H is maximally flexed at the BDC and as much as 20° after the TDC, which does not follow from the above argument. Furthermore, the Θ_C for Θ_{MAX} and Θ_{MIN} varied by $\sim 20^\circ$ in this study. The explanation for this can be found in the large variations in Θ_A that occur between cyclists at these points in the pedal stroke. This is because while the crank angle domains of Θ_H and Θ_K are not very sensitive to changes in saddle height (Figure 30), Θ_A is more a result of neuromuscular activation patterns and learned technique. Therefore, perhaps the most valuable subject specific evaluation is that of Θ_A .

As in Figure 33, Θ_A is generally roughly constant and near zero during the first quarter of the crank revolution, after which it enters plantarflexion to deliver power in the second half of the downstroke. In the third quadrant, during the first half of the upstroke, the heel typically stays lifted as the pedal rises and thus there is minimal change in the ankle flexion. However, between 270° - 360° the heel drops again relative to the pedal which brings the ankle back to a neutral or slightly dorsiflexed position for the start of the next pedal stroke.

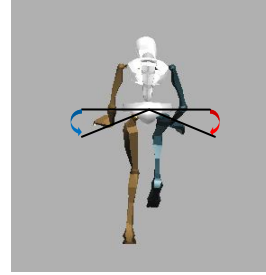
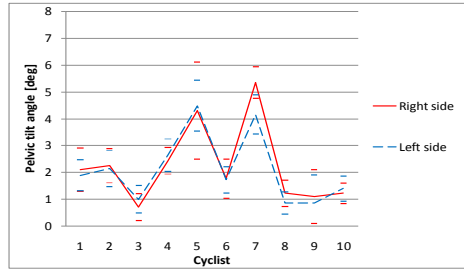
A comparison of Θ_A between Cyclist 1 and 7 in Figure 33 demonstrates that there are notable differences between cyclists and between left and right joint flexion. It can be seen that the range of Θ_A for Cyclist 7 is significantly higher than for Cyclist 1. This is primarily because Cyclist 7's heel lift in the fourth quadrant is much more pronounced. Cyclist 1's left ankle remains in plantarflexion throughout the entire pedal stroke and level for the majority of the upstroke, whereas the right ankle already begins recovering to a neutral position before the BDC. Similarly, there are notable differences between Cyclist 7's left and right ankle flexion patterns. The left leg curve has a similar shape to Cyclist 1, although there is almost double as much range of flexion. This is because the heel is slightly more lifted at 270° and more dropped between 0 - 90° , resulting in higher plantarflexion and dorsiflexion respectively. However, Cyclist 7's right heel is lifted much higher during the middle

of the upstroke, resulting in a high peak plantarflexion of almost 40° and sudden recovery to the neutral position in the last quadrant.

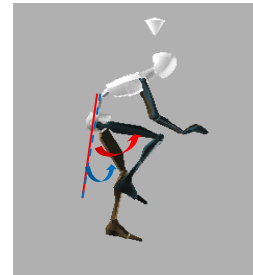
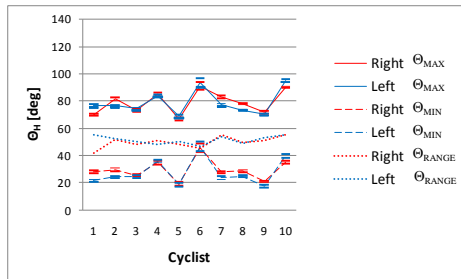
4.3.2. Bilateral asymmetry

As shown in the previous subsection, Θ_A (as well as Θ_H and Θ_K) can vary between left and right joints. One of the aspects of cycling kinematics related to dynamic bicycle fit for which there is a lack of research is bilateral asymmetry. A recent research review of bilateral asymmetry in running and cycling found that bilateral asymmetry is common and highly variable in cycling (Carpes, F.P *et al.*, 2010). According to Carpes *et. al.*, the origins of bilateral asymmetry are not clearly understood, although it is suspected that differences in neuromuscular patterns associated with limb dominance are a major factor. Furthermore, no studies have investigated the effect of asymmetry on performance or risk of injury. Early literature thus far also contains very few evaluations of kinematic asymmetry, with most focussing on asymmetry in kinetic variables such as power, torque and force (Carpes, F.P *et al.*, 2010). Results suggest that asymmetry varies with cadence and workload, although the correlations are not clear (Smak, W *et al.*, 1999). An evaluation of the factors affecting asymmetry in joint kinematics would therefore be a valuable contribution to this new field of study.

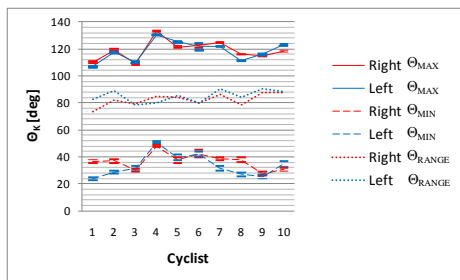
Therefore the difference between right and left leg flexion was investigated using the MVN. Figure 34 shows Θ_{LEFT} and Θ_{RIGHT} for all three joints as well as the pelvic tilt in the lateral plane. Lateral pelvic tilt is important to consider in studies of asymmetry because it is a dynamic factor which can affect Θ_H , Θ_K and Θ_A by changing the orientation of the pelvis. This effectively alters the position of the hip joint centre and thus the distance between the pelvis-saddle and pedal-shoe interfaces. The results for the pelvis (Figure 34a) show that the left and right lateral tilt was almost identical for all the test subjects, with the exception of Cyclist 7 who had a slightly larger tilt on the right side. Furthermore, it can be seen that for most cyclists the pelvic tilt was fairly regular, the standard deviation being approximately 1° (which is negligible) except for Cyclist 5 whose pelvic tilt was slightly irregular at a standard deviation of approximately 2°. However, all in all, the pelvic tilt values are acceptably low. Cyclists 3, 8 and 10, especially, demonstrated exceptionally stable pelvic girdles during the testing, suggesting superior bicycle fit.



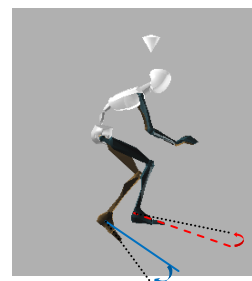
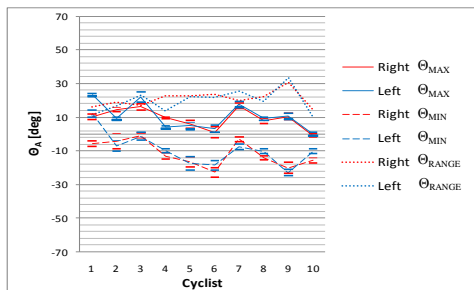
(a)



(b)



(c)



(d)

Figure 34: Asymmetry in (a) pelvic tilt and (b) Θ_H , (c) Θ_K and (d) Θ_A

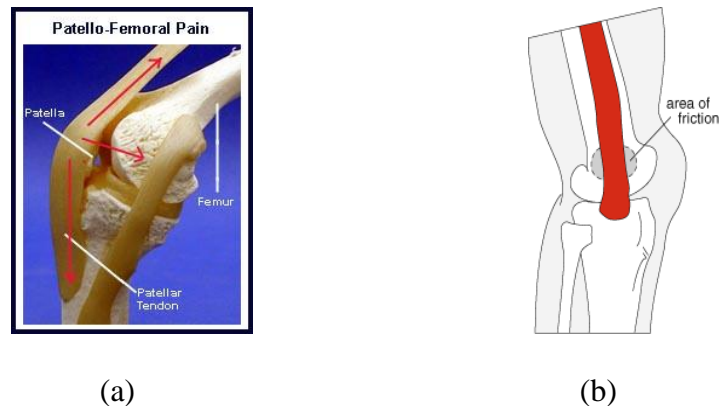
However, the results for Θ_H do show asymmetry for some of the cyclists (Figure 34b). Cyclist 1's Θ_{RANGE} is much higher for the left hip than the right, with a difference of over 10° . This is caused by the lower Θ_{MAX} and higher Θ_{MIN} of the right hip. Cyclists 2, 7, 8 and 9, on the other hand, have almost identical ranges of Θ_H although there is an offset between the Θ_{LEFT} and Θ_{RIGHT} . This indicates that the right thigh (and therefore knee joint) rises higher around the TDC and does not drop as low near the BDC as the left thigh. Cyclist 10 has the same asymmetry problem, although this time the left Θ_H is higher than the right. Conversely, Cyclist 3, 4, 5 and 6 have almost perfect symmetry between left and right Θ_H , although Cyclist 6 seems to have less consistency in his hip motion (note larger deviation).

There is also notable asymmetry in Θ_K . Interestingly, there is very little difference ($<5^\circ$) between most of the left and right Θ_{MAX} values for Θ_K , while some values for Θ_{MIN} are considerably disparate ($>15^\circ$). The Θ_{MAX} values, with the exception of Cyclist 6, also are considerably more consistent than for Θ_{MIN} . This leads to some significant differences in Θ_{RANGE} , especially for Cyclists 1, 2, 7 and 8 whose right knees are noticeably more flexed than the left towards the bottom of the downstroke. On the other hand, just as with the Θ_H results Cyclist 10's range of Θ_K is equal, although the left limb measurements are higher. Conversely, Cyclists 3, 4, 6 and 9 demonstrate almost perfect symmetry for Θ_K .

Finally, the Θ_A measurements clearly show how large the variation in ankling technique is between cyclists, as well as how much larger the standard deviation is for each cyclist. Whereas Θ_H and Θ_K are more consistent (proportionally), here Θ_{MAX} and Θ_{MIN} vary by more than 20° between cyclists. However, despite this, the range of flexion is still relatively stable around $\sim 20^\circ$, with the exception of Cyclist 9 ($\sim 30^\circ$) and Cyclists 1 and 10 ($\sim 10^\circ$). This suggests that although there is a very high variability in Θ_{MAX} and Θ_{MIN} for Θ_A between cyclists, Θ_{RANGE} is more predictable. Surprisingly, however, despite the variability between cyclists the ankles are not any more asymmetrical than the hips and knees for specific cyclists. In fact, upon closer inspection, the left and right ankle values are quite well matched. Cyclist 1 is the clear exception with a large offset between the left and right ankle flexion. The left ankle remains in relatively high plantarflexion throughout the crank cycle, so much so that there is almost no overlap between the left and right ankle's range of flexion! Cyclist 2 and 3 also show some asymmetrical heel lift in the recovery phase, while Cyclists 5-10 demonstrate slight asymmetry in dorsiflexion on the downstroke. Lastly, Cyclist 4 has less left ankle flexion at both ends of the pedal stroke.

4.3.3. Prevention of knee injuries

Another key aspect to consider during bicycle fit is injury prevention. Due to the linear pedalling action and associated lack of sudden muscle contractions during cycling, muscle-related injuries are considered a low risk injury in road cycling. However, the repetitive nature of cycling does lead to overuse injuries, particularly in the knee ligaments. Since there is relatively little abduction/adduction and rotation of the knee joint, most knee injuries occur anteriorly, particularly in the patellofemoral joint (PFJ) and the iliotibial band (ITB). A recent review of lower body problems and injuries in cycling claims that a third of all knee pain can be attributed to the PFJ and that the second highest percentage of knee pain (7%) occurs in the ITB (Callaghan, M.J, 2005). According to Callaghan, the reason for patellofemoral pain in cyclists, more commonly known as ‘biker’s knee’, is still debated. However, it is almost certainly associated with the high reaction force which develops at the surface of the PFJ (see Figure 35a) during maximum flexion of the knee ($\sim 110^\circ$). On the other hand, injuries such as iliotibial band friction syndrome (ITBFS) occur near 30° knee flexion. This is just within range of the lowest point of typical cycling knee flexion near the end of the downstroke. ITBFS is believed to occur, not due to excessive forces (as with PFJ pain), but rather due to repetitive friction of tissue fibres in the impingement zone ($\sim 30^\circ$ knee flexion), which is shown in Figure 35b.



(Source: (Knee Pain Info Website))

Figure 35: The (a) forces leading to PFJ pain and the (b) ITB friction zone

Figure 34c shows that only three subjects (Cyclists 4, 5 and 6) do not have at least one knee joint passing through the impingement zone. Cyclists 2, 8 and 9 are especially susceptible to ITBFS due to flexion minima of $\sim 25^\circ$. However, since range

of motion for knee flexion is quite similar between the cyclists, those with a negligible risk of ITBFS run a higher risk of PFJ pain at the opposite end of the pedal cycle. Cyclists 5 and 6 flex their knees more than 120° , and Cyclist 4 more than 130° , which is very high. It may be therefore inferred that the upper and lower knee flexion boundaries for overuse injuries need to be negotiated by adjusting bicycle fit parameters, most importantly the saddle position. When the saddle is too high or in an overly forward position, the knee flexion decreases which in turn increases the risk of ITBFS and anterior knee pain. On the other hand if the saddle is too low, knee flexion increases and the risk of PFJ pain increases. Therefore, the saddle position should be adjusted vertically and horizontally to ensure that overuse injuries in the knee are reduced near both the TDC and BDC.

4.4. Conclusions

Section 4.1 presented the validation of the MVN outdoor data. This included an analysis of the magnetometer data, results of a benchmark test against the Vicon system and comparisons between the outdoor data and flexion measurements from other studies. The assessment of the magnetic field parameters during testing revealed that the road bicycles caused variable and unacceptable interference to the MVN system. The sensors near the hands and feet were most strongly affected, resulting in a lack of compensation for gyroscopic errors which ultimately degraded the biomechanical model. Therefore, the only measurements the MVN could conduct accurately were hip, knee and ankle flexion using the KiC algorithm. The KiC algorithm performed well in the benchmark tests, showing that accurate measurements of Θ_H , Θ_K and Θ_A can be taken with the MVN even within magnetically disturbed environments. The average values for Θ_{OUT} were also shown to be in line with other studies, although Θ_{RANGE} for the knee was shown to be slightly high. This corresponds to the slightly high Θ_{MAX} and low Θ_{MIN} measurements for Θ_K during the Vicon test. All in all, however, the MVN measurements for outdoor cycling kinematics were proven valid.

Section 4.2 presented results of the investigation into the difference between indoor and outdoor cycling kinematics. It was found that there were small but statistically significant changes in Θ_H , Θ_K and Θ_A between the indoor and outdoor measurements. The changes in hip and knee flexion are hypothesized to be related to subconscious adaptations in body position made during the outdoor tests due to environmental factors. For instance, cyclists may adopt a lower upper body position when sensing

the wind resistance on the road, thus having a more inclined pelvis and therefore a higher hip joint flexion. It is also probable that in adopting a lower trunk position, the cyclist shifts slightly forward on the saddle, leading to a more forward knee joint position and thus higher Θ_K values. In such a situation, the more forward knee position may also lead to a lower heel position and thus a slightly decreased dorsiflexion (greater Θ_{MIN} since dorsiflexion is negative). Furthermore, cyclists on a trainer do not have to worry about their environment or balance and therefore can focus much more on ankle patterns during pedalling, which may also explain the decrease in plantarflexion (Θ_{MAX} for ankle) seen in the outdoor measurements. It was also found that there were some statistically significant differences in cycling kinematics between low and high power. This is a significant result. It rejects the claim quoted from Exercise and Sport's Science that rider kinematics is independent of workload. Moreover, outdoor flexion measurements appear to be more affected by workload. The correlation between low and high power kinematics dropped considerably from the laboratory to the field tests. This may be due to the fact that the wheel fixtures on the stationary trainer restrict the lateral movement of the bicycle.

Section 4.3 demonstrated the applications of the MVN data for improving cycling kinematics. The high variability in the outdoor joint flexion angles between cyclists was used to support the claim that optimal cycling kinematics is not highly correlated with specific values for Θ_H , Θ_K and Θ_A . This showed that static fit methods are poor approximations of bicycle fit and that the MVN data should be used for dynamic bicycle fit. The detailed MVN measurements offer valuable insight into the way a cyclist is pedalling across the entire pedal stroke. It was also shown that bilateral asymmetry is relevant to dynamic bicycle fit and cycling technique, although it is a young field of research which requires more quantitative kinematic studies. Mocap systems such as the MVN offer fitters an improved ability to identify asymmetries with accurate and simultaneous data for both limbs. The results show that kinematic asymmetry is not affected systematically by changes in workload. Conversely, the consistently high asymmetry of some of the subjects (such as Cyclists 1 and 2), may indicate that for these cases cyclist-specific factors, such as discrepancies in leg length, joint flexibility or muscle strength, may be responsible. This illustrates that asymmetry in cycling technique may require different interventions. Some may require a corrective training protocol to improve technique or conditioning, while others may use spacers in one shoe to correct a shorter leg. Lastly, the MVN data can also be used to identify the risk of overuse injuries such as ITBFS and PFJ pain.

5. DISCUSSION

This chapter presents a discussion of the outcomes of this study. Conclusions are made from the experimental results concerning the research questions. Some of the practical lessons learned using the MVN system are given. Recommendations are also made regarding future research in road cycling kinematics using IMCT. Finally, in closing, the wider significance of the research outcomes is discussed.

5.1. Research Conclusions

As stated in the Chapter 1, the primary objective of this study was to evaluate the use of the MVN system for the analysis and optimization of cycling kinematics. Three research questions were formulated in order to guide the evaluation process. This section summarizes the work done and answers obtained for each question.

The first research question was: Can the MVN system be used to conduct field measurements of cycling kinematics? To the author's best knowledge, road cycling kinematics have never been measured before on the road. This presented an opportunity to showcase the portability of the MVN system. However, it was necessary to identify potential barriers to outdoor data collection on the road and validate the accuracy of the MVN measurements. Therefore, the cycling kinematics of ten male competition-level cyclists was recorded with the MVN on an open stretch of road. Each test included three one-minute long sessions at low, medium and high cycling power (2, 3.5 and 5.5 W.kg⁻¹). The cyclists rode their own bicycle and were pursued by a vehicle containing a laptop and the wireless receivers within wireless signal range. Although the outdoor data capture with the MVN was successful there were visible signs of kinematic errors in the biomechanical model. Therefore, in order to assist in validating the outdoor measurements it was necessary to assess the level of magnetic interference caused by road bicycles on the MVN's accuracy.

This was accomplished by analyzing the magnetometer data from each individual MTx for every cyclist. The raw magnetometer signal was extracted from the MVNX files and used to calculate the intensity and inclination angle of the local magnetic field around each MTx on the subject's body. The results of the magnetic analysis, given in Section 4.1, showed that the magnetometer measurements of many of the MTxs on the body segments furthest from the bicycle frame, in other words the upper body torso, were not distorted. However, there was significant interference evident in

the data from the magnetometers near the handlebars and pedals (distal limb segments). Magnetic intensity levels deviated from the nominal value by up to almost 50% in some cases, which resulted in some unrealistic hip abduction/adduction angles of over 45° for some joints. Therefore, it can be concluded that even though most competition-level road bicycle frames and components are manufactured with light-weight materials such as carbon fibre and nonferrous metal alloys, there is still an unacceptable level of magnetic interference to the MVN system caused by road bicycles. This means that the normal MVN fusion engine which makes use of magnetometer heading data to calculate joint angles cannot be used in most cases to capture road cycling kinematics accurately. However, the KiC fusion engine calculates lower limb joint angles in the sagittal plane without the magnetometer data. Therefore, the measurement of hip, knee and ankle flexion is still possible despite magnetic interference during the road cycling tests.

As a result, the short answer to the first research question is that the MVN system is not capable of measuring full-body 3D cycling kinematics on the road. Angles in the coronal and transverse planes (abduction/adduction and internal/external rotation) can thus not be measured accurately with the current technology. However, the outdoor KiC data was found to be valid. The flexion curves calculated by the KiC engine showed a very strong correlation with those in other studies. The general flexion pattern along the crank cycle was almost identical with those in the literature and the flexion maxima and minima occurred at approximately the same crank angles. However, due to the lack of comparative data, it was impossible to validate the KiC data directly. Instead, the KiC algorithm was benchmarked against the Vicon system for an indoor test, since the magnetic environment is inconsequential. The Vicon and MVN KiC data for the validation test showed very high correlations ($R^2 > 0.956$), as well as good accuracy ($RMSE < 3.5^\circ$) for all joints. This validates the accuracy of the KiC algorithm and suggests that the accuracy of the flexion data obtained in the outdoor tests is also very high. It is thus proposed that field measurements of hip, knee and ankle flexion can be successfully conducted using the MVN. Fortunately, these are some of the most important angles.

The second research question was: Is there a significant difference between cycling kinematics measured on a laboratory trainer and on the road? Thanks to the novel outdoor cycling kinematic data obtained with the MVN, the difference between indoor and outdoor cycling kinematics could now be investigated for the first time. To do this, the outdoor test protocol was repeated on a stationary trainer in a

laboratory and the joint flexion measurements for each corresponding power session were compared. The results (given in Section 4.2) showed that on average outdoor flexion at competition-level intensity (medium power) was $\sim 5^\circ$ higher ($P < 0.062$) for the hip and knee $\sim 2^\circ$ higher ($P < 0.198$) on the road, while the ankle flexion was lower by $\sim 4^\circ$ ($P < 0.039$). It was also found that the relationship between rider kinematics and cycling power was significantly different in the laboratory and road tests. While the indoor high and low power session data correlated relatively well for the hip ($R^2 > 0.936$), knee ($R^2 > 0.891$) and ankle ($R^2 > 0.56$), the outdoor correlations were much lower: 0.368, 0.613 and 0.086 respectively. Therefore, the answer to the second research questions is that there is definitely a significant difference between cycling kinematics measured on a stationary trainer in a laboratory and out on the road.

The third and final research question was: How can the MVN system be used for improving cycling kinematics? Although it is generally understood that the optimal body position on a bicycle is highly specific to each cyclist, there is a general lack of scientific data available which quantifies the differences in joint angle excursions by competition-level cyclists. As expected, the joint angles measured for the cyclists demonstrated a large variability. The average maximum, minimum and range of hip flexion varied by approximately 20° , 19° and 10° respectively. Similarly, the variations for the knee (15° , 15° and 13°) and ankle (18° , 18° and 14°) are significant. This large variability in lower limb joint flexion strongly suggests that even though the test subjects may not all have had the perfect bicycle fit, it is not feasible to prescribe optimal bicycle fit parameters such as seat height based on specific hip, knee or ankle flexion angles. This brings into question the validity of performing bicycle fits using static measurements and anthropometrical data alone. Therefore, it is suggested from these results that optical bicycle fit is not defined by specific joint angles in sub-elite cyclists. Furthermore, the primary way in which the MVN system can be used for improving cycling kinematics is through dynamic bicycle fitting.

One of the aspects of cycling technique which is relevant to dynamic bicycle fits is that of bilateral asymmetry of the lower body. Interestingly, kinematic asymmetry was found to be significant in over a third of the test subjects, which supports the findings of other studies. However, discrepancies between left and right joint excursions were found to be relatively unaffected by workload. Rather, asymmetries were specific to the cyclist. These findings demonstrate that the MVN data can be used to diagnose bilateral asymmetry and thereby introduce technical and training

interventions in order to reduce limb dominance and other muscular and anatomical differences. Rider kinematics is often different statically and dynamically and this is especially relevant when evaluating bilateral asymmetry. Therefore, Mocap technologies such as the MVN system have a strong advantage over manual techniques in interpreting the actual kinematics during cycling. Another aspect which was considered was the link between joint excursions and overuse injuries in the knee. The MVN data showed that several of the cyclists were running the risk of ITBFS due to excessive knee extension near the BDC, while others were flexing the knee quite rigorously and were at risk of PFJ pain. Therefore, the MVN system also has value as a diagnostic tool for injuries related to overuse and poor technique.

Therefore, in conclusion, the results of this study indicate that due to magnetic interference caused by road bicycles IMCT cannot yet be used to its full potential in analyzing and improving road cycling kinematics. However, the limited data which was captured accurately outdoors does indicate that field measurements are more realistic than indoor data captured on a trainer. Furthermore, the scope of dynamic fit applications for Mocap data was shown to be comprehensive and vastly superior to approaches not using Mocap technology. These outcomes suggest that the MVN system, with its novel outdoor kinematic measurement capability, has considerable potential of leading to the world's first comprehensive dynamic fit system that can be taken out of the laboratory and out onto the road.

5.2. Lessons Learned

The following section presents some of the lessons learned during the research. This includes discussions of the aspects of the MVN and the indoor and outdoor protocols that can be improved in future work.

5.2.1. MVN operating principles

The first step in this study was to research the working principles of the MVN system. Firstly, this was important because there was a need for greater technical expertise in IMCT in BERG. Secondly, it provided a strong theoretical groundwork for the work in this study. The task involved reviewing the PhD dissertations and research publications which led to the design of the MVN system, as well as the official MVN documentation. The results of this literature study are presented in Section 2.1. The entire Mocap process (MVN sensor fusion scheme) was discussed in detail, including the inertial navigation system, the Kalman filtering techniques

employed for sensor fusion and a review of the biomechanical model. The methods employed for eliminating the errors prevalent in the inertial sensor data were also explained. The sensor fusion used to reduce integration error in the gyroscope measurements was described. Furthermore, an overview was given of the kinematic constraints in the biomechanical model used to compensate for accelerometer drift error. Most significantly, the various types of magnetic interference compensated for by the MVN were discussed, including *a priori* mapping of permanent constant distortions, disturbance rejection Kalman filtering for temporary constant or varying disturbances and KiC for permanent varying disturbances. Lastly, the appendices provide supplementary information on the MVN; an overview of the internal operation of the inertial sensors (Appendix A.2) and technical specifications for the MVN hardware (Appendix B.1).

5.2.2. Practicalities of data collection using the MVN

It should be noted that the calibrations of the biomechanical model are perhaps the single most important (and underestimated) factor in determining the accuracy of the MVN recordings. While lower quality calibrations may render a realistic-looking body model sufficient for visual purposes such as animation work, the actual kinematic data will not be sufficiently accurate for biomechanical analysis. Firstly, as previously mentioned, it is important to perform the calibration in an undisturbed area. This is more important than avoiding magnetic distortions during recording, since the system can reject many of these if the initial condition is undisturbed.

Secondly, the posture of the test subject during calibrations is of utmost importance. Care should be taken to strictly align the sensors and body segments with the assumed position shown in the MVN instructions. For instance, the orientation of the sensors should be in the right plane, especially for the MTx on the pelvis, which must point exactly up the spine and be in the coronal plane. In terms of the stationary poses, one should ensure that the width of the feet is the same as the width of the hips, that the thumbs point forward during the N-pose and that the palms are parallel to the ground during the T-pose. For the movement poses, the correct technique is required for the squat and the right grip is crucial for correct wrist joint location in the hand-touch calibration. As mentioned earlier, the squat calibration could not be performed during testing due to the cleats on the subjects' cycling shoes. However, it is recommended that a platform be designed for the cyclists to stand on that negates the effect of cleat protrusion during the squat calibration. Lastly, it is also important

that all calibrations be performed on a flat surface. This is especially relevant to outdoor tests where footing may not be level.

The accuracy of the anthropometrical data used to scale the body model should also be considered. The accuracy of the segment lengths is lowered when using the default inputs of only height and foot size since the rest is estimated statistically. These incorrect segment lengths affect the estimation of joint centres and angles. However, anthropometrical measurements are subject to error and should only be carried out by qualified personnel. Furthermore, discrepancies between MTx positioning on different subjects is common and should be considered as a source of measurement inaccuracy. Since skeletal dimensions vary between test subjects, MTxs are often positioned in slightly different positions on the body relative to the joint centres for the same size Lycra suit. This can be remedied by replacing the estimated distances between the joints and sensors used in MVN Studio with the actual measured distance. However, this also requires accurate clinical measurements.

Another important issue regarding the MVN data is the initial magnetic conditions of the recording. Although it may seem sensible to record only the kinematics that is of interest (in the case of this study the constant power session of the test protocol), this is not recommended. The seated position of the subject on the bicycle should be considered a magnetically disturbed scenario for the suit due the metal on the bicycle. Therefore, if the recording is started when the cyclist is already riding the Kalman filter begins with a magnetically disturbed initial condition. This hinders the Kalman filter's ability to map and reject the presence of distortions in the magnetic field. It is therefore recommended that any recording should be started with the test subject walking in a totally undisturbed area for a few seconds before climbing on the bicycle. This allows for successful reprocessing of the MVN files in MVN Studio, which is not possible if the recordings begin with the cyclist on the bicycle. Unfortunately, this instruction is not made explicit in the MVN BIOMECH user's manual and was therefore not known or carried out for the majority of the testing phase. However, this is more of a general issue with the MVN and did not affect the KiC measurements.

5.2.3. Indoor and outdoor measurement of road cycling kinematics

The use of a stationary trainer presents many challenges. First of all, trainers usually contain large amounts of ferrous material which distort the magnetic field around the subject's lower body. Even when the frame was replaced with an aluminium replica,

the brake unit near to the feet still interfered with the magnetometer signals. This resulted in incorrect ankle joint measurements. It is highly probable that the magnetic brake system distorted the local magnetic field more so than some other brake types may. However, the choice of brake was also determined for realism and the option of power metering. Wind brake systems, which are the economical option, provide a poorly simulated road 'feel' and generate large quantities of noise. However, commercial fluid-based brakes systems, which offer more realistic power-speed curves and make far less noise, do not usually offer built-in power measurement.

One of the solutions to the magnetic interference of the brake would be to design a customized indoor trainer for use with the MVN. Either power metering could be integrated with a fluid trainer, or the magnetic brake could be distanced from the cyclist using power transmission methods (for instance with a belt and pulley system). For future indoor studies, it is suggested that a fluid trainer be used and that the power measurements be carried out externally from the brake system. However, this presents a problem for testing since the only other place for a power meter is on the bicycle and would require each participant to own one, which would limit the size of the test population considerably.

The trainer is also not the only source of magnetic interference in the laboratory. The metal reinforcement in buildings presents a hostile environment for the MVN system. Indoor testing is possible for cycling research with the MVN, however, it is not recommended. As expected, the outdoor recordings with the MVN generally experienced less magnetic interference than the indoor tests. The only problem that was experienced was a poor signal range when placing the wireless receivers close to each other in the vehicle. This was remedied by using USB extension cables and placing the receivers an appropriate distance apart. Since the stretch of road used for testing was generally undisturbed by traffic, the pursuit vehicle was able to easily maintain an adequate following distance. However, there is a minor risk of losing the wireless connection during a test, which can result in a lost recording. Care should be taken to select the software setting for saving a partial recording during signal loss. Another consideration for outdoor testing is gradual inclinations on the test route, which are not immediately noticeable. These can significantly alter the power-to-speed correlations used for testing and care should be taken to complete each test in the same direction on the stretch of road.

5.2.4. Recommendations for future testing

It is crucial that the data collection be developed qualitatively and quantitatively in order for future work to be effective. The current data needs to be both improved and expanded. Firstly, it is highly recommended that the first priority of future work be to eliminate the magnetic interference caused by the road bicycles. If the magnetic problems can be solved, the full potential of the MVN system can be realised for the analysis of road cycling performance and the scope of measurement data would be greatly enlarged. This includes the measurement of joint angles in all three dimensions, instead of only flexion angles. Abduction and rotation angles are necessary to perform full biomechanical analysis of pedalling technique (for example patella tracking in the frontal plane), rotations of feet at the cleat-pedal interface etc. Furthermore, the inclusion of upper body data would enable further research into optimal bicycle fit such as for aerodynamic efficiency and positioning of the arms.

However, there are many complications involved with removing the magnetic interference. The only feasible way of doing this is to design a magnetically neutral road bicycle. This would involve adapting a top-end carbon fibre bicycle with customized components made of metals such as aluminium and other alloys and would involve considerable design and testing to accomplish. One of the greater concerns with a custom bicycle is its ability to accommodate different cyclists. The advantage of athletes being tested on their own bicycles is that the bicycle frame is already sized according to their height and body size. Furthermore, the types of saddles and pedals (to name a few) also vary between bicycle makes and this may have an impact on the rider's comfort and cycling technique. Before testing each cyclist, a complete bicycle fit would need to be conducted. This may even involve changing the frame, cranks or handlebar stems. Therefore, a custom road bicycle would present challenges in terms of the variability of cyclists' physiques and preferences in cycling brands.

One way to overcome this would be to develop a stationary bicycle with adjustable frame tubes and cranks, which could be adapted easily for different cyclists. The advantage of such a setup would be that the measurement process would be more controllable than on the road. However, it would introduce a loss of realism due to the laboratory environment as well as potential magnetic interference from the building. The former problem should be considered in the light of the testing requirements and ecological validity, whereas the latter would require the stationary bicycle to be used outdoors if necessary. Another way to overcome the problem of

having to adjust the bicycle would be to design a proper outdoor road bicycle and acquiring multiple size frames, cranks, handlebar stems and other components so that the bicycle could be fitted to the test subject. This would solve the challenges associated with the stationary bicycle and enable outdoor testing, which is most desirable. However, it would involve a considerable amount of work to complete the pre-test bicycle fit.

It is also highly recommended that a protocol be developed for clinical measurements of a test subject's anthropometry required for the MVN biomechanical model. Certified anthropometrical measurements are needed to improve the accuracy of the kinematic measurements. For example, a cyclist with abnormally long femur bones would have different knee angles when pedalling than the MVN system would estimate using the normal femur length for that cyclist's height and shoe size. Therefore, by inputting subject specific anthropometrical data into the biomechanical model the measurement performance of the MVN would be improved. However, attempts at taking clinical measurements of body dimensions should be approached with caution by untrained personnel since there is a high risk of measurement error. For this reason, these were not carried out for this study and the body dimensions were instead estimated automatically by the MVN system using a statistical model (based on height and foot size only) and regression equations.

Moreover, due to slight variations in body fit for each cyclist, the Lycra suit does not fix the MTxs to exactly the same anatomical landmark each time. Although some of these inconsistencies are eliminated during the calibration, it is necessary to account for this discrepancy in order to maximize the accuracy of the kinematic measurements. Fortunately, this is accommodated for in MVN Studio (for the lower body) by inputting further clinical measurements of the distance between each MTx and a bony landmark on the corresponding proximal joint. Therefore, it is crucial for accurate kinematic measurements that detailed anthropometrical data be used to scale the MVN biomechanical model and improve the segment and joint centre approximations.

5.3. Recommendations for Future Cycling Research

Future studies in road cycling performance using the MVN should recognise the secondary nature of kinematics in most cases. Most often, technique is a means to an end. For example, although cycling kinematics is important, it is ultimately the

kinetics of cycling (the forces propelling the bicycle), which ultimately determine the performance. Therefore, the MVN data should ideally be used along with force measurements, such as cycling power, to assess optimal bicycle fit. Modern equipment allows for a diversity of force measurements in cycling, such as 3D pedal forces for individual feet and even pressure distributions across the sole of the shoe during pedalling. These forces can also be used to calculate joint moments using inverse dynamics. Furthermore, the process of power production before the pedal forces are exerted is very important to understand for performance enhancement. This includes the cardio-respiratory system, the indicators of which are volume of oxygen (measured in a VO_2 test) and heart rate (measured using heart rate monitors). Once the oxygen inhaled reaches the muscles, power production is realised through coordinated muscle contractions. These muscle activation patterns are measured using electromyography (EMG) devices. It is highly recommended that future work be focused on integrating the MVN data with force, metabolic and neuromuscular data to gain a more comprehensive outlook of the performance parameters.

There are a broad number of key focus areas for future research. Perhaps the key application of the MVN suit is in the area of dynamic bicycle fit and biomechanical analysis. Studies considering the effect of interventions to technique on cycling kinematics and performance would be of value in implementing improved training methods. It is recommended that dynamic fit protocols be developed and tested for improving biomechanical efficiency and reducing the risk of injuries. This type of work would not only be relevant to elite and sub-elite cyclists, but to the amateur field as well. Moreover, research into the differences in kinematics between male and female athletes may offer insight into how cycling equipment could be made more gender specific. Similarly, the cycling technique of younger athletes could be researched in order to understand the way in which children and teenage cyclists should adapt their technique at different stages of physical development.

The effect of fatigue on cycling kinematics should also be investigated. In this study, steady state cycling was recorded for extremely short periods, thus effectively making each recording a “best effort” by the cyclist. However, longer recordings using the MVN suit are possible and would provide insight into how technique changes over time in a race. This would be especially valuable if conducted outdoors. Furthermore, Mocap recordings of entire races would include data from various inclinations (hills) as well as during changes of direction (cornering). Only straight and level cycling was considered in this study, although cycling kinematics during climbing,

descending and cornering are significantly different and should also be optimized for best performance.

Finally, the analysis of cycling kinematics would benefit greatly from the software tools available today. Due to the complex interdependencies between multidimensional factors in cycling performance, it is the author's strong opinion that attempts to create standardized optimizing protocols for aspects such as bicycle fit should be focused on creating neural network prediction models. The high computational power of neural networks is required to handle cyclist diversity and find the trends in anatomical, physiological and mechanical measurement data. Of course, such a model would demand extremely large databases and comprehensive measurements which would be a challenge. In a similar vein, an emerging software tool for biomechanical analysis is dynamic biomechanics simulation software packages such as LifeModeler, that can be used to create virtual cyclists to simulate kinematics and kinetics during cycling. The MVN system's kinematic data could possibly be used to drive the simulations and validate the kinetic estimations of the software with force measuring instruments.

5.4. Significance of Research

Overall, it can be said that the research presented in this thesis successfully fulfilled the research objective. Each of the three research questions was systematically addressed, providing valuable insight into the use of the MVN for road cycling analysis. Furthermore, a significant knowledge base was also built up for future work using the MVN system. Therefore, this study stands as a technical reference for BERG researchers and students in forthcoming projects. In addition, as mentioned in the research motivation (Section 1.2), the results of the study also have a wider relevance to the fields of motion capture, sports science and road cycling.

The magnetic analysis and validation of the KiC algorithm is a valuable contribution to the field of Mocap at large. It supports the accuracy of clinical measurements of lower body flexion taken with the MVN, even in magnetically disturbed environments. This is especially applicable for researchers conducting ambulatory testing in buildings, for example gait analysis, since it is primarily the legs which require immunity to the magnetic interference caused by ferrous metals in the floor. Furthermore, the experiments demonstrate the novel clinical implication of IMCT (provided there is no magnetic interference). The MVN's ability to conduct accurate

field measurements of full-body kinematics opens up new and promising clinical applications for motion capture outside of the entertainment field, like telemedicine, ergonomics in the workplace etc.

The results of this study also demonstrate the use of IMCT for clinical outdoor measurement of sports technique to the sports science community. Besides a few exceptions, sports scientists have generally been slow to adopt any Mocap technology for research purposes, probably because of the high cost and limited scope of testing associated with the traditional optical systems. This is now beginning to change as Mocap improves and sport becomes more technology-orientated. However, although the IMCTs are provided at a much lower cost systems and have a much wider scope for measurement compared to optical systems, there are still barriers to its wide-scale adoption: a lack of validation studies, the MVN's image as an entertainment technology and the perceived sufficiency of the Vicon system. Another factor may be the lack of collaboration between sports science practitioners and engineers required to bridge the ever-widening technology gap associated with Mocap systems. However, this study illustrates the value of understanding the inner workings of systems such as the MVN in order to perform project-specific analysis (for example magnetic analysis of raw sensor data). Furthermore, this study contributes to the necessary exposure for IMCT to act as a catalyst for future sports science studies of outdoor sports kinematics.

Finally, the results of this study contribute to the field of road cycling in a number of ways. Firstly, they contain the first documented field measurements of road cycling kinematics using a clinical Mocap system. The differences found between the indoor and outdoor tests suggest that rider kinematics are statistically different and are more affected by changes in cycling power on the road than on a trainer. This opens up an interesting discussion about the use of indoor data to assess road cycling performance and may alter the perception of the ecological validity of laboratory road cycling. Secondly, this study also displays the relevance of IMCT for performing better bicycle fits. The combination of the outdoor measurement capability of the MVN with the applications of the data for dynamic bicycle fit holds the prospect of a major breakthrough in bicycle fitting for road cycling. This is the most notable contribution made by this study.

APPENDIX A THEORETICAL WORK

A.1 Mocap Overview

This section provides an introduction to the concept of Mocap, covering its general working principles and the prominent Mocap technologies in the industry.

A.1.1 General working principles

Mocap can be described as the tracking and digital replication of physical motion. Human Mocap, therefore, involves the tracking of a person's full body kinematics, which can then be rendered on a computer screen. Mocap systems track external markers placed on the body and then translate the marker kinematics into predicted body kinematics using computer software. Therefore, digital rendering of captured motion is generally conducted in two stages: firstly, tracking the markers representing individual landmarks on the body and secondly, assembling the anatomical body model using estimation algorithms and a predefined biomechanical model. This process is illustrated in Figure 36.

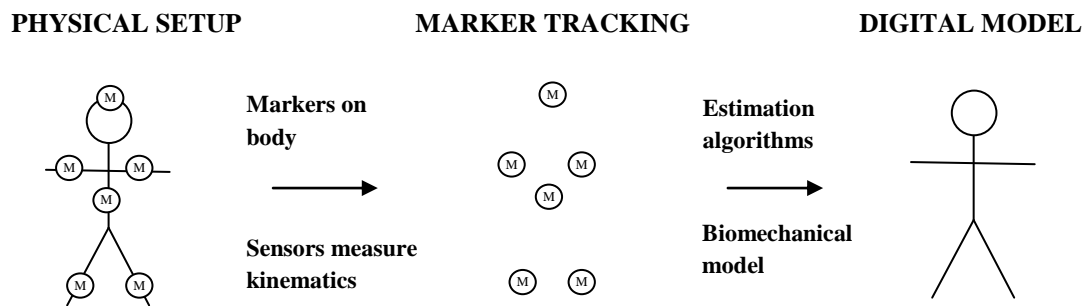


Figure 36: Basic universal Mocap principles

The marker tracking in all Mocap involves a source (signal transmitter) and a collector (sensing receiver). Mocap systems use either transmitter markers or receiver markers. If the markers are transmitters, the receiver will be an external sensor which tracks the movement signal of the markers, for example a camera. Alternatively, if the body markers are receivers the markers will contain some form of sensor to track their own motion with reference to an external transmitter signal.

A.1.2 Types of Mocap

There are three basic categories of Mocap based on the placement of receivers and transmitters: outside-in, inside-out and inside-in (Menache, A, 2000). These different Mocap implementations are illustrated in Figure 37.

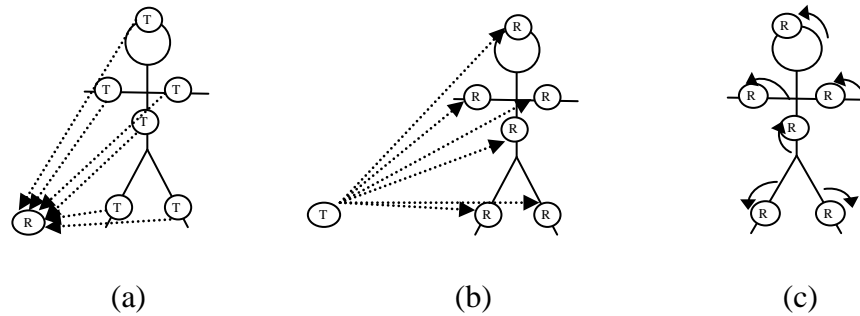


Figure 37: The (a) outside-in (b) inside-out and (c) inside-in Mocap methods

Receivers can either be placed ‘inside’ or ‘outside’ the moving system (human subject). The words ‘in’ and ‘out’ likewise refer to the placement of the transmitter, also relative to the subject. Therefore, in outside-in systems (Figure 37a), the receiver is externally located and the markers transmit a signal to it from the body. On the other hand, inside-out systems have receivers on the human body which measure an external signal (Figure 37b). Finally, inside-in systems have receiver markers which can actually sense their own kinematics and thus the transmitted signal is actually the body motion itself (Figure 37c). In order to illustrate this concept, the dominant technologies in each of these three categories are briefly described.

The most successful implementation of the outside-in approach is optical systems. Optical technologies utilize vision-based methods of Mocap which have developed from the field of computer vision and use cameras as receivers to capture the motion of the markers. In these systems numerous light-emitting markers are placed on bony landmarks of the body. These markers can be either passive or active. In passive marker systems the markers are made of retroreflective materials that reflect external light and can thus be located in 3D space using multiple camera images. Active markers, on the other hand, emit their own light using multiple LED’s which enlarges the capture volume at the cost of powering each marker. Optical systems can track large numbers of markers, have minimal attachments to the body and deliver high accuracy measurements at high frame rates. However, they are expensive systems that have long setup times and suffer from capture area restrictions due to the use of

fixed cameras and marker occlusion when line of sight between the cameras and the markers is obstructed.

Although marker-based optical systems still dominate optical Mocap, new markerless technologies are emerging which use advanced feature detection algorithms from the field of pattern recognition to quantify human motion from video. Since they remove the need for transmitters, these markerless systems are seen as the future for many Mocap applications (Mündermann, L *et al.*, 2006). However, markerless Mocap has not yet been validated for clinical applications that require very accurate kinematic measurements.

Secondly, inside-out Mocap is mostly used in magnetic systems. These use an external electromagnetic field generator as a transmitter and multiple magnetic sensors as receiver markers. The sensors measure the low frequency field and then an onboard control unit uses these measurements to determine the marker position and orientation in the transmitted magnetic field. The advantages of magnetic systems are their relatively lower pricing and lack of occlusion errors. However, the use of magnetic fields means that the capture volume is small and extremely vulnerable to magnetic disturbances.

The third and last type of Mocap, inside-in, is implemented in two popular technologies: mechanical and inertial. Mechanical systems consist of an exoskeleton worn by the subject, which comprises multiple angular encoders (goniometers), connected by links that are fixed to the limb segments. The goniometers act as receiver markers and measure joints angles directly using trigonometry. Mechanical systems are highly accurate for simple joints and can be used outdoors, although they are quite cumbersome and present sensor alignment issues in multiple-degree-of-freedom joints such as the shoulder.

Inertial Mocap, on the other hand, uses inertial sensors as markers, fixed to body segments (instead of joints) to directly measure the physical segment kinematics. This is possible because inertial sensor units can sense their own position and orientation using miniature internal accelerometers and gyroscopes. The signals for these sensors are converted into full body kinematics using inertial navigation systems, sensor fusion schemes and a biomechanical model. Inertial systems can be used outdoors, have extremely low setup times and high sensitivity to movement nuance. However,

they are susceptible to drift errors from integration of the sensor signals and thus experience cumulative measurement errors.

In conclusion, optical systems are the current Mocap benchmark in terms of accuracy although they are restricted to laboratory use and require direct line of sight. Magnetic systems cost less and are occlusion-free although they have the smallest capture area and are highly susceptible to magnetic disturbances. However, both require highly controlled environments in which to perform measurements. Mechanical systems are untethered and therefore solve the problem of spatial restrictions, although they can impede certain movements. Inertial Mocap has the same strengths and is less cumbersome, although sensor drift and magnetic interference are a problem.

A.2 MVN Inertial Measurement Units

This section contains a description of the operating principles of the three sensors used in the MVN MTxs: damped mass accelerometers, vibratory structure gyroscopes and AMR magnetometers.

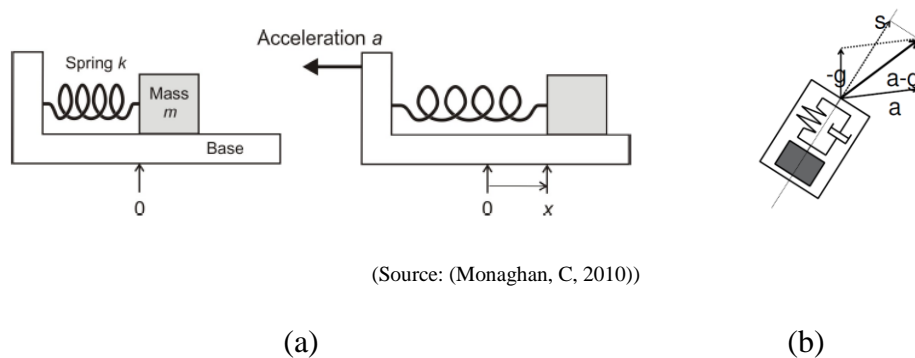


Figure 38: Accelerometer (a) principles and (b) signal output vector diagram

Figure 38 is a simplified 2D schematic of the accelerometers used in the MTxs for the purposes of illustration. According to Newton’s second law of motion, when the MTx experiences an acceleration a the proof mass m_a is displaced by a distance x_s from its initial position and thus stretches the spring (Figure 38a). In keeping with Hooke’s law of elasticity, the reaction force in the attached spring is equal and opposite to the force exerted on the MTx and proportional to the displacement x_s and spring constant k_s of the spring (ignoring friction). Therefore, the accelerometer can measure linear

acceleration by detecting the displacement for the known spring constant and proof mass according to Equation 12.

$$\begin{aligned}
 F_a &= -F_s \\
 \therefore m_a a_a &= k_s x_s \\
 \therefore a_a &= \frac{k_s x_s}{m_a} \tag{12}
 \end{aligned}$$

The accelerometer also senses the direction of the gravitational acceleration g which must be subtracted from the acceleration vector to get the pure sensor acceleration. This is done by using a filter to separate the high frequency accelerations from the constant g (Figure 38b). The 3D acceleration signal, which is inputted to the MVN sensor fusion scheme, is thus calculated in vector form as in Equation 13.

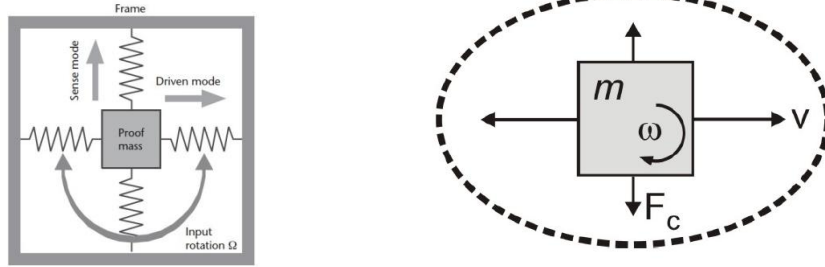
$$s_s = s_a - s_g \tag{13}$$

The angular MTx data is obtained using a specific type of gyroscope called a vibratory structure gyroscope, or Coriolis vibratory gyro. This device measures rate of turn (angular velocity) based on the Coriolis Effect. The Coriolis Effect refers to the apparent deflection of an object when viewed from a rotating frame of reference. This can be illustrated by the example of an airplane, which travels along a path that appears straight to the pilot but is curved when observed from the ground due to the rotation of the Earth. Newton's laws cannot be directly applied in this situation since they govern motion occurring in an inertial frame of reference. However, when transforming Newton's equations to a rotating frame of reference, the Coriolis Effect comes into play. The so-called Coriolis acceleration, which causes the apparent deflection of the flight path, is similar to centrifugal force and is proportional to the cross product of the velocity of the airplane v and the angular velocity of the Earth Ω as in Equation 14.

$$a_c = -2(\Omega \times v) \tag{14}$$

The gyroscope's vibratory structure contains a proof mass m which is vibrated using tuning forks. This driven vibration due to the resonating tuning forks occurs in a specific plane. When the sensor unit is rotated at angular velocity ω , the proof mass experiences a vibration due to the Coriolis force F_c which is perpendicular both to the plane of the driven axis v and the axis of the rotation. This orthogonal vibration can

be detected by capacitive electrodes under the masses and, by a known relationship with the Coriolis force, be used to calculate the angular velocity of the sensor unit.



(Source: (Tawfik, H, 2009))

Figure 39: Schematic of vibrating mass gyroscope working principals

Due to this known relationship, the gyroscopes in the MTxs can be used to determine the rotation of the MTx using a vibratory structure similar to the diagram in Figure 39. The Coriolis force is given in Equation 15 by substituting a_c from Equation 14 into Newton's equation $F_c = ma_c$. The Coriolis force can be measured for the known vibratory mass m , and then used to solve for Ω and thus the angular velocity ω .

$$F_c = -2m(\Omega \times v) \quad (15)$$

Thirdly, magnetometers are employed to obtain the bearing of the MTx in a global reference frame. The magnetometers used in the MTx contain a nickel-iron (NiFe) permalloy thin-film resistor, which has a property called anisotropic magnetoresistance (AMR). The film has a unidirectional magnetization vector that aligns itself with the local (usually the Earth's) magnetic field. Significantly, the electrical resistance of this ferromagnetic material is dependent upon the phase angle between its magnetic field and the current running through it.

The AMR magnetic sensor in Figure 40a measures voltage across the permalloy resistors, as shown in Figure 40b, for a given current to calculate the electrical resistance. This resistance is then used to calculate the angle between the current and the local magnetic field from a known relationship. By fixing the angle of the current in the magnetometer in a known direction (usually 45° to the permalloy structure), the angle of the magnetic field can be calculated by measuring the resistance value of the

magnetometer resistor and solving for the angle measured from the offset value of the current angle in Equation 16.

$$R = f(\cos^2 \theta) \quad (16)$$

In conclusion, each MTx contains three 3D MEMS sensors: a damped-mass accelerometer, a vibrating-mass gyroscope and an AMR magnetometer. The signals from these three sensors include 3D linear acceleration (m.s^{-2}), 3D angular velocity (rad.s^{-1}) and 3D Earth magnetic field (mGauss). These measurements are the inputs to the INS in the MVN sensor fusion scheme.

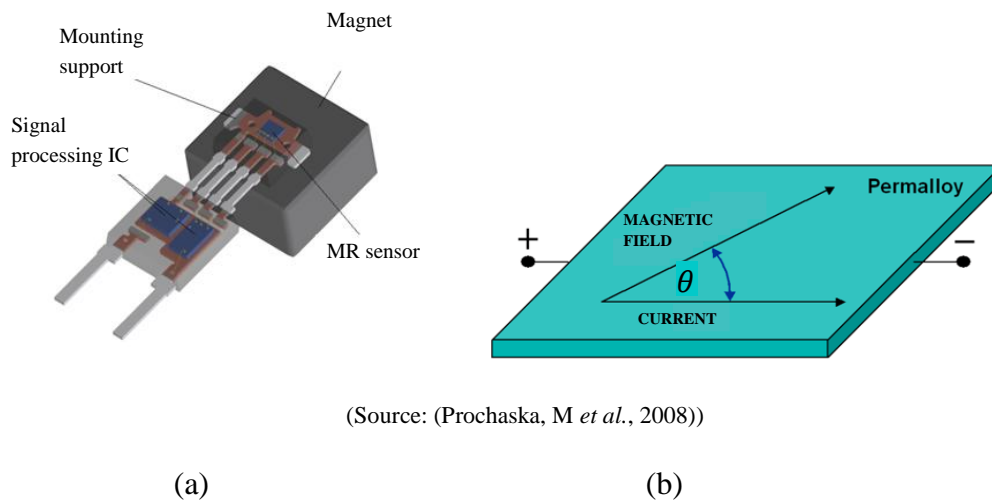


Figure 40: An AMR (a) sensor and (b) the AMR principle.

A.3 Road Cycling

This section presents a supplementary review of research findings in the area of optimal cycling kinematics. It provides theoretical background on road cycling performance and bicycle fit.

A.3.1 Cycling kinematics and performance

The basic goal of cycling performance optimization is to complete a race in the shortest possible time. Therefore, optimal performance occurs when the highest average speed for a race is achieved. This equates to maximizing the forces propelling the bicycle (in other words power production), and minimizing the forces repelling the bicycle motion (power demand). It also includes minimizing fatigue, discomfort and injury. Therefore, in broad terms, IMCT systems such as the MVN

should be used to optimize the body position of cyclists in order to maximize pedalling efficiency and minimize aerodynamic drag, fatigue, discomfort and injury so that the highest possible average speed is attained. However, this is a complex challenge which is sometimes obscured by the diversity and intricacy of human bodies.

Firstly, it is important to identify the elements of cycling which fall under the broad categories of power production and power demand. Factors affecting cycling performance include a plethora of overlapping aspects such as cyclist genetics, physiology and training, aerodynamic and biomechanical efficiency, muscle recruitment and gross mechanical efficiency, pedalling cadence and gearing, aerobic economy and intensity, bicycle technology, pacing strategy and environmental conditions (Atkinson, G *et al.*, 2003; Faria, E.W *et al.*, 2005b). However, research has also highlighted that these factors have varying degrees of importance. For instance, it has been shown that besides training, the largest performance improvements can be gained by relatively small changes in body position (Jeukendrup, A.E and Martin, J, 2001).

However, it is also important to understand the interaction of these factors when wanting to optimize cycling performance. One of the main challenges is the high level of complex interdependencies between performance factors (Atkinson, G *et al.*, 2003). A good example is that of choosing the best cadence. There appear to be different cadences for optimal heart rate, metabolic efficiency and power output, meaning that optimal cadence selection remains unclear. Therefore, despite vast amounts of research there is still a lack of successful multivariable studies which investigate the correlations between factors (Abbiss, R *et al.*, 2009). Furthermore, the influence of some performance factors on power production and power demand appears to be antagonistic. For instance, studies have shown that although a lower body position reduces aerodynamic drag, it also has a negative effect on cardio-respiratory (Gnehm, P *et al.*, 1997) and neuromuscular (Dorel, S *et al.*, 2009) performance. This further strengthens the case against research which considers optimization of isolated aspects of cycling. Therefore, it is clear that IMCT technology might serve the purpose of providing more comprehensive kinematic data for the analysis of body position in relation to these other performance variables.

Body position on the bicycle (cycling kinematics), plays a major role in determining many of the abovementioned cycling performance factors. The stationary upper and mobile lower body have distinct, although interrelated, functions. The angle of the

joints and orientation of these body segments, which affect most other performance aspects are defined by the body position and thus the interaction between the bicycle and the cyclist. Therefore, optimal road cycling kinematics should always be discussed in the context of optimal bicycle fit.

A.3.2 General principles of bicycle fit

This section covers the basic principles of static and dynamic bicycle fit as laid out in a review conducted by Silberman (2005). It covers the optimization of lower and then upper body positioning first approximately with static methods and then more accurately with dynamic methods.

During a static fit, the bicycle is setup to achieve the approximated optimal body position based on general guidelines for joint angles and positions. The size of the bicycle is usually the first consideration and relates primarily to the geometry of the frame. The lengths and angular inclinations of the seat tube, top tube, down tube and head tube define nominal boundaries for the three interface points and are fixed. After this, however, the saddle, handlebar and pedal positions are still slightly adjustable (Figure 11 is repeated here in Figure 41 for convenience).

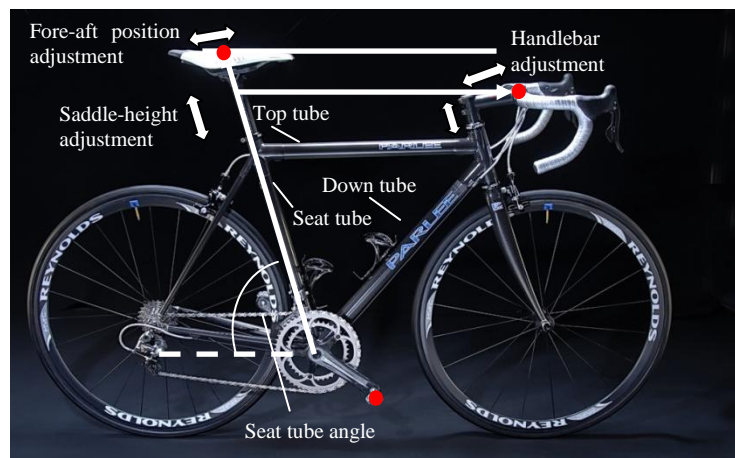


Figure 41: Basic bicycle fit parameters

The seat can be moved horizontally by changing the fore-aft position, and the saddle-height can be adjusted by lengthening or shortening the seat tube. It should be noted, however, that changes in saddle-height also equate to changes in fore-aft position due to the fact that both the railing and seat tube are angled and similarly, that changes in fore-aft position cause the saddle height to increase or decrease. Secondly, the height

and horizontal position of the handlebars can be adjusted by changing the lengths of the head tube and stem respectively. Lastly, the pedal position can be fine-tuned by choosing the most suitable crank length and adjusting the cleat position and orientation on the cyclist's shoe.

The first step in a static bicycle fit is to determine the proper pedalling kinematics of the lower body. This is achieved by adjusting the cleat position, saddle height and saddle fore-aft position. Cleat positioning should be done to maximize power and reduce injuries by ensuring that the first metatarsal in the foot is situated directly above the pedal axle. Various adjustments to the cleat position, as well as the insertion of shims or wedges, can be made to compensate for abnormalities or discrepancies in leg length and alignment. When determining saddle height, the goal is to position the saddle as high as possible without causing stress injuries to the lower extremities. This is because the higher the seat height, the higher the power output (the knee being most powerful at lower flexion angles) and the lower the aerobic cost. It should be noted that changes to the normal cleat position allow for higher or lower saddle heights. The saddle fore-aft position determines the flexion of the knee at specific pedal positions, and can thus be used to optimize crank torque. Usually, the knee should be directly above the pedal axle when the crank is forward and parallel to the ground, although positions that are further forward are used for riders competing in shorter, faster races who need more power in the downstroke.

Once the lower body kinematics have been optimized by positioning the pelvis-saddle and shoe-cleat-pedal interfaces, the upper body kinematics are optimized for power, aerodynamics, comfort and injury prevention by adjusting the stem length and handlebar height (in other words the "reach"). The greater the vertical distance between the saddle and the handlebars, the lower the cyclist and the smaller the frontal surface area; which leads to better aerodynamic efficiency. However, lower trunk positions reduce cycling power and increase strain on the back, meaning that optimal handlebar height is a balancing factor between power gains and power demand losses. Stem length, on the other hand, determines the extension of the upper body and is as vital to proper performance. The athlete's core musculature should not be too elongated or compacted, as this will increase fatigue while reducing power in both cases.

After the static fit, dynamic fits are generally conducted to optimize the static fit approximations. Again, the lower limb is taken into consideration first. The

biomechanical efficiency of the pedalling technique is especially relevant to competitive cycling. The effective transfer of forces to the pedals reduces wasted energy and improves power output and this is accomplished by optimizing the body position during dynamic fit. Out-of-plane muscular forces (those not exerted perpendicular to the crankshaft) are minimized by ensuring the correct crank hub width and pedal-cleat contact position and orientation. This essentially corrects bad tracking of the knee joints in the coronal plane as well as excessive internal and external knee rotation. These out-of-plane forces should be differentiated from non-muscular (inertial) tangential forces, which do not lead to fatigue. Furthermore, the pedalling forces at the various phases of the pedal stroke can be maximized through dynamic bicycle fit. This includes limiting negative forces on the upstroke, minimizing 'dead spots' at the top and bottom of the crank cycle and maximizing peak and total power. To do this, saddle height, fore-aft position and crank length are used to position the knee joint and adjust its range of motion for optimal collective crank torque. Cleat position on the shoe affects the role of the ankle in power delivery and should also be considered, although not in isolation, since it affects the effective seat position.

The upper body position is also a crucial component of dynamic bicycle fit. Most important, for competitive cycling, is the aerodynamic efficiency of the body position. Research has shown that aerodynamic drag represents 80% of the power demand at 30 km.h⁻¹ and that changes in body position reduce drag by up to 14% (Garcia-Lopez, J *et al.*, 2009). Therefore, along with narrow arm and leg profiles, the frontal surface area of the cyclist should be minimized by changing the height of the handlebars. The metabolic efficiency of the cyclist is also affected by upper body position. The cardio-respiratory system resides in the trunk, supplying energy to the actuating muscles in the lower extremities as well as the stabilizing muscles in the arms and core musculature. Constriction of the diaphragm and arterial system therefore leads to metabolic inefficiency (Gnehm, P *et al.*, 1997). The reach and pelvic tilt of the cyclist should thus also be adjusted for optimal heart rate and VO₂. Furthermore, the posture of the cyclist's back and arms plays an important role in the reduction of fatigue relating to weight distribution between the skeleton and core musculature. The position of the saddle relative to the handlebars should also be reconsidered in this light (Burke, E.R, 2003). In conclusion, the angles of the torso, shoulders, elbows and wrists need be adjusted with all these factors in mind in order to achieve the optimal performance.

APPENDIX B EXPERIMENTAL WORK

This section includes a more detailed description of the test instruments used for data collection. The technical specifications are given for the MVN hardware and Powerbeam Pro trainer and miscellaneous items are briefly mentioned.

B.1 The MVN Hardware

The MVN Lycra suit is designed with two external pouches on the lower back for storing the XBus Masters. Inner pouches hold each MTx sensor firmly in place on a prescribed body segment and there are hems that allow for the wiring, which connects all the sensor units in a daisy chain configuration, to be neatly stowed away. The XBus Masters provide power to the MTxs, synchronize all the MTx measurement signals and handle wireless communication with the computer. See Table 7 for more technical information on the MVN XBus Masters.

Table 7: MVN XBus Master specifications

Specification	Description	Value	Unit
Weight	-	300	g
Dimensions	-	100 x 150 x 40	mm
Input voltage range	-	4-14	V
Typical operating time	When using wireless mode	3	h
Power source	4x AA NiMH rechargeable	2700	mAh
Wireless connection	Spread spectrum link	2.4	GHz
Range	Outdoors/indoors	150/50	m

The typical battery life of the MVN system is three hours, which is sufficient for most cycling tests, although it tends to be much lower after many cycles. The operating time may drop below an hour when the batteries are older. In terms of mass, the XBus Masters can be considered negligible. In fact, the total weight of the on-body system is 1.9 kg (MVN user manual), which does not inhibit the technique of the cyclist for non-endurance testing. Furthermore, the placement of the XBus Masters is on the (stationary) lower back and is therefore not a hindrance to body position on the bicycle. The range of the wireless transmission is suitable for most testing situations, although these values are dependent upon the correct positioning of the two wireless receivers relative to one another. It was found that the outdoor range could be lower than 10 m when the receivers were placed very close to each other. Therefore, USB

extensions were required to move them further apart, where the range was about 40 m.

Table 8: MVN MTx sensor specifications

Specification	Description	Value	Unit
Weight	-	30	g
Dimensions	-	38 x 53 x 21	mm
Rate gyroscope	Range of rotation rate	± 1200	deg/s
Accelerometer	Range of linear acceleration	± 180 (18 g)	m/s^2
Magnetometer	Error	< 0.5	deg ³
	Resolution	0.5	deg
Sensor signals	Sampling rate	60-120	Hz

Table 8 contains more technical information on the MTx sensor units. The sensor specifications exceed the requirements for cycling testing. Assuming that the lower leg segment is the fastest moving part of the body in cycling, one could estimate the maximum rotation rate experienced by the MTx on this segment, in other words if the rotation was purely about one axis of the gyroscope sensor. Taking a maximum expected pedalling rate of 120 rpm, there would be two pedal strokes per second. To get the rotation of the segment in the plane, a range of motion of twice the knee flexion (which is usually a maximum of 100°) can be used. Therefore, the lower leg segment will experience a maximum rotation rate of approximately 400 °.s⁻¹, which is a factor of three slower than the gyroscope specification. Furthermore, it is assumed that the linear acceleration of the MTxs would be far lower than the maximum of 180 m. s⁻². Lastly, assuming a crank rotation of 720 °.s⁻¹ (120 rpm), the sampling rate would be sufficient for a minimum measurement rate of one every 6° at 120 Hz, or 60 samples per pedal stroke. This equates to a minimum of one sample at approximately every 3° of crank cycle, which is an acceptable resolution for the purpose of this study.

B.2 Powerbeam Trainer

Indoor testing requires the simulation of road race conditions on a stationary bicycle trainer. There are many categories of trainers, primarily differentiated by the type of resistance unit employed to imitate the energy demands of cycling, as well as the ‘feel’ of the road. When comparing results between indoor and outdoor tests it is desirable to have a high quality brake system that provides riding conditions that will have a minimal effect on outdoor technique. Furthermore, the control and

measurement of cycling power during the laboratory test protocol is required in order to obtain comparable results between individual cyclists. It is therefore necessary to use an indoor trainer, which has a realistic road feel and can execute pre-programmed workouts within a target range for power output. Therefore, a CycleOps Powerbeam Pro trainer was purchased for use in the indoor testing phase of the research, and is shown in Figure 42.



(Source: (Powerbeam Manual, 2009))

Figure 42: The Powerbeam Pro stationary bicycle trainer

The Powerbeam Pro is an advanced trainer system which fulfils the requirement for realistic road cycling conditions. It uses a magnetic brake that applies variable resistance to a roller with a flywheel attached to it. The roller resistance is controlled by a linear stepper motor which adjusts the distance between the magnet and the inner rim of the flywheel. The Powerbeam handlebar display unit, shown in Figure 43, transmits command signals wirelessly from an onboard closed-loop control system to the stepper motor. In this way, the inertia of the flywheel (roller resistance) can be adjusted to control cycling power, depending on the riding mode or specific workout selected on the handlebar unit by the cyclist. Power is measured with Powertap strain-gauge technology and two magnetic strips on the roller that provide torque (T) and rotational speed (ω) measurements respectively. These are used calculate the power exerted by the cyclist on the trainer as in Equation 17.

$$P = T\omega \tag{17}$$



(Source: (Powerbeam Manual, 2009))

Figure 43: Powerbeam wireless handlebar display unit

The Powerbeam Pro comes with a computer software package that can be used to set up customized workouts and view recorded workout data after a session is complete. The programmable workouts can be configured for specific power targets, meaning that the Powerbeam meets the test protocol requirements for the trainer, since cycling power can be measured and controlled. This power data, along with other measurements, is wirelessly streamed in real-time to the display unit for immediate visual feedback and can also be stored for later computer analysis if needed. Refer to Table 9 for more information on the Powerbeam data.

Table 9: Powerbeam specifications

Specification	Description	Value	Unit
Power measurement accuracy	Powertap sensor error	± 5	%
Measurement frequency	Rate of data sampling	1	Hz
Maximum power	Power range at high speed	1000+	W
Minimum power	Lowest possible resistance	30	W

B.3 Miscellaneous

One of the challenges that arose with the use of the Powerbeam trainer was that the frame caused unacceptable interference to the MVN sensors during testing. This was due to the proximity of the frame to the pedals. It was therefore necessary to design an aluminium frame to which the brake could be mounted. Brass was used for the skewer mounts, as can be seen in Figure 44. The change in frame made a significant difference to the level of magnetic interference. Although the magnetic brake still continued to have a lesser influence on the MVN sensors, the magnetic brake remained the best option due to the artificial ‘feel’ of wind brakes and the lack of

built in power measurement for oil-based brakes. Rollers were also not considered due to the increased risk of injury during testing.

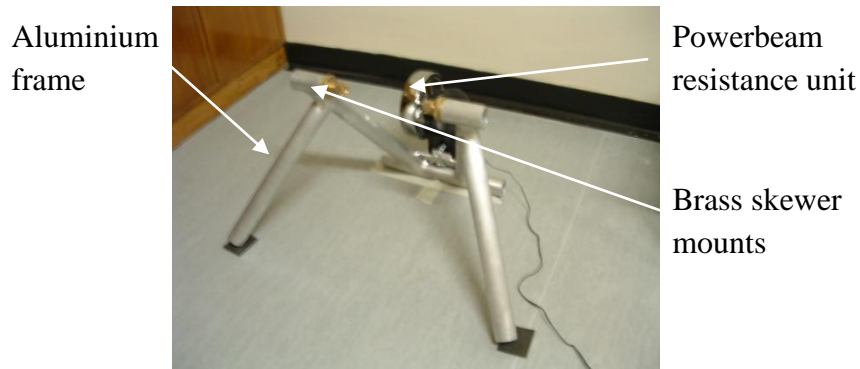


Figure 44: Manufactured aluminium frame for trainer

Two computers were utilized for the data collection. A desktop PC was used for the indoor testing and a laptop for the outdoor testing. Therefore, MVN Studio was installed on both machines. The Powerbeam software, which allowed for the programming of unique workouts for each cyclist and the collection of testing power data, was installed on the desktop PC. The laptop made it possible to keep the MVN suit within range of the transceivers while doing outdoor tests with a bicycle on the road. It was placed in the passenger seat of a pursuit vehicle during outdoor testing, in order to maintain wireless communications with the MVN suit, as the cyclist rode down the road. Furthermore, in the indoor tests, a high powered fan was used to reduce the heating effect due to lack of wind resistance and ventilation in the room.

APPENDIX C ANALYSIS WORK

This appendix is an overview of the analysis work performed in Matlab. It contains sections on the data management and numerical analysis which was conducted for the data analysis show in Chapter 4.

C.1 Data Management

The large volume of measurement data produced for each MVN recording created the need for efficient data management. The flow of information from MVN Studio to Matlab required the writing of numerous Matlab functions to import and structure the data effectively.

C.1.1 Importing MVNX data files into Matlab

The first step of the importation of the data into a Matlab workspace was exporting it from MVN Studio. The kinematic data from the 3 power sessions was exported from the indoor and outdoor MVN recording files for all 10 cyclists (20 files) into separate MVNX files (60 files). Then, the MVNX files were imported and stored in 60 Matlab data structures (Figure 45). Importing the MVNX files into Matlab was done using a toolbox, called XML_IO_TOOL, which is available freely for download on the Internet (File Exchange 2009). The XML toolbox contains a function for reading XML files and converting the output data into Matlab structures. This is normally in the form of nested structures and cells, with the field names based on the XML tags. Figure 45 summarizes the flow and quantity of the recorded cycling data.



Figure 45: Flow of measurement data from MVN Studio into Matlab

C.1.2 Data structuring

The raw MTx and Mocap data was stored in Matlab structures for convenience and efficient retrieval of information. The different stages of the data analysis (Figure 46) required transformations of the data, and thus structures were created for the imported raw data file and joint data, as well as structures for feature extraction and numerical

and statistical analysis. Each structure also acted as a backup for the consequent data in the process. This was especially relevant for the large raw data files which take a very long time to import into Matlab with the XML toolbox.

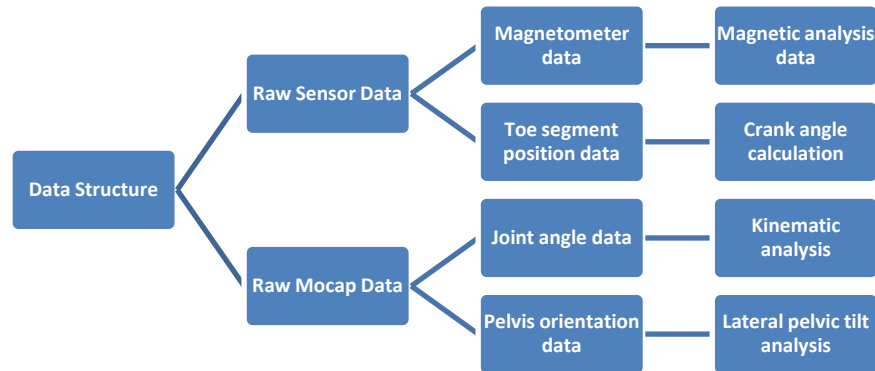


Figure 46: Matlab Data structure

The raw sensor data consisted of the magnetometer measurements for each MTx, as well as position data calculated with the biomechanical model from the foot MTx data. This data was sampled at 120 Hz, meaning that there were 7200 samples per sensor axis in each of the 60 second recordings. Since there are 17 MTxs in the MVN system, there were 17 magnetometers each measuring three vector quantities (x, y and z). Therefore, there were 60 matrices of the size 7200x51 for the magnetic analysis, corresponding to the three constant power recordings completed during indoor and outdoor testing with ten cyclists. Furthermore, there were sixty 7200x6 matrices containing the x, y and z position coordinates of each cyclist's left and right toe segments.

The raw Mocap data for each test was a matrix containing all the joint angles for the biomechanical model. Each full body sample contained 3 angular joint measurements for each of the 22 joints in the biomechanical model, one for each of the three anatomical planes. This means there are sixty 7200x66 matrices per cyclist in the raw data structure. This structure was used as the original unprocessed data source during analysis and no data manipulations were performed on it. Due to magnetic interference, only the flexion\extension joint angles were analyzed in this study. Furthermore, only the hip, knee and ankle joint were considered. Therefore, it was necessary to group these joint angles into a new data structure. The columns containing these joint angles were retrieved from the MVNX data table, with the index corresponding to the standard order of joint IDs in the MVN file. Each joint is

represented by three columns (one for each plane in space), with flexion/extension being the third. Therefore, for example, in order to obtain the flexion/extension values for the right knee, the 48th column of the raw data matrix was accessed since the right knee is the 16th joint in the MVN sequence (see illustration in Figure 47).

	Joints			Right Knee (#16)			Right Ankle (#17)		
Sample	Anatomical planes			Adduction	Rotation	Flexion	Adduction	Rotation	Flexion
	Columns			#46	#47	#48	#49	#50	#51
1									
2									
3									
.									
.									
.									

Figure 47: The MVNX data table for joint ankles

In this way, the joint data structure was used to store the flexion/extension sample vectors of the hip, knee and ankle measurements. These make up a total of 6 joints. Therefore, the joint data structure consists of sixty 7200x6 matrices. This data was used for the numerical analysis and feature extraction which followed. After the assimilation of the desired joint data into the relevant Matlab structure, this information could be evaluated. Feature extraction was performed with basic numerical analysis, calculations and curve fitting which allowed for the examination of kinematics for each cyclist. The results were stored in the analysis structure.

Raw Sensor Data	Raw Kinematic Data	Joint Data
<ul style="list-style-type: none"> • 23 segments • Magnetic/position data • All planes • 60 matrices • 7200x51 and 7200x6 cells 	<ul style="list-style-type: none"> • All 22 joints • Joint angles • All planes • Sixty matrices • 7200x66 cells 	<ul style="list-style-type: none"> • 6 joints • Joint angles • Flexion/extension • Sixty matrices • 7200x6 cells

Figure 48: Contents of Matlab data structures

C.2 Numerical Analysis

This section explains the calculations performed to obtain the magnetic field parameters for the magnetic field analysis, the crank angle Θ_C and the kinematics parameters Θ_{MAX} , Θ_{MIN} and Θ_{RANGE} for Θ_H , Θ_K and Θ_A .

C.2.1 Magnetic flux and inclination calculation

The magnetometers in each segment's MTx sense the local magnetic field in order to provide global orientation for the biomechanical model. The assumption, therefore, is that the local magnetic field measured by the MTxs is essentially the Earth's undisturbed magnetic field.

Two parameters used to represent the Earth's magnetic field are the magnetic field strength and inclination angle. Magnetic field strength, equivalent to the flux density of the magnetic field, is a vector quantity which describes the force experienced by other magnetic materials (or moving electrical charges) at a specific point in the field. Magnetic inclination, on the other hand, describes the orientation of the magnetic field with regard to the ground. Traditionally, this has been defined as the angle between a magnetic needle and the horizontal plane. In a homogenous magnetic field, such as would be the case for a magnetically undisturbed test, the field strength and inclination would remain constant at a specific geographical location.

Therefore, in order to quantify the disturbances to the MTx magnetometer data the magnetic field strength and inclination were considered. This was done using the raw sensor data, which was extracted from the MVN XML files. The magnetometer data is in the form of an unscaled three-dimensional vector as in Equation 18:

$$M_t = m_{x,t} + m_{y,t} + m_{z,t} \quad (18)$$

where $m_{x,t}$, $m_{y,t}$ and $m_{z,t}$ are normalized components of the total magnetic field M_t measured within the local x-y-z coordinate system of the MTx. It should be noted that the orientation of the MTx is unknown in the global frame (in which the Earth's magnetic field is defined) and therefore cannot be used to rotate the local coordinate system. Therefore, to overcome this, intuitive methods were used to obtain an indication of the field strength and inclination.

$$FS_t = \sqrt{m_{x,t}^2 + m_{y,t}^2 + m_{z,t}^2} \quad (19)$$

Firstly, the scalar magnitude of the field strength was calculated as in Equation 19. This value is most useful in evaluating distortions near moving MTxs, since it can be used irrespective of the orientation of the MTx relative to the Earth’s magnetic field. Basically, a change in the magnitude readings at different positions indicates a non-homogenous (and thus disturbed) field.

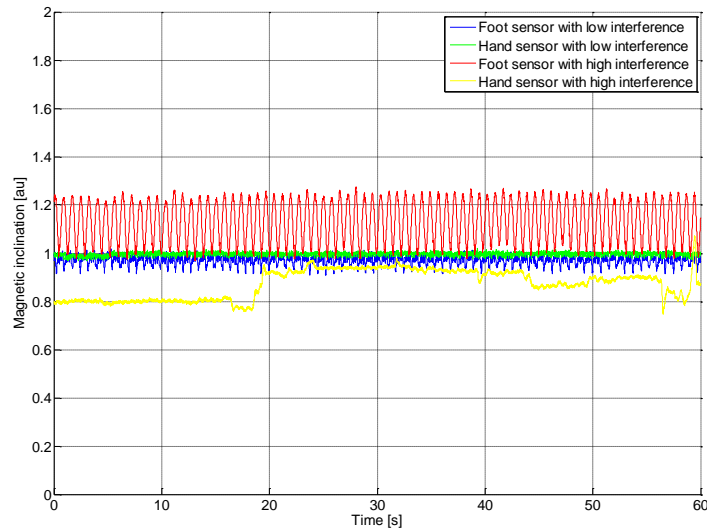


Figure 49: Example of magnetometer readings over time

Figure 49 shows typical high and low interference readings taken during the one-minute-long cycling tests in this study for the hand and feet sensors. The intensity readings are in arbitrary units and are scaled to a undisturbed value of 1 in this graph (whereas the undisturbed value is 50 in the magnetic analysis in Section 4.1.1. Therefore, it can be seen in Figure 49 that a stationary hand sensor in an approximately homogenous magnetic field (green line) is fairly stable. However, some of the hand sensors experienced significant changes in magnetic intensity during the testing, presumably due to the cyclist moving their hands nearer to ferrous metals (such as changing gears or leaning on the brakehoods). On the other hand, both the low and high interference cases for the foot sensors show sinusoidal intensity readings. This is because a cyclist’s foot moves in a circular path past various certain metal objects such as the bicycle chain and sprockets. The extent of change in amplitude represents the level of heterogeneity of the magnetic field on the path of the moving foot sensor.

However, FS on its own is not useful for determining homogeneity around stationary magnetometers (such as in the MTxs on the hands) because it only represents the field strength at a singular point. Therefore, since the values were not scaled to the standard gauss units, the interpretation of the calculated magnitude requires a reference value for the Earth's magnetic field. An undisturbed intensity value of 50 was measured for the magnitude FS , during calibration tests taken outdoors.

$$A_t = a_{x,t} + a_{y,t} + a_{z,t}$$

(Error! Bookmark not defined.)

Secondly, the local inclination angle measured with the components of the magnetometer data M_t can be rotated to the global frame using the accelerometer data A_t (Equation 20), albeit only for stationary MTxs. This can be done because a stationary accelerometer will effectively act as an inclinometer. The sensor output will then correspond to the gravity vector, with a magnitude of 9.81 m.s^{-2} in the downwards direction. Therefore, since gravitational vector is perpendicular to the global horizontal plane (ground), the global inclination angle can be obtained (Figure 51). This is accomplished by calculating the angle between the magnetometer vector and a vector perpendicular to the accelerometer vector (the Earth's horizontal).

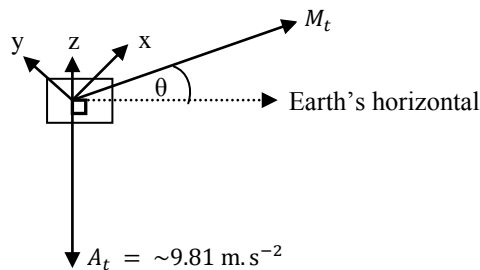


Figure 50: Method used to obtain the magnetic inclination angle

Figure 51 shows $\theta_{MA,t}$, the angle between the magnetometer and accelerometer vectors. This angle was solved using the cosine rule for triangles which states that any internal angle of a triangle can be obtained provided that lengths of the three sides are known. The equations for the lengths of these vectors are also given.

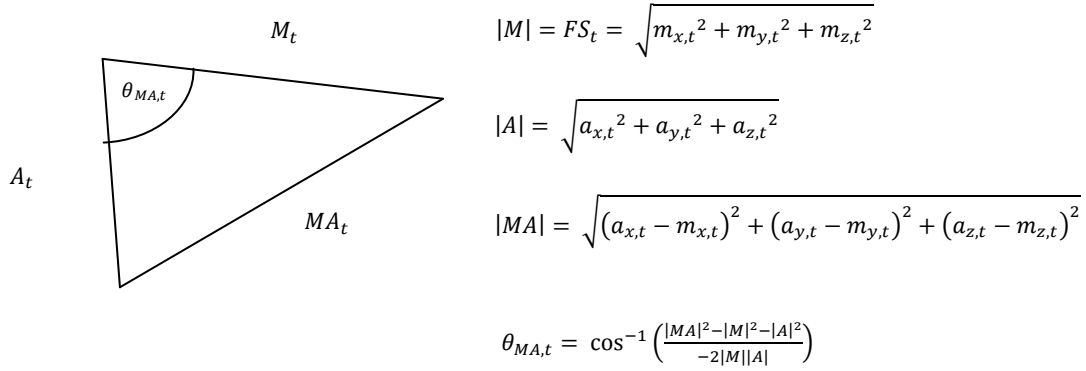


Figure 51: Cosine method used to obtain angle $\theta_{MA,t}$

In the equations in Figure 51 $|M|$ and $|A|$ represent the magnitude of the magnetic field strength and gravity vector respectively and are the two sides of the triangle adjacent to the angle $\theta_{MA,t}$. The side of the triangle $|MA|$ opposite to $\theta_{MA,t}$ represents the resultant magnitude of A_t and M_t . Therefore, once $\theta_{MA,t}$ is calculated the inclination I_t can be found as in Equation 21.

$$I_t = \theta_{MA,t} - 90^\circ \quad (20)$$

The accuracy of this method is largely determined by the validity of using the accelerometer as an inclinometer. If the sensor is moving and accelerates, the gravitational vector is more difficult to separate from the other acceleration components. In the MVN Kalman filter, advanced frequency analysis is used to eliminate high-frequency noise (due to vibrations) and medium-frequency disturbances (due to body movements) from the constant gravitational acceleration. However, this was beyond the scope of this study. Since the inclination was only a secondary part of the magnetic analysis, the gravitational vector was approximated by removing the accelerations due to vibrations and movements in less sophisticated way. Firstly, it was assumed that the vibrations experiences by the accelerometers was approximately Gaussian white noise, and thus could be averaged out.

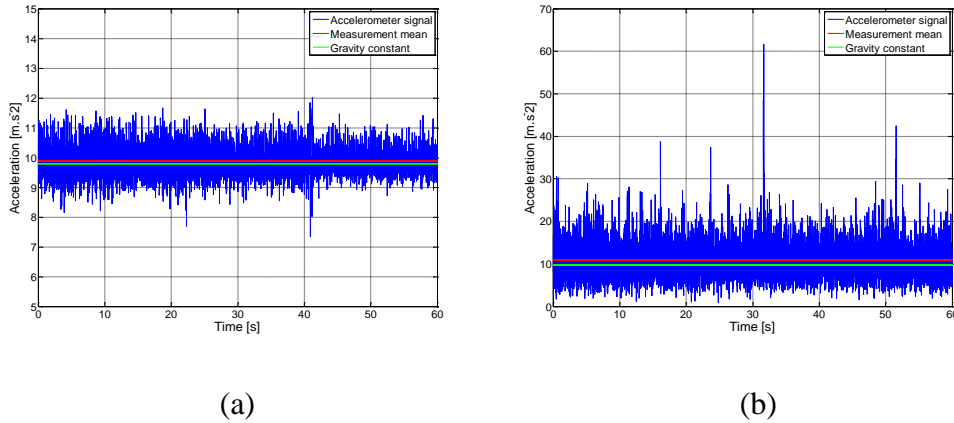


Figure 52: Hand sensor acceleration (a) indoors and (b) outdoors

An example of this can be seen in Figure 52, which shows the raw accelerometer signal for a stationary hand signal during an indoor and outdoor test respectively. Here it can be seen that the vibrations are roughly random since the mean of the acceleration signal is almost equal to the gravitational constant $g = 9.81 \text{ m.s}^{-2}$. This is especially true for the indoor measurements on the stationary trainer, which oscillate on average between $9\text{-}11 \text{ m.s}^{-2}$. On the other hand, the outdoor hand sensor experienced far higher deviation in acceleration ($\sim 5\text{-}20 \text{ m.s}^{-2}$), probably due to the inertia of the bicycle on the road and less controlled power level due to wind resistance and lateral movement etc. This results in a slightly less accurate average acceleration. However, both the indoor and outdoor average accelerations for the stationary sensors are relatively accurate approximations of ‘ g ’. Furthermore, Figure 53 illustrates that while the approximated gravitational vector of the stationary sensors is roughly constant in direction and magnitude, the moving sensors are not.

The inclination angle of the Earth’s magnetic field around Stellenbosch University during the time of testing was taken as 67° (International Geomagnetic Reference Field, Inclination Chart, 2000). Therefore, I_t can be used to evaluate the disturbances to the local magnetic field around stationary MTxs that experience negligible accelerations. However, this not only excludes the moving sensors (which obviously cannot be used as inclinometers), but also the outdoor test results. This is because the accelerometers experience inertial forces due to the movement along the road. Therefore, only the indoor tests conducted on a stationary trainer can be used to obtain the inclination angle. However, a comparison between the inclination angles

around the various MTx still serves to indicate the effect of ferrous materials on the bicycle, even though offset errors may be due to building-related disturbances.

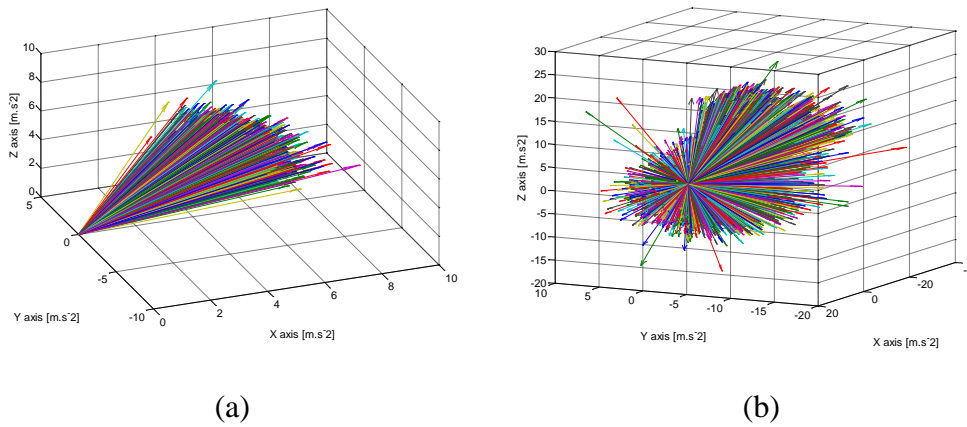
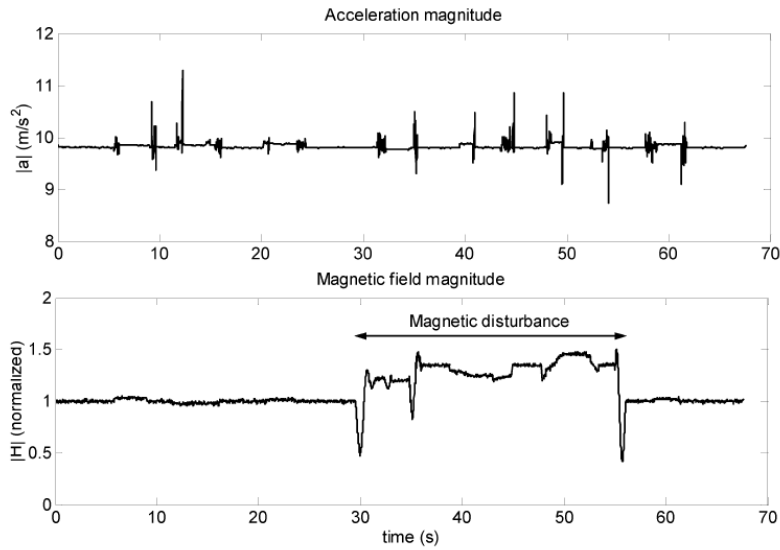


Figure 53: Acceleration vectors for indoor (a) hand and (b) foot sensors

The magnetic analysis performed in this study was modelled on two studies (on methods of compensation for magnetic interference) by Roetenberg (2005; 2007), which contributed to the development of the MVN BIOMECH system. In the 2005 paper, Roetenberg gives an example of considerable magnetic interference measured by an MTx when placed near an iron cylinder (Figure 54). When compared to the levels of interferences experienced by the MTx in this study (Figure 49), it can be seen that the road bicycles do indeed distort the magnetic field considerably. Furthermore, Roetenberg also gives the accelerometer readings during the quasi-static trial with the MTx, which shows accurate readings of g with spikes occurring when the MTx was slowly rotated. When compared with Figure 52a, it can be seen the vibrations of the hand sensor during testing in this study are in the same order of magnitude as a slow rotation, which is very low.



(Source: (Roetenberg, D *et al.*, 2005))

Figure 54: Example of severely disturbed magnetometer readings

C.2.2 Cadence and crank angle calculation

A method was found to calculate the crank angle, used in the kinematic results section, with the MVN data. Since the toe section (distal part of the foot above the cleat) is fixed to the pedal in the sagittal plane, the global position of the toe segment in the biomechanical model was assumed to closely approximate the position of the pedal in space. Figure 55 shows how the point (x_i, y_i) of the pedal in the sagittal plane at a specific point should theoretically be a fixed radial distance from the crank spindle, equal to the length of the crank arm. The crank length L_C is simply the hypotenuse of x and y . The top of the pedal stroke was defined as zero degrees, such that the crank angle Θ_C is calculated as the clockwise angle between the crank arm and the positive y -axis (assuming the positive x -axis is in the direction of the front wheel of the bicycle). This is calculated using the four-quadrant tangent angle between x and y .

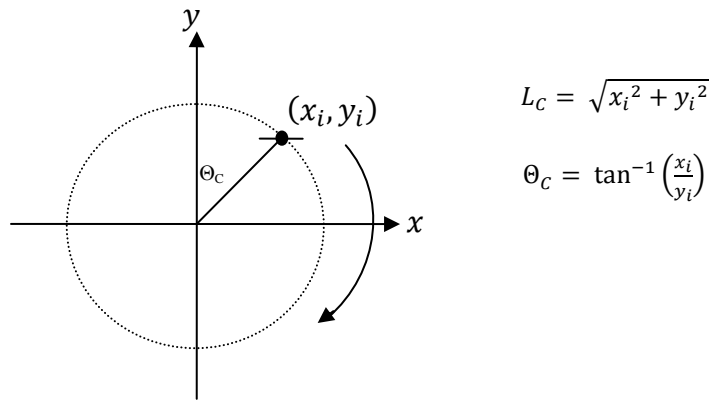


Figure 55: Crank angle as calculated using the position of the pedal

The MVN data contains three-dimensional position data for the toe segment (see example case in Figure 56a). Similar to the kinematics data, the position data is sinusoidal due to the rhythmic motion of pedalling. The positions are calculated in the Kalman filter using the initial position of the biomechanical model and are therefore not normalized. As can be seen by the sloping green line, the foot segment experiences drift error in the Z-plane. Fortunately, the X- and Y-axis measurements are stable and the pedal position in the sagittal plane can be taken as drift free. However, the ranges of motion for the X and Y measurements (which should both be equal to the double the crank arm length) differ considerably. Therefore, when they are normalized and plotted against each other (Figure 56b) the measured position of the pedal is roughly elliptical, which is of course not true.

Upon closer inspection, the range of Y-axis measurements is approximately 0.35 (-0.175, 0.175) which is very close to a standard crank length available today. However, the range of position for X is only 0.2 (-0.1, 0.1) which is too small for a crank arm. It is thus acceptable to assume that Y represents the true crank position, whereas X contains a significant bias error. After careful analysis of the MVN recordings, it was found that the reason for the bias error was that the sagittal plane was slightly rotated about the Y-axis (in other words the X-axis was not perfectly parallel to the bicycle). This was due to the asymmetrical magnetic interference of the bicycle, especially in the hands, which caused the biomechanical model to be slightly asymmetrical (especially in the upper body). Therefore, the X-axis measurements are not the true length of the crank arm because the sagittal plane was not exactly

perpendicular to the pedal. Therefore, the X-axis measurements were not valid for calculating the crank angle.

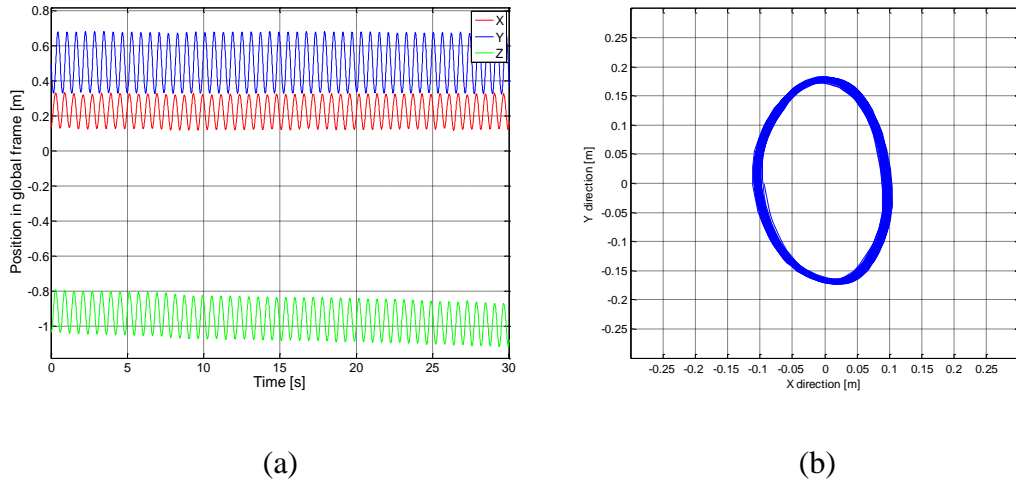
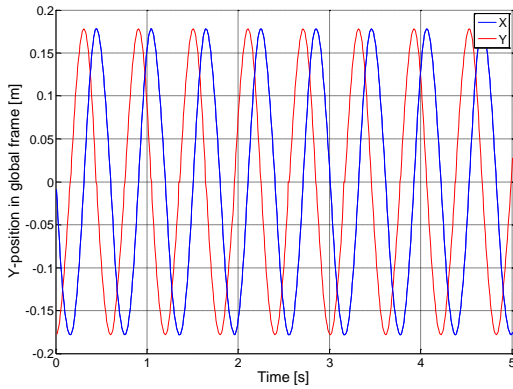


Figure 56: (a) Raw position data and (b) path of toe segment

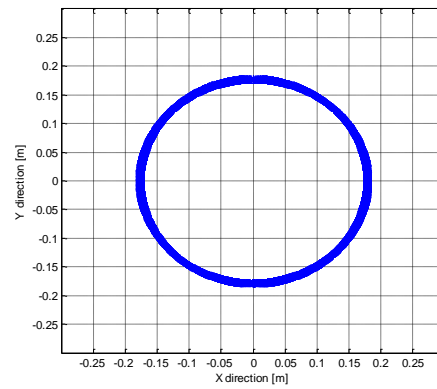
Fortunately, since it was known that the pedal path is circular, only the Y-axis measurements were necessary. The crank length was taken as half the range of motion in the Y-direction (~0.175m), and a Matlab function was written to calculate the X-coordinate. This was done using knowledge of which quadrant the Y-data was in and the crank length, based on Equation 22.

$$x_i = \sqrt{L_c^2 - y_i^2} \quad (21)$$

The corrected data is shown in Figure 57a. The measurements were normalized and now had the same diameter. The final pedal path (Figure 57b) is very near the actual path and could be used to calculate the angle of the crank arm for the kinematics results to be plotted against. The validity of the crank angle was supported by the fact that the crank angle domains at which the leg joint angles were maximum and minimum were almost identical to studies in which the crank angle was measured using an optical encoder.



(a)



(b)

Figure 57: Corrected pedal path using Y-data

The value of the crank angle calculation is that it provides information about where in the pedal stroke the joint angles occur, as opposed to simply plotting kinematics over time. This is crucial for being able to analyze bicycle setup using the MVN. Furthermore, this method of calculating the crank angle makes use of the available data instead of taking measurements using an encoder on each different bicycle which would take extra money, time and effort. It is also better than using an encoder in that the position data is already synchronized with the kinematic data in the MVN measurements, and eliminates the need for synchronizing encoder data with the motion recording. Lastly, the crank angle can also be used to measure pedalling cadence by measuring the time it takes for one full pedal revolution. Even the instantaneous cadence can be found at different points in the pedal stroke, which is useful for analyzing the dynamics properties of the crank during each pedal stroke.

C.2.3 Joint flexion calculations

The Θ_H , Θ_K and Θ_A data required some basic numerical analysis to extract Θ_{MAX} , Θ_{MIN} and Θ_{RANGE} . The joint angles follow a sinusoidal pattern, which made it easy to parameterize the data with these three values. Matlab functions were thus written to locate the maxima and minima, which were then used to obtain the range. As shown in Figure 58, Θ_{MAX} and Θ_{MIN} were calculated using five moving points along the data curve. When a value was greater than three points on either side of it, it was taken as a maximum (similarly for the minimum values). This was done to eliminate the capture of anomalous peaks or troughs in the data (see graph) which are possible at

high sample rates using Kalman filter estimation of joint kinematics. A vector of Θ_{MAX} , and Θ_{MIN} values, along with their corresponding indices, were thus extracted for each joint in each test.

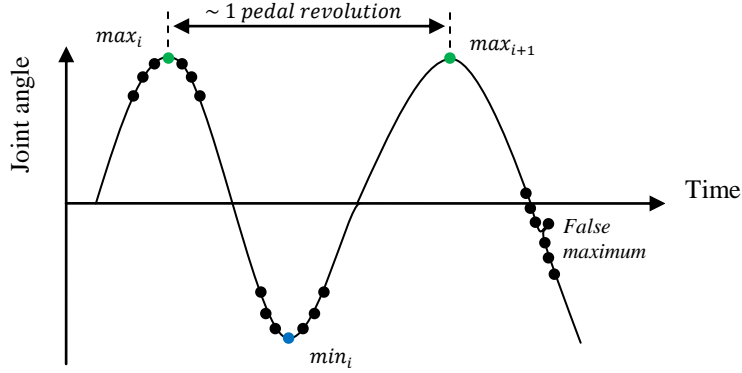


Figure 58: Method used to calculate the kinematic parameters

Due to natural variations in technique, the peak and trough values were slightly different for each pedal revolution. Therefore, the crank cycles were split up and then averaged. Θ_{MAX} and Θ_{MIN} are thus calculated as in Equation 23 and 24 respectively. Θ_{RANGE} could then be calculated as in Equation 25. Finally, the deviations used in the plots in the data analysis chapter were obtained from Equations 26 and 27.

$$Max_{avg} = \frac{1}{j} \sum_{i=1}^j max_i \quad (22)$$

$$Min_{avg} = \frac{1}{k} \sum_{i=1}^k min_i \quad (23)$$

$$Range_{avg} = Max_{avg} - Min_{avg} \quad (24)$$

$$Max_{dev} = \sqrt{\frac{1}{j-1} \sum_{i=1}^j (max_i - Max_{avg})^2} \quad (25)$$

$$Min_{dev} = \sqrt{\frac{1}{k-1} \sum_{i=1}^k (min_i - Min_{avg})^2} \quad (26)$$

It should be noted that the above equations were not coded manually . Rather, the corresponding Matlab functions were used in the numerical analysis.

REFERENCES

- 3D Allusions Studio 'Xsens MVN - Inertial Motion Capture' [online] (Cited 5 December 2010) Available from
URL:<http://www.3dallusions.com/201010252097/News/Xsens-MVN-Inertial-Motion-Capture.html> >
- Abbiss, R., Peiffer, J., and Laursen, P. (2009) 'Optimal cadence selection during cycling', *International SportsMed Journal* 10.1, pp.1-15.
- Ahmad, A., Rowlands, D., and James, D. (2009) 'Deriving upper arm rotation from Vicon to enhance the first serve in tennis', *Journal of Science and Medicine in Sport* 12.S68, S1-S83
- Ashby, B. and Heegaard, J. (2002) 'Role of arm motion in the standing long jump', *Journal of Biomechanics* 35.12, pp.1631–1637.
- Atkinson, G, Davison, R, Jeukendrup, A, and Passfield, L (2003) 'Science and cycling: current knowledge and future directions for research', *Journal of Sports Sciences* 21.9, pp.767-787.
- Baker, R. (2007) 'The history of gait analysis before the advent of modern computers', *Gait & Posture* 26.3, pp.331–342.
- Bini, R., Diefenthaler, F., and Mota, C. (2008) 'Fatigue effects on the coordinative pattern during cycling: Kinetics and kinematics evaluation', *Journal of Electromyography and Kinesiology* 20.1, pp.102-107.
- Braune, W. and Fischer, O. (1988) *Determination of the moments of inertia of the human body and its limbs*, Springer-Verlag: Berlin
- Brodie, M., Walmsley, A., and Page, W. (2008) 'Fusion motion capture: a prototype system using inertial measurement units and GPS for the biomechanical analysis of ski racing', *Sports Technology* 1.1, pp.17-28.

Burke, E.R. (2003) *High-Tech Cycling: The science of riding faster*, Human Kinetics: Colorado

Callaghan, M.J. (2005) 'Lower body problems and injury in cycling', *Journal of Bodywork and Movement Therapies* 9.3, pp.226-236.

Carpes, F.P., Mota, C.B., and Faria, I.E. (2010) 'On the bilateral asymmetry during running and cycling: A review considering leg preference', *Physical Therapy in Sport* 11.4, pp.136-142.

Cavanagh, P. and Sanderson, D. (1986) 'The biomechanics of cycling: Studies of the pedaling mechanics of elite pursuit riders', *In The Science of Cycling*, Human Kinetics: Champaign

Chan, Y., Fong, D., Chung, M. *et al.* (2010) 'Identification of ankle sprain motion from common sporting activities by dorsal foot kinematics data', *Journal of Biomechanics* 43.10, pp.1965-1969.

Chapman, A.R., Vicenzino, B., Blanch, P. *et al.* (2008) 'The influence of body position on leg kinematics and muscle recruitment during cycling', *Journal of Science and Medicine in Sport* 11.6, pp.519-526.

Chung, C.S. (1989). The kinetics and kinematics of the shoulder and elbow during the volleyball spike. *In: XII Congress.* Seoul, Korea: International Society of Biomechanics, pp.997.

Cloete, T. (2008). *Benchmarking full-body inertial motion capture for clinical gait analysis (MSc)*. University of Stellenbosch.

Cutti, A., Ferrari, A., Garofalo, P. *et al.* (2010) '“Outwalk”: a protocol for clinical gait analysis based on inertial and magnetic sensors', *Medical and Biological Engineering and Computing* 48.1, pp.17-25.

Cycling SA (2010) 'Cycling SA unveils impressive "2020 vision"' [online] (Cited 4 December 2010) Available from

URL: <http://www.cyclingsa.com/Article.aspx?uid=68> >

Design News Magazine 'Xsens sensors go Hollywood' [online] (Cited 20 November 2010) Available from

URL: <http://www.xsens.com/en/news/entertainment-news/inertial-sensors-go-hollywood> >

Dorel, S., Couturier, A., and Hug, F. (2009) 'Influence of different racing positions on mechanical and electromyographic patterns during pedalling', *Scandinavian Journal of Medicine & Science in Sports* 19.1, p.44–54.

Eberhart, H. and Inman, V. (1947). Fundamental studies of human locomotion and other information relating to design of artificial limbs. *Report to the National Research Council of the University of California*.

Egana, M., Ryan, K., Warmington, S.A., and Green, S. (2009) 'Effect of body tilt angle on fatigue and EMG activities in lower limbs during cycling', *European Journal of Applied Physiology* 108.4, pp.649-656.

Elliot, B., Alderson, J., and Denver, E. (2007) 'System and modelling errors in motion analysis: Implications for the measurement of the elbow angle in cricket bowling', *Journal of Biomechanics* 40.12, pp.2679–2685.

Ephanov, A. and Hurmuzlu, Y. (2002) 'Generating pathological gait patterns via the use of robotic locomotion models', *Technology and Health Care* 10, pp.135–146.

Faria, E.W., Parker, D.L., and Faria, I.E. (2005a) 'The Science of Cycling Part 1: Physiology and Training', *Sports Medicine* 35.4, pp.285-312.

Faria, E.W., Parker, D.L., and Faria, I.E. (2005b) 'The Science of Cycling Part 2: Factors Affecting Performance', *Sports Medicine* 35.4, pp.313-337.

Farrell, K.C., Reisinger, K.D., and Tillman, M.D. (2003) 'Force and repetition in cycling: possible implications for iliotibial band friction syndrome', *The Knee* 10.1, pp.103–109.

Faupin, A. and Gorce, P. (2008) 'The effects of crank adjustments on handbike propulsion: A kinematic model approach', *International Journal of Industrial Ergonomics* 38.7-8, pp.577-583.

Ferrari, A., Cutt, A., Garofalo, P. *et al.* (2010) 'First in vivo assessment of “Outwalk”’: a novel protocol for clinical gait analysis based on inertial and magnetic sensors', *Medical and Biological Engineering and Computing* 48, pp.1-15.

Garcia-Lopez, J., Rodriguez-Marroyo, J.A., Juneau, C. *et al.* (2009) 'Reference values and improvement of aerodynamic drag in', *Journal of Sports Sciences* 26.3, pp.277–286.

Ghasemzadeh, H., Loseu, V., Guenterberg, E., and Jafari, R. (2009). Sport Training Using Body Sensor Networks: A Statistical Approach to Measure Wrist Rotation for Golf Swing. *BodyNets: Proceedings of the Fourth International Conference on Body Area Networks*.

Gnehm, P., Reichenbach, S., Altpeter, E. *et al.* (1997) 'Influence of different racing positions on metabolic cost in elite cyclists', *Medicine and Science in Sports and Exercise* 29.6, pp.818-823.

Gregor, R.J. (2000) 'Biomechanics of Cycling', *In Exercise and sport science*, Philadelphia: Lipincott Williams and Wilkins

Gregor, R. and Conconi, F. (2000) *Biomechanics of cycling*, Blackwell Science Limited Oxford

Hull, M.L. and Jorge, M. (1985) 'A method for biomechanical analysis of bicycle pedalling', *Journal of Biomechanics* 18.9, pp.631-644.

ICG Magazine 'The Avatar Effect' [online] (Cited 20 November 2010) Available from

URL: <http://www.xsens.com/en/news/entertainment-news/the-avatar-effect> >

IOL Sport (2010) 'IOL News' [online] (Cited 3 December 2010) Available from

URL: <http://www.iol.co.za/sport/cycling/argus-riders-to-wear-black-arambands-1.614376> >

Jeukendrup, A.E. and Martin, J. (2001) 'Improving Cycling Performance: How Should We Spend Our Time and Money', *Sports Medicine* 31.7, pp.559-569.

Jobson, S. A., Nevill, A. M., George, S. R. *et al.* (2008) 'Influence of body position when considering the ecological validity of laboratory time-trial cycling performance', *Journal of Sports Sciences* 26.12, pp.1269–1278.

Jobson, S.A., Nevill, A.M., Palmer, G.S. *et al.* (2007) 'The ecological validity of laboratory cycling: Does body size explain the difference between laboratory- and field-based cycling performance?', *Journal of Sports Sciences* 25.1, pp.3-9.

Jones, A. and Doust, J. (1996) 'A 1% treadmill grade most accurately reflects the energetic cost of outdoor running', *Journal of Sports Sciences* 25.1, pp.321-327.

Knee Pain Info Website, 'Patellofemoral Joint Pain ' [online] (Cited 2 December 2010) Available from

URL: <http://www.kneepaininfo.com/kneepatellofem.html> >

Lapinski, M., Berkson, E., Gill, T. *et al.* (2009). A Distributed Wearable, Wireless Sensor System for Evaluating Professional Baseball Pitchers and Batters. *In: International Symposium on Wearable Computers*, pp.131-138.

Lloyd, D. and Rubenson, J. (2008). Ostriches, ligaments and chucking: Research at the University of Western Australia. *Vicon: Setting the Standard for Life Sciences*. [online] Available from:

URL: http://www.vicon.com/standard/archives/2008/uni_westaus.htm >

Louw, Q., Grimmer, K., and Vaughanc, C. (2006) 'Biomechanical outcomes of a knee neuromuscular exercise programme among adolescent basketball players: A pilot study', *Physical Therapy in Sport* 7.2, pp.65–73.

Luinge, H.J. (2002). *Inertial Sensing of Human Movement (PhD)*. University of Enschede, the Netherlands.

Mavrikios, D., Karabatsou, V., Alexopoulos, K. *et al.* (2006) 'An approach to human motion analysis and modelling', *International Journal of Industrial Ergonomics* 36.11, pp.979–989.

Menache, A. (2000) *Understanding motion capture for computer animation and video games*, Morgan Kaufman Publishers

Monaghan, C. (2010). *Pros and Cons of Inertial Sensing for Human Motion Analysis*. [online]. Available from:

URL: <http://download.xsens.com/XsensProsCons20091105.wmv> >

Mündermann, L., Corazza, S., and Andriacchi, T.P. (2006) 'The evolution of methods for the capture of human movement leading to markerless motion capture for biomechanical applications', *Journal of NeuroEngineering and Rehabilitation* 3:6.

Muybridge, E. (1887) *Animal Movement*, Philadelphia: J.B. Lippincott

Noakes, Prof. T. (2010). Personal communication, 16 August, Cape Town

(2009) 'Powerbeam Manual' [online] (Cited 8 June 2010) Available from URL: http://www.cycleops.com/pdfManuals/19063_PowerBeam%20User%20Manual%20with%20Joule.pdf >

Prochaska, M., Klabunde, B., and Butzmann, S. (2008) 'Modeling and simulation of magnetoresistive sensor systems ' [online] (Cited 6 June 2010) Available from URL: www.embedded.com/design/210300298 >

Redfield, R. and Hull, M. L. (1986) 'On the relation between joint moments and pedalling rates at constant power in bicycling', *Journal of Biomechanics* 19.4, pp.317-329.

Retul Studios 'Retul bicycle fit' [online] (Cited 4 December 2010) Available from URL: <http://www.retul.com/> >

Roetenberg, D. (2006). *Inertial and Magnetic Sensing of Human Motion (PhD)*. University of Enschede, the Netherlands

Roetenberg, D., Baten, C., and Veltink, P. (2007) 'Estimating Body Segment Orientation by Applying Inertial and Magnetic Sensing Near Ferromagnetic Materials', *IEEE Transactions on Neural Systems and Rehabilitation Engineering* 15.3, pp. 469-471

Roetenberg, D., Luinge, H.J., and Baten, C.T. M. and Veltink, P.H. (2005). Compensation of Magnetic Disturbances Improves Inertial and Magnetic Sensing of Human Body Segment Orientation, *IEEE Transactions on Neural Systems and Rehabilitation Engineering* 13.3, pp. 395-405

Roetenberg, D., Luinge, H., and Slycke, P. (2009) 'Xsens MVN: Full 6DOF Human Motion Tracking Using Miniature Inertial Sensors' [online] (Cited 10 January 2010) Available from

URL: http://www.xsens.com/images/stories/PDF/MVN_white_paper.pdf >

Roetenberg, D., Luinge, H., and Veltink, P. (2003). Inertial and magnetic sensing of human movement near ferromagnetic materials. *In: Proceedings of the Second IEEE and ACM International Symposium on Mixed and Augmented Reality (ISMAR '03)*. IEEE Computer Society.

Schache, A., Blanch, P., Rath, D. *et al.* (2002) 'Three-dimensional angular kinematics of the lumbar spine and pelvis during running', *Human Movement Science* 21.2, pp.273-293.

Silberman, M.R., Webner, D., Collina, S., and Shiple, B.J. (2005) 'Road Bicycle Fit', *Clinical Journal of Sports Medicine* 15.4, pp.271-276.

Slawinsk, J., Bonnefoy, A., Ontanon, G. *et al.* (2010) 'Segment-interaction in sprint start: Analysis of 3D angular velocity and kinetic energy in elite sprinters', *Journal of Biomechanics* 43.8, pp.1494–1502.

Smak, W., Neptune, R.R., and Hull, M.L. (1999) 'The influence of pedaling rate on bilateral asymmetry in cycling', *Journal of Biomechanics* 32.9, pp.899-906.

Steinwender, G., Saraph, V., Scheiber, S. *et al.* (2000) 'Intrasubject repeatability of gait analysis data in normal and spastic children', *Clinical Biomechanics* 15.2, pp.134-139.

Tawfik, H. (2009) 'A glimpse at MEMS' [online] (Cited 5 July 2010) Available from URL: <http://knol.google.com/k/a-glimpse-at-mems#> >

Thies, S.B., Tresadern, P., L. Kenney, L. *et al.* (2007) 'Comparison of linear accelerations from three measurement systems during “reach & grasp”', *Medical Engineering and Physics* 29.9, pp.967-972.

Timmer, C. (1991) 'Cycling Biomechanics: A Literature Review', *Journal of Orthopedic and Sports Physical Therapy* 14.3, pp. 106-113

Tokuyama, M., Ohashia, H., Iwamoto, H. *et al.* (2005) 'Individuality and reproducibility in high-speed motion of volleyball spike jumps by phase-matching and averaging', *Journal of Biomechanics* 38.10, pp.2050-2057.

Weber, W. and Weber, E. (1836) *Mechanik der menschlichen Gehwerkzeuge.*,
Göttingen: Dieterich

Welch, G. and Bishop, G. (2001) 'An Introduction to the Kalman Filter', *In*
SIGGRAPH